Characterization of Motor Unit Discharge Rate in Patients with Amytrophic Lateral Sclerosis (ALS)

Thesis Submited by
Patrick K. Kasi

In partial fulfilment of the requirements for the
Master of Science in Electrical and Computer Engineering
Department of Electrical and Computer Engineering

Worcester Polytechnic Institute
May 2009

Thesis Committee:
Edward A.Clancy, PhD Chair

Lisa S. Krivickas, MD

Paolo Bonato, PhD

Abstract

In this study, we used a custom made quadrifilar needle electrode and multichannel electromyography (EMG) software tool to decompose EMG signals and investigate the behavior of motor unit discharge rate (MUDR) of concurrently active motor units in patients with amyotrophic lateral sclerosis (ALS). Decomposition is a technique used to break down the complex EMG signal into its constituent motor units. A motor unit is a single alpha motor neuron and all the muscle fibers it innervates. ALS is a progressive degenerative disorder of both the upper and lower motor neurons.

We recorded four differentially amplified EMG signals from the first dorsal interosseous (FDI) muscle of six ALS patients (four with predominant lower motor neuron pathology and two with predominant upper motor neuron pathology) and seven control subjects. Recordings were made from force contractions of 20 and 50 % of maximum voluntary contraction (MVC). All control subjects were between the ages of 40 and 70 years and were examined by a practicing physiatrist for exclusion criteria including neuromuscular disorders or any medications that might affect muscle activity.

We observed differences in initial firing rates and variability of active motor units between control subjects and ALS patients. Furthermore we observed differences in firing rates and variability of active motor units between ALS patients with predominant upper motor neuron pathology and ALS patients with predominant lower motor neuron pathol-

ogy. Initial motor unit firing rates for control subjects were 16.22 $\pm$ 2.06 Hz at 20% MVC and 19.79 $\pm$ 1.66 Hz at 50% MVC. As expected, initial motor unit firing rates from patients with predominant lower motor neuron pathology were higher than those of control subjects; 18.87 $\pm$ 4.73 Hz at 20% MVC and 24.28 $\pm$ 5.01 Hz at 50% MVC. ALS patients with predominant upper motor neuron pathology, as expected, had initial motor unit firing rates that were lower than those observed in control subjects; 9.22 $\pm$ 1.68 Hz at 20% MVC and 12.83 $\pm$ 2.26 Hz at 50% MVC. Motor unit firing rate time series in ALS patients with predominant upper motor neuron pathology showed decreased variability, 0.99 $\pm$ 0.17 Hz at 20% MVC and 1.70 $\pm$ 0.52 Hz at 50% MVC, when compared to control subjects, 2.37$\pm$0.67 at 20% MVC and 4.20$\pm$ 1.00 at 50% MVC. Variability of motor unit firing rate time series in ALS patients with predominant lower motor neuron were high, 3.38 $\pm$ 1.2 Hz at 20% MVC and 4.07 $\pm$ 1.56 Hz at 50% MVC, compared to control subjects. At 50% MVC, motor unit substitution was observed in ALS patients with predominant upper motor neuron pathology despite the contractions lasting just a few seconds. Motor unit action potentials (MUAPs) recorded from patients were polyphasic when compared to those from control subjects, as is characteristically found in practice.

Acknowledgments

I am truly grateful to all my thesis committee members and I cannot possibly thank you enough. I extend my sincere appreciation to Dr. Edward Clancy, my super thesis advisor, for encouragement, knowledge shared and the patience reading through this manuscript several times. You have always provided feedback that has helped me advance. Dr. Lisa Krivickas, it is always a pleasure learning from you and thank you for sharing your wealth of knowledge on neurophysiology and neuropathies. Thank you once again for reading through this manuscript and all the suggestions you have provided. Many many thanks go to Dr. Paolo Bonato for your enthusiasm, novelty, dedication and broad knowledge. This in conjunction with the broad number of projects we are exposed to in the Motion Analysis Laboratory have had a profound impact on my view of research.

I would like to express my thanks to others who have, in different ways, contributed to this work: Dr. Gary Kamen, Mel Meister, Dr. Effie Chew and Todd Hester. Rita Brugalores thank you for you help in analyzing data.

Funding for this project was provided by the Harvard NeuroDiscovery Center.

Finally I would like to thank my family, especially my grandparents for raising me since I was a child, and friends for all the support.

Contents

1 Introduction **8**

1.1 Preface 8

1.2 Objective 8

1.2.1 Neurophysiologic Measures 9

1.3 Hypotheses 9

1.3.1 Specific Goals 10

1.4 Study Contribution 10

2 Motor Neuron Diseases **11**

2.1 Introduction 11

2.2 Amyotrophic Lateral Syndrome (ALS) 11

3 Physiology of EMG **14**

3.1 Introduction 14

3.2 History 15

3.3 Anatomy And Physiology Of The Motor Unit 16

3.3.1 Muscle Fibres 17

3.3.2 Sarcolemma 18

3.3.3 Action Potential 18

3.3.4 Motor Unit 21
3.3.5 Motor Unit Recruitment 22
3.3.6 Action Potential Analysis 23
3.3.7 Conduction Velocity 23
3.3.8 Muscle fiber conduction velocity 24

4 EMG Signal Detection and Acquisition 26
4.1 Introduction 26
4.2 Indwelling Electrodes 27
4.3 Conditioning and Amplifying the EMG Signal 28
4.3.1 Common Mode Rejection Ratio (CMRR) 28
4.3.2 Input Impedance 29
4.3.3 Slew Rate 29
4.3.4 Distance from Signal Source 29
4.3.5 Filtering 29
4.4 Sampling 30
4.4.1 Quantization 30

5 Decomposition of EMG Signals 32
5.1 Introduction 32
5.2 Pre-processing 33
5.3 Detection/Segmentation 34
5.4 Classification 34
5.5 Superposition resolution 35
5.6 Existing EMG Decomposition Tools 37

6 Methods & Procedures 39
6.1 Subject Recruitment 39
6.2 Instrumentation 40

6.3 Experimental Protocol 43
6.4 Data Analysis 46
6.4.1 Decomposition 46
6.4.2 Motor Unit Firing Rate Time Series 50

7 Results **56**

8 Discussion **69**

9 Conclusion and Future Work **73**
9.0.3 Conlusion 73
9.0.4 Future Work 74

A Development of Data Acquisition System **75**
A.0.5 Hardware Development 75
A.0.6 Software Development 77

B Interactive Multi-Channel EMG Decomposition Tool **78**
B.1 Introduction 78
B.2 Multichannel EMG Decomposition Tool Box 78
B.3 Loading Data 82
B.4 Choosing the repetition 82
B.5 Choosing the time frame 83
B.6 Preprocessing data 84
B.7 Setting the thresholds (Detection) 85
B.8 Extracting Templates 87
B.9 Classification 91
B.10 Super position Resolution 92
B.11 View Firing Rates 95
B.12 Conclusion 96

C Stochastic Processes **98**

C.1 Stationary Stochastic Processes 98

C.1.1 Ergodic Stochastic Processes 99

C.2 Analytic methods 100

C.2.1 Digital Filtering 100

C.2.2 Autocorrelation Function Estimation 102

C.2.3 Spectral Density Functions 103

C.2.4 Coherence 109

C.3 Entropy 110

C.3.1 Introduction 110

C.3.2 Sample Entropy 110

C.4 Synchrony 112

C.4.1 Phase Synchrony Based on The Hilbert Transform 112

C.4.2 Hilbert Transform 113

Bibliography 115

Chapter 1

Introduction

1.1 Preface

This manuscript details a multi-disciplinary approach towards scientific research by combining engineering techniques and neurophysiology as way to learn more about motor neuron diseases. The first part (chapters 2 through 3) provides an overview of neurophysiology and electromyography. The second part (chapter 4 and beyond) gives an engineering (signal processing) background, principles upon which the practical aspects of this project are based, and results.

1.2 Objective

The goal of this project is to assess the behavior of motor unit discharge rate (MUDR) in patients with amyotrophic lateral sclerosis (ALS) as compared to a control population. ALS is a progressive degenerative disorder of both the upper and lower motor neurons. Several clinical trials have been carried out as a way of identifying drugs that will slow the progression of ALS [DeCarvalho et al 2005]. Critically important in clinical trial design is the selection of the most appropriate outcome measures and these have included functional scales as well as neurophysiologic measures. In order to detect small changes

in the rate of disease progression, multiple outcome measures are normally used. Neurophysiologic (and Revised ALS Function Rating Scale) outcome measures have been reported to be the best available [DeCarvalho et al 2005].

1.2.1 Neurophysiologic Measures

The neurophysiologic measures that have been utilized to date are: (1) Compound motor action potential (CMAP) amplitude, (2) Motor unit number estimate (MUNE), and (3) Neurophysiologic index (derived from motor nerve conduction study parameters). Both the CMAP amplitude and MUNE decline simultaneously over time in ALS [Shefner et al 2004]. All of the neurophysiologic measures mentioned above relate to the number of remaining motor units, however they do not assess the firing characteristics of the motor units. Since functional impairment in ALS is caused by muscle weakness (i.e. inability to generate force), and given that in addition to motor unit number, firing rate influences muscle force generation, it is therefore essential to characterize the motor unit firing rate (in addition to motor unit number) in order to further understand the etiology of weakness in ALS.

1.3 Hypotheses

We hypothesize that the MUDR is abnormal in patients with ALS when compared to their age matched control subjects. We further hypothesize that that the observed abnormalities in patients are a function of the relative degree of upper motor neuron (UMN) and lower motor neuron (LMN) pathology, variability in ALS patients is abnormal when compared to their age matched control subjects, ALS patients with predominant lower motor neuron pathology will have increased variability in motor unit firing rates, and that ALS patients with predominant upper motor neuron pathology will have decreased variability.

1.3.1 Specific Goals

Our specific goal is to characterize MUDR in patients with ALS and compare these rates with those from healthy control subjects. We hypothesize that ALS patients (1) with predominant lower motor neuron pathology will have increased MUDR and increased MUDR variability; (2) with predominant upper motor neuron pathology will have decreased MUDR and decreased MUDR variability.

1.4 Study Contribution

To date, no studies of MUDR in ALS have been published. By characterizing MUDR in patients with ALS, we hypothesize that it is possible to track motor unit behavior longitudinally. This capability may be useful in assessing rate of disease progression and as an outcome measure in clinical trials. As an initial study, we have collected MUDR measurements as well as muscle force, and CMAP amplitude measurements from the first dorsal interosseous (FDI) muscle in 6 patients with ALS. In addition, we have also collected the same information from eight control subjects with no known form of motor neuron disorder. This study will allow us to learn more about motor unit dysfunction in people with ALS and other motor neuron disorders. Further understanding of motor unit behavior in this population may contribute to better clinical trial design in the future because of the potential use of these variables as outcome measures.

Chapter 2

Motor Neuron Diseases

2.1 Introduction

Motor neuron diseases (MNDs) are a group of disorders of the nervous system responsible for the progressive degeneration of motor neurons [Preston 2004]. MNDs are subdivided into three clinical subtypes:(1) primary lateral sclerosis (PLS), which affects upper motor neurons (motor neurons within the brain); (2) primary muscular atrophy (PMA), which affects lower motor neurons (motor neurons that originate from the spinal cord and terminate at the muscles of the body); (3) classic ALS which affects both the upper and lower motor neurons. Spasticity and exaggerated reflexes indicate damage to the upper motor neurons. A progressive wasting (atrophy), fasciculations and weakness of muscles that have lost their nerve supply indicate damage to the lower motor neurons [Leigh and Swash 1995]. The purpose of this chapter is to give a general idea of the classic ALS pathology. In this document, the term ALS will refer to classic ALS.

2.2 Amyotrophic Lateral Syndrome (ALS)

First identified in 1874 by the French physician Jean Martin Charcot [Leigh and Swash 1995], ALS is the most common variant of motor neuron diseases [Preston 2004]. ALS is a pro-

gressive neurodegenerative disorder that affects both the upper and lower motor neurons. ALS is also known as Lou Gehrig's disease (after Lou Gehrig, a famous baseball player who was diagnosed with ALS in 1939). ALS can occur among young individuals, but it most commonly affects people between the ages of 40 - 70, with a slight male predominance. It can be difficult to diagnose in the early stages because its symptoms may mimic other disorders. However, there are clinical signs that can be indicative of a wasting of either the upper or lower motor neurons. A lower motor neuron lesion is characterized by muscle atrophy, weakness, fasciculations and cramps. An upper motor neuron lesion can manifest as stiffness, spasticity, weakness, pathologic hyperreflexia, and Babinski responses. Currently, 30,000 Americans have the disease with over 5,600 people in the United States being newly diagnosed with ALS each year. Five to ten percent of people with ALS have a hereditary form of the disease whereas 90 to 95 percent of ALS is sporadic. In the past, a high incidence of ALS was observed in the Western Pacific (Guam, Kii Peninsula of Japan, Papua New Guinea) [Leigh and Swash 1995]. It is believed that the high incidence rate was tied to specific dietary toxins (amino acids found in seeds of casin). During the last few years, a dramatic decline in ALS incidence in the Western pacific region has been observed. Investigators are attributing this decline mainly to a change in diet (replacement of traditional foods with western due to introduction of western foods). ALS is not contagious. Over time, as the disorder progresses, ALS robs those affected of most physical activity. It destroys motor neurons that are vital in the functioning of the nervous system, and through which the brain controls voluntary muscles in the body. As a result, leg and foot muscles (controlled by motor neurons in the lower spinal cord), arm, hand and finger muscles (controlled by motor neurons in the upper spinal cord), speaking, swallowing and chewing (controlled by motor neurons in the brain stem) are progressively affected. ALS symptoms, and the order in which they occur, vary from person to person. The rate of muscle wasting varies significantly from person to person. Some patients have long periods with very slow degeneration. Life

expectancy of newly diagnosed people is roughly three to five years. Twenty percent of patients diagnosed with ALS live more than five years, and 10% live more than 10 years [Leigh and Swash 1995]. Over time, ALS may spread throughout the body and may affect muscles required for breathing. However, ALS does not affect the senses of sight, hearing, taste, smell and touch. It also does not affect the mind, eye muscles, and the heart. Principal features of ALS disease at a microscopic level include: loss of large motor neurons, cytoplasmic inclusions, proximal and distal axonopathy with axonal spheroids, degeneration of motor nerve fibers, and tract degenerations. To date, despite years of research, the cause of ALS has not been determined, making the search for a cure very difficult [Leigh and Swash 1995].

Chapter 3

Physiology of EMG

3.1 Introduction

Electromyography (EMG) is the investigation of muscle activity through electrical signals from muscles. For the purposes of this document, we will restrict ourselves to skeletal muscles. Electromyography is subdivided into two kinds: clinical (diagnostic) and kinesiological. Clinical EMG focuses on characterizing motor unit action potentials during muscle contraction. A motor unit is a single alpha motor neuron and the muscles fibers it activates. A more detailed description of a motor unit is given in subsection 3.3.4. Clinical electromyography is carried out to help diagnose neuromuscular disorders, while kinesiological EMG mostly deals with human movement analysis. Kinesiological EMG investigates the relationship of muscular function to movement of the body segments and evaluates timing of muscle activity with regard to the movements. Recording of EMG signals can be achieved by placing electrodes on the surface of the skin (surface EMG) or fine wire or needle electrodes which are inserted deep in the muscle (indwelling EMG). When recording from deep within the muscle, a needle or fine wire electrode is inserted into the muscle (approximately 0.25-0.5 cm deep). An advantage of indwelling EMG is its selectivity which strongly attenuates cross talk (a phenomenon in which action potentials from muscles further away also contribute to the recording through volume conduction

contributing to the recorded EMG signal), and can be used when targeting small muscles. In this document, EMG shall refer to clinical EMG signals recorded within the muscle (indwelling).

3.2 History

The study of EMG originated from the discovery of the role that electricity plays in the nervous system of animals. The first written documents on biolelectric events, which describes the catfish as a fish that ”releases troops” due to the electric shocks it generated, can be found in the ancient Egyptian hieroglyph of 4000 B.C. [Malmivuo]. Francesco Redi, in the mid 1600’s, documented that a highly specialized muscle was the source of an electric ray fish’s energy. Direct observation of the relationship between muscles and electricity was performed in dissected frogs, by Luigi Galvani (1791- 1797) [Malmivuo]. Galvani’s results enticed Alessandro Volta to develop the Voltaic pile, the earliest known electric battery. He then used it to study animal electricity (such as electric eels) and the physiological responses to applied direct-current voltages. Also, following Galvani’s work, Carlo Matteucci demonstrated that cell membranes had a voltage across them and could produce direct current. German physiologist Emil du Bois-Reymond, who was inspired by Matteucci’s work, went on to discover the action potential in 1848. The conduction velocity of action potentials was first measured in 1850 by du Bois-Reymond’s friend, Hermann von Helmholtz. In 1880, Wollaston hypothesized that a sound is generated during muscle contraction. Due to limitations technologically, he proved his theory by comparing the frequency of muscle sounds to distant carriages moving along cobblestone roads. A carriage was driven at various speeds until the noise frequency generated from the carriage matched that of contracting muscle that Wollaston heard through his thumbs. By knowing the size of cobblestones and the diameter of the carriage wheels, Wollaston estimated the sound generated by muscles to be approximately 25 Hz. In this

way, he demonstrated that energy generated by muscles was in a range that is audible [Yamamoto and Takano 1994]. To establish that nervous tissue was made up of discrete cells, the Spanish physician Santiago Ramn y Cajal and his students used a stain developed by Camillo Golgi to reveal the myriad shapes of neurons. For their discoveries, Golgi and Ramn y Cajal were awarded the 1906 Nobel Prize in Physiology. EMG signals were first displayed on an oscilloscope in the 1920's. This advance intellectually stimulated researchers to further investigate the anatomy and physiology of skeletal muscles. As a result, investigators such as Basmajian have been able to demonstrate a deeper comprehension of EMG and its application. This knowledge has increased the curiosity among several investigators in the field of electromyography.

3.3 Anatomy And Physiology Of The Motor Unit

Figure 3.1 shows the organization of skeletal muscles. They are covered by a layer of connective tissue called epimysium. The epimysium protects muscles from friction against other muscles and bones. Fascia, a connective tissue outside the epimysium, surrounds and separates different muscles. Portions of the epimysium project inward to divide the muscle into compartments. Each compartment contains a bundle of muscle fibers. Each bundle of muscle fibers is called a fascicle and is surrounded

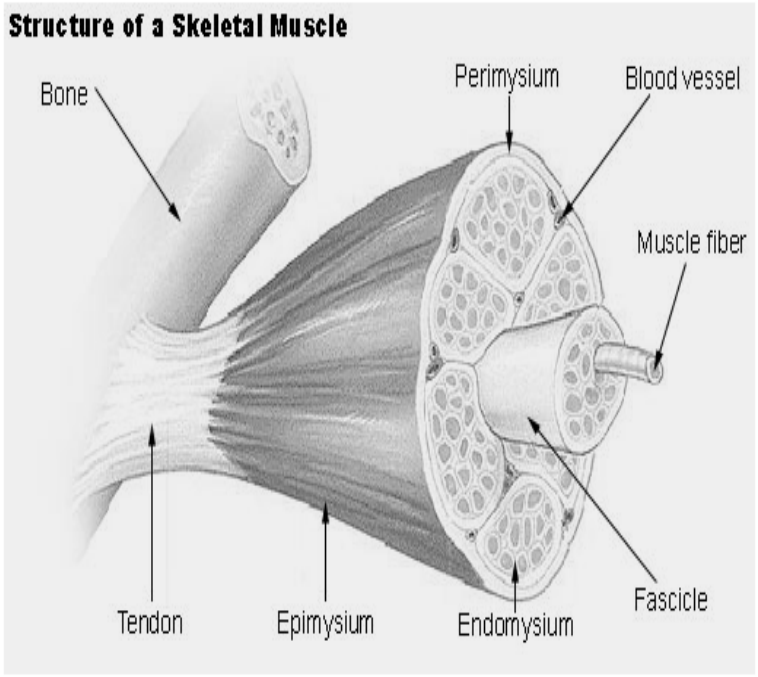

Figure 3.1: Shows organization of muscles structure [Young]

by a layer of connective tissue called the perimysium. Within the fascicle, each individual muscle cell, called a muscle fiber, is surrounded by connective tissue called the endomysium. Skeletal muscles are composed of up to 2,000,000 muscle fibers. The majority of muscles fibers have diameters ranging from approximately 20 micrometers to greater than 100 micrometers [Guyton]. Each muscle fiber is composed of smaller subunits known as myofibrils. It is the nerve endings that are responsible for activating muscle fibers.

3.3.1 Muscle Fibres

Skeletal muscle is made up of thousands of cylindrical muscle fibers most often running all the way from origin to insertion. The fibers are bound together by connective tissue through which run blood vessels and nerves. Muscle fibers have an elongated cylindrical shape. The nuclei of these muscle cells are located in the peripheral part of the cell. The cell is densely packed with contractile proteins, energy stores and signaling mechanisms. A single muscle fiber that is 100μm in diameter and 1 cm long contains approximately 8000 myofibrils. In turn, each myofibril has some 4500 sacromeres, 16 billion thick

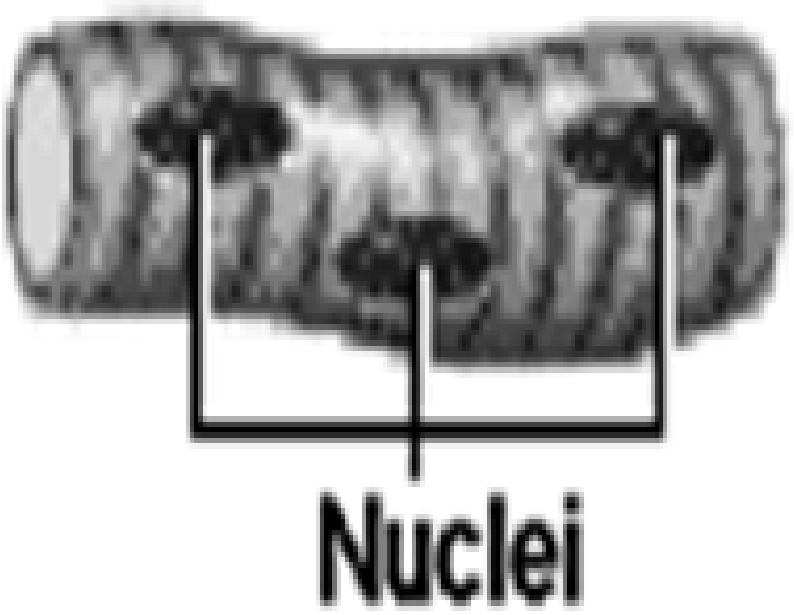

Figure 3.2: Muscle fiber, an elongated cylindrical shape with multiple nuclei (picture adapted from [Young])

filaments and 64 billion thin filaments [Krivickas 2008].

3.3.2 Sarcolemma

The cell membrane of the muscle fiber is called the sarcolemma. It is composed of cell membranes called the plasma membrane. The outer coating of the sarcolemma is made up of a thin layer of polysaccharide material that contains several thin collagen fibrils. At the end of each muscle fiber, the surface layer of sarcolemma fuses with the tendon fiber and the tendon fibers in turn group to form muscle tendons which insert into bones.

3.3.3 Action Potential

The fundamental function of a peripheral nerve is to transmit information from anterior horn cells, in the spinal cord, to muscles for the motor system and from sensory receptors to the spinal cord for the sensory system. Nerves are much like electrical wires in terms of how they function. They serve as a conduit through which an electrochemical signal propagates. In most regions of the body, positive and negative charges (i.e., ions) are maintained such that overall charge is equalized (principle of electrical neutrality).

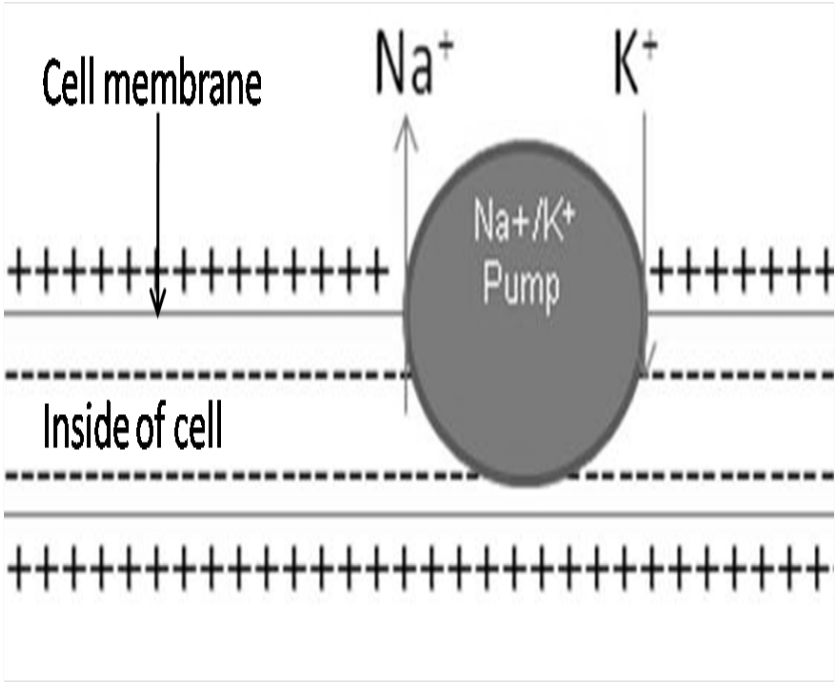

Figure 3.3: Resting membrane potential. At rest the membrane is negatively polarized on the inside relative to the outside.

When soduim ions (Na^+) are pumped to the outside of the membrane, lining up along the outside of the membrane and in turn K^+ ions pumped inside the cell membrane, there

is a higher concentration of positive charge on the outside of the cell when compared to that on the inside of the cell. This causes the inside of the cell membrane to be negatively charged. This action creates a dipole layer of positive and negative charges, as shown in Figure 3.3. This arrangement is similar to an electrical capacitor and is known as the resting potential of nerves (-90mV). The membrane is said to be polarized. Therefore axonal membranes of all nerves have a charge due to this maintainance of sodium (Na^+) ions and potassium (K^+) ions across the membrane.

A typical action potential is initiated when the membrane is depolarized. When depolarization occurs, the membrane suddenly becomes permeable to sodium ions allowing tremendous numbers of positively charged sodium ions to flow to the interior of the axon (axons become more positive internally), increasing voltage. Once the voltage increases past a critical threshold, typically 15 mV higher than the resting value, the sodium current dominates and a runaway condition results; the cell "fires," producing an action potential. Once initiated, the action potential hops (in axons with a myelin sheath) down the axon. Action potentials hop because myelin is an insulating sheath formed by Schwann cells that surround vertebrate peripheral neurons only leaving some areas exposed, see Figure 3.5. It is at the exposed areas with very high densities of sodium channels (nodes of Ranvier) that action potentials hop without

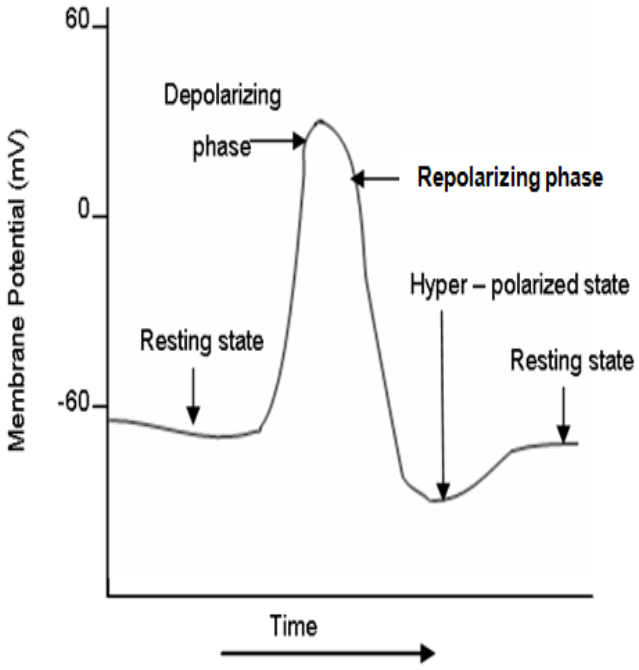

Figure 3.4: Action potential. When depolarization takes place, sodium channels open causing an influx of Na^+ The action potential is momentary because Na^+ channels are blocked within a millisecond thereby increasing K^+ conductance.

involving the intermediate axon.

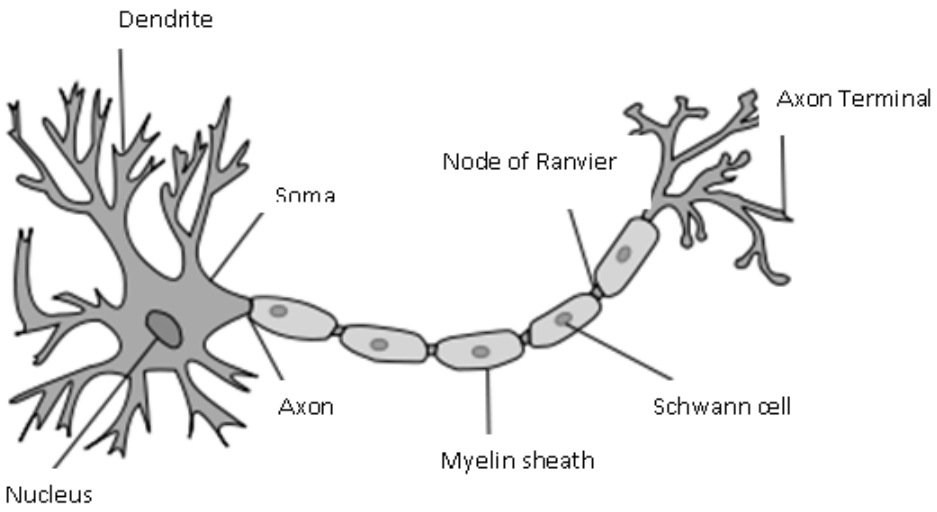

Figure 3.5: Showing structure of a neuron [Young].

Propagation of action potentials as described above is known as saltatory conduction. Action potentials that do reach the ends of the axon generally cause the release of a neurotransmitter into the synapse, which may combine with other inputs to provoke a new action potential in the post-synaptic neuron or muscle cell. As the potential rapidly rises positively, the membrane voltage overshoots beyond zero volts as shown in Figure 3.4.

3.3.4 Motor Unit

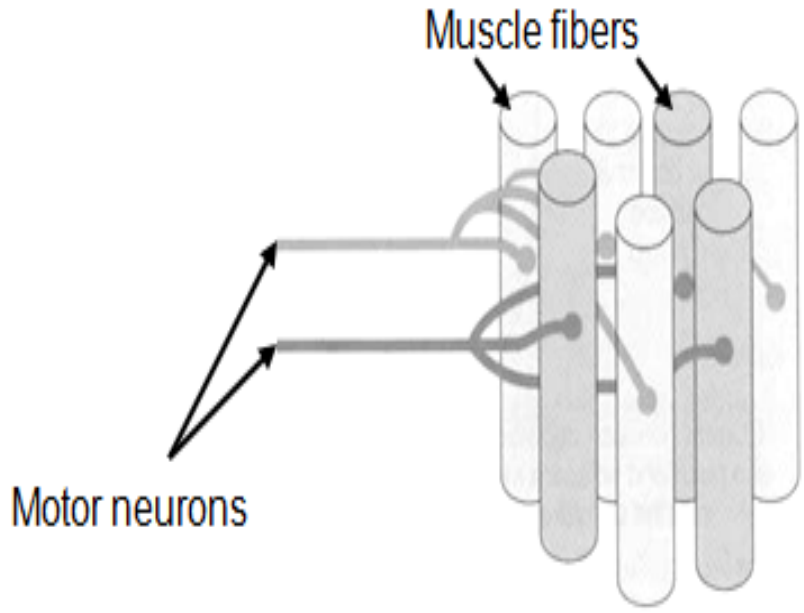

Figure 3.6: Two different motor units. The light shade motor neuron innervates light shade muscle fibers and the dark motor neuron innervates the dark muscle fibers to which it is attached [Young].

A motor unit (MU) is the basic component of the peripheral nervous system. An MU is comprised of a single alpha motor neuron and all the muscle fibers it innervates (activates). An alpha motor neuron is a lower motor neuron of the brainstem and spinal cord. It innervates extrafusal muscle fibers of the skeletal muscle. It is also responsible for initiating muscle contraction. Large muscles (low fine control demands) such as quadriceps muscles, are organized into larger motor units and may have as many as 2000 fibers per motor unit. On the contrary, muscles for controlling high precision movements like those required in the fingers or the eyes are organized into smaller motor units with typically few (roughly 10) fibers per motor unit. Groups of motor units can function together to coordinate contractions of a single muscle. All motor units active in a muscle are known as a motor unit pool. The size of a motor unit (i.e. the number of muscle fibers) varies considerably according to the muscle's function. The motor neuron branches into many terminals, and each terminal innervates a specific muscle fiber. The motor unit is the brain's smallest functional unit of force development control; for example, if a motor unit comprising 1000 muscle fibers is stimulated, then all 1000 of those fibers will contract at the same time. The brain cannot stimulate individual muscle fibers one at a time. The territory of a motor unit ranges between 5 - 10

mm in adults.

3.3.5 Motor Unit Recruitment

The central nervous system (CNS) combines two control mechanisms to regulate the force a single muscle produces. The first is recruitment and the second is rate coding. Progressive activation of muscle fibers by successive recruitment of motor units to achieve increased intensity of muscle contraction is known as motor unit recruitment. During a muscle contraction, small motor units (slow conduction velocity/fewest fibers) are excited first and as the strength of muscle contraction increases, larger motor and larger units (fast conduction velocity/most fibers) are recruited last. As a result, the number of motor units recruited increases. This process is known as ”Henneman’s Size Principle.” The size principle is important because it allows gradual increase of muscle force during weak contractions whereas changes are larger when large force is desired. Small motor units are fatigue resistant and they provide fine control for most activities. On the other hand, big units fatigue easily and are only used occasionally in instances such as running when fine control is not required. Muscle fibers belonging to one motor unit overlap spatially other motor units in micro bundles of three to fifteen muscle fibers. Therefore, separate motor units contract in support of one another due to this interdigitation [Guyton]. The activation of one motor neuron will result in a weak but distributed muscle contraction. The activation of more motor neurons will result in more muscle fibers being activated, and therefore a stronger muscle contraction. It is important to note that different motor units are driven asynchronously by the spinal cord so that contraction alternates among motor units one after another and as a result a smooth contraction is provided even at low frequencies [Guyton]. Note that MU firing produces a short mechanical twitch about 4 ms in duration. Subsequent firing is continuously required in order to sustain a contraction.

3.3.6 Action Potential Analysis

MUAPs recorded from needle EMG represent the extracellular compound potential of the muscle fibers of a motor unit. The recorded signal is heavily weighted towards the fibers nearest to the needle. The amplitude decreases as the distance between needle and membrane increases. MUAPs are classified as normal or pathological based on morphology, polyphasia and amplitude (as well as other measures). Polyphasia is a measure of synchrony within a MU - that is the extent to which the muscle fibers within a motor unit fire at the same time. The number of phases is defined as the number of baseline crossings of the MUAP plus one. Normally, MUAPs have two to four phases. Therefore MUAPs that have significantly more than four phases indicate either a nerve or a muscle that is not healthy. Highly polyphasic/complex motor action potentials that are small in amplitude usually indicate that a muscle is pathologic whereas an action potential that is large in amplitude and polyphasic is indicative of a reinnervated nerve fiber (due to injury or motor neuron disease) that is pathologic. Serrations are similar to polyphasia with the exeption that phases observed do not cross the baseline, see Figure 3.7. When the muscle loses nerve supply (denervation) due to a disease or injury, atrophy begins. After denervation, muscle fibers are often reinnervated by collateral sprouts from adjacent intact motor nerves. The newly formed sprouts are thinly myelinated and therefore exhibit slow conduction. Because of this slowness, reinnervated muscle fibers are seen as time-locked satellite potentials that trail the main MUAP. Over time the sprout matures increasing its thickness of myelin and hence conduction velocity. The satellite potential then fires closer to the main and ultimately becomes an additional phase or serration.

3.3.7 Conduction Velocity

The action potential propagates as a wave along the axon. Conduction velocity is therefore the measure of the conducting speed, computed as the distance travelled divided by

the conduction time taken. Conduction velocity in nerve fibers ranges from 0.25 m/s in extremely small unmyelinated fibers to 100 m/s in very large myelinated fibers [Guyton]. Velocity increases roughly by the square of fiber diameter in unmyelinated fibers where as with myelinated fibers it increases roughly by fiber diameter. Some diseases such as Guillain Barre Syndrome degrade myelin and slow conduction velocity of action potentials [Purves et al].

3.3.8 Muscle fiber conduction velocity

Muscle fiber conduction velocity (MFCV) is the speed at which a depolarization wave travels along the muscle fiber membrane (sarcolemma). Depolarization waves travel at speeds ranging from 3 m/s to 5 m/s. The depolarization of the muscle fiber membrane is one of the steps in the sequence that ultimately causes the muscle fibers to contract. The speed of depolarization of MFCV has important influences on the aspect of the M-wave as well as on the shape of the MUAP. Direct measurement of the MFCV is not a standard technique in clinical EMG, and is only sparsely used for research purposes [Hoeven].

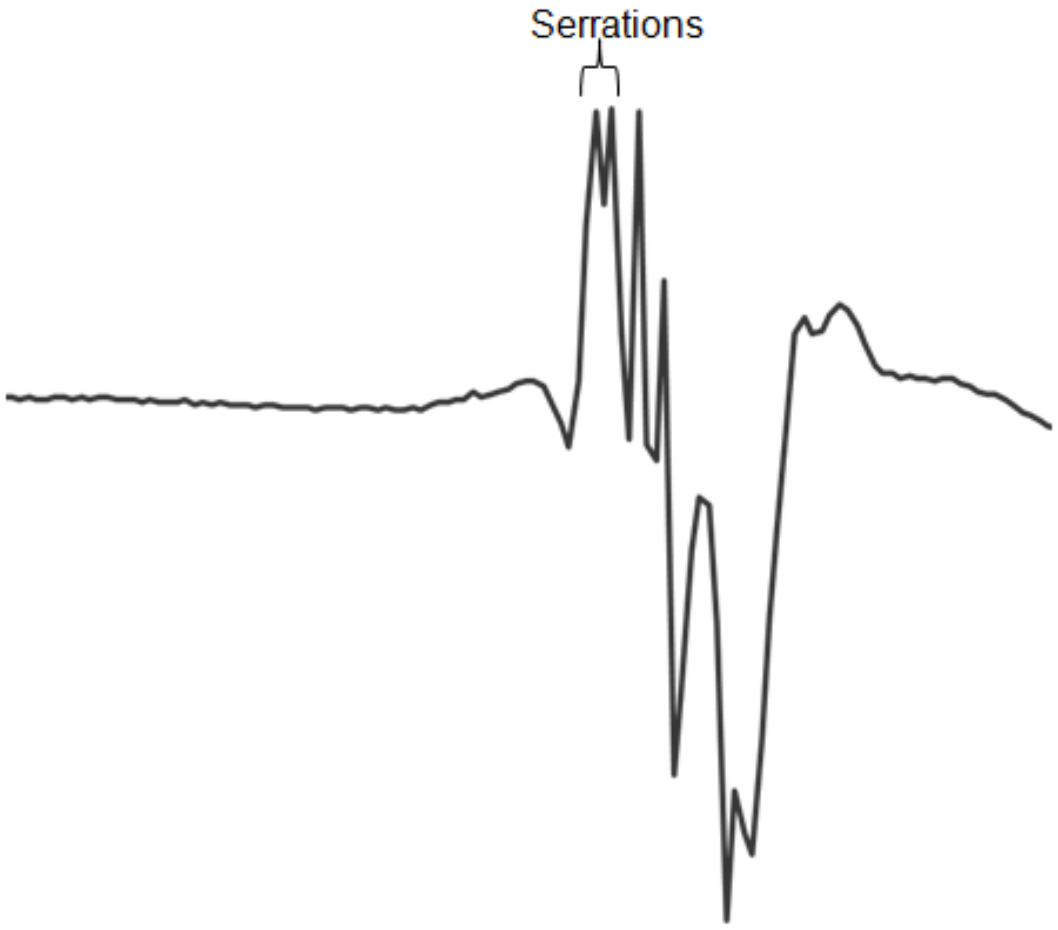

Figure 3.7: Polyphasic MUAP

Chapter 4

EMG Signal Detection and Acquisition

4.1 Introduction

Methods used to acquire data are heavily dependent on the nature of signals to be acquired. EMG signals are complex signals, controlled by the nervous system and are dependent on the anatomical and physiological properties of muscles. Also, it is important to realize that just like any other signals in transit, the EMG signal gets contaminated with undesirable signals (noise) as it traverses from its source to the recording apparatus, making it very difficult to detect. Fortunately, there are techniques that can be used to minimize noise embedded in signals. One such technique is through the process of differential amplification. As a result, the recording of small signals buried in larger common signals is possible. Employing similar techniques, small EMG signals can reliably (high signal to noise ratio) be detected and recorded. Care should be taken when selecting electrodes and type of amplifiers. Electrode and internal amplifier noise may distort the recording of the EMG signal. Filtering is normally performed so that unwanted signals such as low frequency motion artifacts are removed from the EMG signal.

4.2 Indwelling Electrodes

The most common indwelling electrodes used to record EMG are monopolar and concentric needle electrodes. In addition there are other EMG recording techniques based on special needle electrode configurations, namely: single-fiber EMG, macro EMG and quadrifilar needle electrode. Figure 4.1 illustrates some of these EMG needle types.

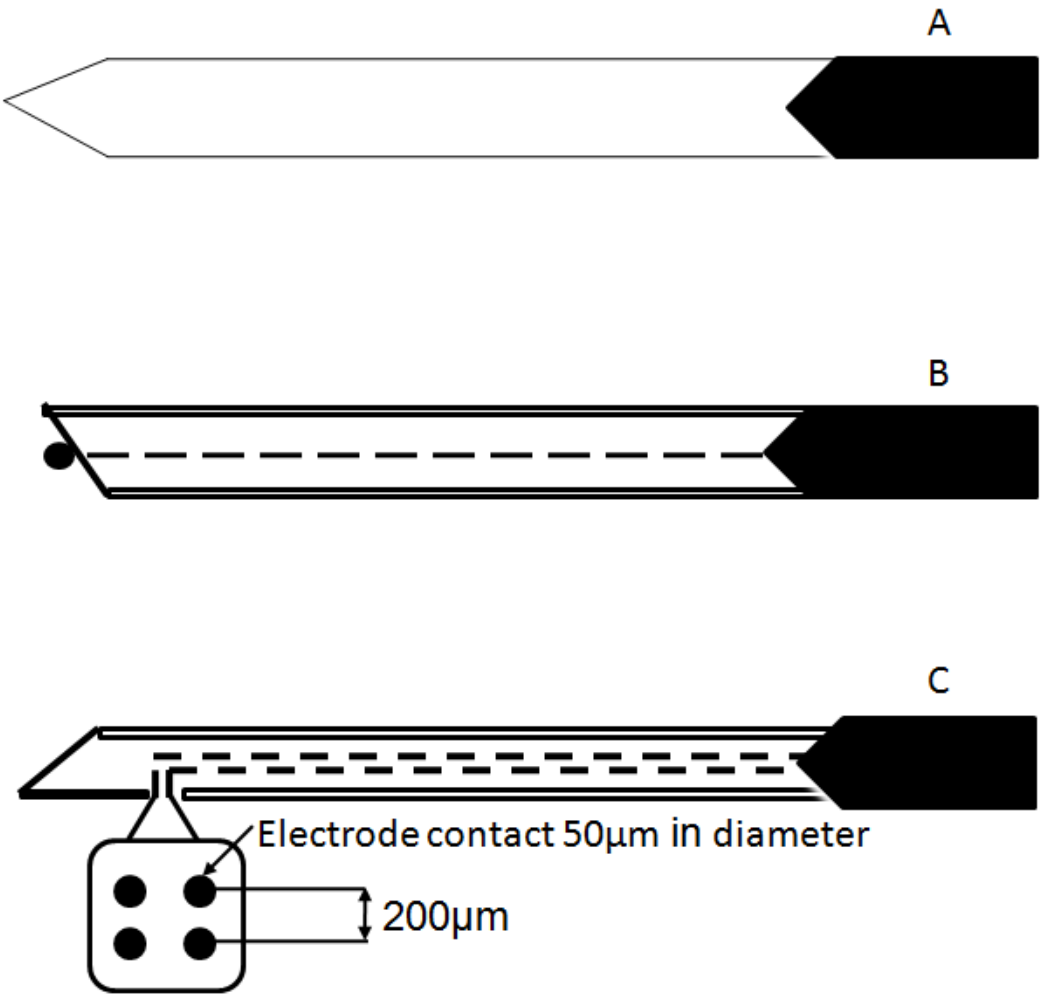

Figure 4.1: Different indwelling needle electrode types. A) In the monopolar design, the needle is Teflon coated and its exposed tip serves as the active electrode. B) The concentric needle has an active electrode running as a thin wire through the needle center and exposed at the tip. The cannula serves as reference. C) The quadrifilar needle electrode is 25-gauge stainless steel. The needle electrode was custom designed with four 50- μm platinum wire electrodes equably exposed on the side port of the cannula

4.3 Conditioning and Amplifying the EMG Signal

Electrical activity of the muscle is usually of very low voltage (generally less than 5-10mV). It is therefore essential to amplify the detected EMG signal so that the signal can be sampled reliably by typical analog to digital converters. Boosting a signal's gain is achieved by using an amplifier. The most practical way of amplifying EMG signals is by using an instrumentation amplifier. The differential input, single-ended output instrumentation amplifier is one of the most useful signal processing amplifiers. It is used for precision amplification of differential dc or ac signals while rejecting large values of common mode interference. It is essential that the EMG signal is amplified without distortion. Ideally, the EMG amplifying circuit should possess the following characteristics;

- High common mode rejection ratio
- High slew rate/bandwidth
- Very high input impedance
- Short distance to the signal source

4.3.1 Common Mode Rejection Ratio (CMRR)

Differential amplifiers have a characteristic of detecting potential differences between recording electrodes and as a result cancel out interfering signals (noise) that are common to the electrode pair, such as power line interference. This is especially true if indeed noise signals get to the recording electrodes with equal amplitudes and without phase shift. The differential amplifier is not able to completely cancel out interfering signals, but the differential mode gain is much bigger than the common mode gain. For EMG, the recommended common mode gain (CMRR) should be at least 95 dB as per ISEK (International Society of Electrophysiology and Kinesiology) specifications [Konrad 2005].

4.3.2 Input Impedance

The input impedance of an EMG amplifier should be very high because EMG signals are of very low power. The higher the input impedance, the lower the input current required from the signal. EMG amplifier input impedance should be roughly as high as 10^9 Ohms [DeOliveira 2005].

4.3.3 Slew Rate

Slew of an amplifier is the rate at which voltage changes with time at any given point in a circuit. Slew rate depends on factors such as; the gain and the compensating capacitors. Limitations in slew rate capability can give rise to non linear effects in electronic amplifiers. Slew rate, usually expressed in units of V/μs, in conjunction with output amplitude limit the highest usable frequency of the amplifier.

4.3.4 Distance from Signal Source

High input impedance can be a disadvantage if power line noise, RF (radio frequency) noise and/or movement artefacts are introduced in the lead wires due to capacitive coupling. With increased length of the leads, the parasitic capacitance increases and the resulting coupled noise is increased (low signal to noise ratio).

4.3.5 Filtering

Today, most EMG filtering is performed digitally, however analog filters are usually applied to the EMG signal during acquisition. The EMG signal passes through high and low pass filters (band filtered) to remove noise such as low frequency noise introduced by motion artifacts as well as high frequency noise. In addition, low pass filtering prevents aliasing. Low pass filters exclude signals above a set frequency whereas high pass filters eliminate

signals below a set frequency. Indwelling EMG signals are usually band filtered between 10 Hz (remove low frequency artifacts such as baseline wonder) and 10 kHz.

4.4 Sampling

Sampling is the conversion of continuous-time signals into discrete time signals by taking samples of the continuous-time signals at discrete instants. It is in most cases done at equally spaced time intervals. For example, if $x_a(t)$ is the analog signal, the sampled version of it is $x_a(nT) = x(n)$ where T is the sampling interval, see figure 4.2.

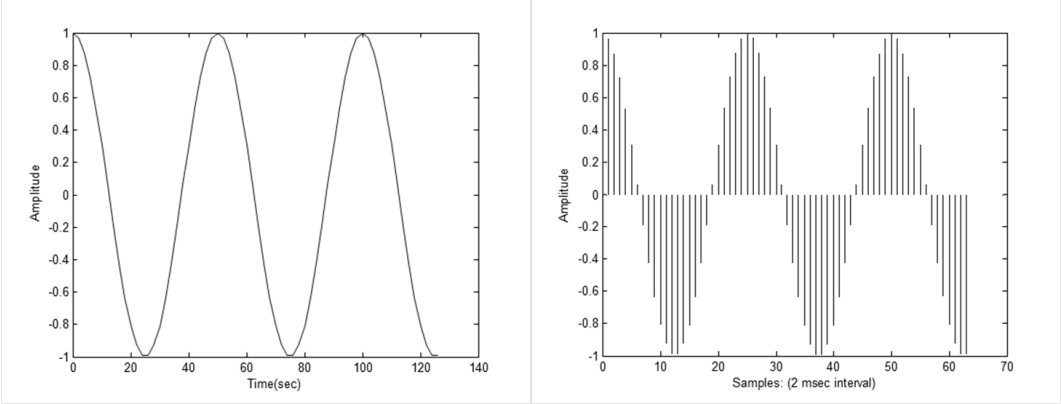

Figure 4.2: A: continuous time signal. B: Sampled version of signal A

It is important to select a proper sampling interval (sample at a rate fast enough) so that all characteristics of the continuous-time signal are captured. The minimum sampling rate should be greater than twice the maximum frequency (Nyquist rate) content of a given signal.

4.4.1 Quantization

Quantization is similar in concept to sampling except that quantization, is related to the amplitude of a signal. It describes steps used to represent the amplitude of a continuous signal in discrete form. The step size (resolution) depends on the arithmetic precision of

analog to digital converters. The digital signal values are known as quantization levels. The distance between the quantization levels is known as quantization steps (resolution). An analog to digital converter board with a resolution of 12 bits ($2^{12} - 1 = 4095$ intervals) with a signal's expected amplitude (after amplification) of $\pm$ 5 volts is sufficient for most kinesiological data acquisition. To achieve good amplitude resolution, very small signals should be amplified to fill the input range of the analog to digital converter.

Chapter 5

Decomposition of EMG Signals

5.1 Introduction

Quantitative analysis of high quality EMG signals recorded using needle electrodes can provide important information for clinical diagnosis of neuromuscular disorders as well as further scientific discovery. For certain purposes, a properly recorded EMG signal has to be fully broken down into its constituent (decomposed) motor unit action potential trains (MUAPTs), see Figure 5.1. A MUAPT is a set of action potentials that represent a given alpha neuron and the muscle fibers it innervates (motor unit). MUAPTs therefore can provide information regarding the way motor units behave during muscle contraction. This information may lead to the diagnosis of various neuromuscular disorders. Also it may give a better understanding of healthy and pathological systems. Assessing of motor unit action potentials (MUAPS) from EMG signals is classically carried out by having a neurologist observe waveforms displayed on an oscilloscope. As an additional aid, a speaker can be connected to the EMG recording channel so that the neurologist can listen to the EMG audio characteristics. In this way, experienced electrophysiologists are able to determine possible disorders in a fairly accurate manner. However, this technique may not suffice when it comes to detecting disorders that are not readily apparent. This technique is also inadequate for research purposes because it is not precise. Since computers have

become ubiquitous, the process of recording EMG and decomposition has been improved upon using personal computers. Today, EMG signals are decomposed into their individual MUAPTs using software routines based on mathematical algorithms, with manual correction/supervision. Despite the new developments, decomposition of an EMG signal is still a complicated undertaking and care must be taken when approaching this task. Some EMG signal characteristics vary depending on the type of electrode used. EMG signal decomposition techniques therefore have to be robust in order to accommodate various EMG signal characteristics. The classical EMG decomposition process is subdivided into four stages; pre-processing, detection, classification and resolution of superimposed waveforms.

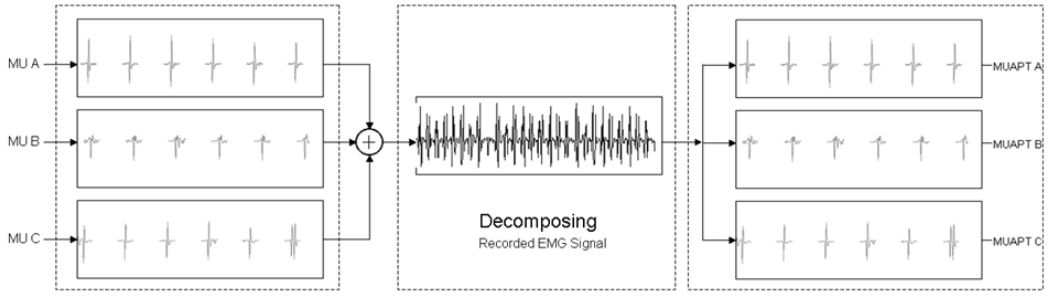

Figure 5.1: The left panel show waveform trains generated by individual MUs. They sum up and result in a complex EMG signal. It is this complex signal (shown in the midle panel) that can be acquired from the muscles and then, this signal is broken down into its contituent motor units as shown in the right hand panel.

5.2 Pre-processing

Preprocessing is necessary in the EMG decomposition process. Filtering may not be excessive during EMG data acquisition (as a precaution). As a result, additional filtering is done (digitally) off-line. In general, high-pass filtering (1000 Hz) and low-pass differentiators shorten the duration of MUAPs, thus reducing the probability of their temporal overlap and therefore reduce the number of superimposed waveforms. These filters also reduce

the amplitude of the many similarly-shaped MUAPs of different motor units that do not have fibers close to the electrode [Stashuk 2001b].

5.3 Detection/Segmentation

The second stage of EMG signal decomposition is the detection of all MUAPs above a set threshold amplitude. Some investigators have used a threshold of 1.5 times the root mean square (RMS) of the filtered EMG signal calculated over the first 1 second interval of the EMG signal [Stashuk 2001b]. This selection ensures that all low amplitude, low frequency MUAPs that would otherwise be extremely difficult to reliably classify are eliminated. There are methods that select variable length sections assumed to contain significant MUAP contributions that are relative to the largest signal components. Others, applied to the raw signal, use a combination of both slope and amplitude thresholds. One method of selecting segments that contain MUAPs that can be consistently correctly assigned is to consider the slope of the EMG signal in some cases pre-filtered through a low pass differentiator [Stashuk 2001b].

5.4 Classification

During the classification stage, action potentials that were detected are grouped into different classes (motor units). The most widely used method in identifying individual MUAPs from a composite EMG signal is known as template matching. Initially, templates are identified. Using action potential shape parameters, the EMG signal is scanned to find action potentials that match the available templates. Other techniques have been applied in order to classify motor units. For example, neural networks have been used to classify MUAPs. Hassoun et al [1994] used a trained neural network to classify individual MUAPs, and Gut and Moschytz [2000] modelled the EMG signal as an [M+1]-ary signaling system

with inter-symbol interference and used a sparse-sequence constrained Viterbi algorithm and MUAP shape and firing pattern information to obtain a maximum a posteriori probability based estimate of the sequences of the active motor units. Each of these algorithms uses the results of an initial clustering stage to assist in making supervised classification decisions [Stashuk 2001b]. One of the most important properties of a neural network is its learning ability. Neural networks are capable of learning patterns of an arbitrary nature, but also need a lot of training data. This property makes neural networks useful in cases where little prior knowledge of MUAPs is available. Difficulty in classification comes when two or more action potentials superimpose on one another. This is known as superposition and classification of such waveforms is described in the section below.

5.5 Superposition resolution

The latter problem is overcome by the superimposition resolution part of an EMG algorithm. Superimposition resolution is the resolving of superimposed MUAPs into their constituent MUAPs. Superimposing occurs because some motor units fire at (almost) the same time, which means that the detected potential is an algebraic sum of individual motor unit potentials from different motor units. Superimposed waveforms can be grouped into three different categories: partially superimposed, completely superimposed and destructively superimposed. In the first situation, the MUAPs overlap but with different peaks still visible. In the second condition, the peaks of individual MUAPs combine to make one large peak. In the third condition, MUAPs are superimposed in such a manner that their out-of-phase peaks are summed together, and end up canceling out one another. Resolving superimposed MUAPs is primarily based on two different methods. One of them is known as the peel-off or sequential approach. It is based on matching MUAPs, one at a time, with the superimposed waveform. Once a match is suitable, the MUAP is assumed to have contributed to the superposition and subtracted from it. The created residual

waveform is then used to search for other contributing MUAPs. MUAP contributions can be assumed to be correct after each subtraction or the final residual can be used to accept the combination of subtracted MUAPs [Stashuk 2001b]. There are a number of algorithms for resolving superimposed MUAPs based on the peel-off approach. These algorithms differ in how they align candidate templates with the superimposed waveform, the order in which they align and subtract templates and the thresholds used to accept suggested resolutions [Stashuk 2001b]. McGill [McGill 2005] implemented the 'peel-off' technique in his EMG decomposition toolbox, called EMGLAB. It resolves superpositions during template matching by identifying larger spikes and 'peeling them off' in order to reveal smaller spikes in the residual. Some superpositions that cannot be resolved during the automated phase are resolved manually. Jianjun Fang et al [1999] have devised a technique that is based on spectrum matching in the wavelet domain. This technique is sometimes considered to be more effective than the waveform matching technique in the time domain, especially when interference is induced by low-frequency baseline drift or by high-frequency noise. The spectrum matching technique in the wavelet domain does not need additional windowing like Fourier spectrum-matching techniques. In addition, the spectrum matching technique in the wavelet domain is immune to interfering white noise to which the Fourier transform is vulnerable, because it can be easily denoised with the soft-threshold method.

The second method of resolving superpositions is the modeling technique. It is based on synthesizing superimposed waveform models by adding up combinations of MUAPT templates with different relative time shifts. Model synthesis and comparison is repeated until an optimal or acceptable match is obtained between one of the model superimposed waveforms and the actual superimposed MUAP of time shifts considered for matching. Several modeling approaches have been reported. All of these techniques are similar in that they reduce the space required to be searched by first selecting a subset of possible contributing MUAPs, limit the number of assumed contributing MUAPs to 2 or 3, initially

align the MUAPs using either peak values or maximal correlation, and use optimization techniques to solve for the model parameters [Stashuk 2001a]. The peel-off approach is faster when compared to the modeling technique. It requires $2NM$ tests to resolve a superimposed MUAP whereas the modeling technique requires $N(N-1)M^2/2$, where N is the number of possibly contributing motor units and M is the number of time shifts considered for matching. On the other hand, the peel-off method is not efficient when superimposed waveforms exhibit destructive properties. Theoretically the modeling approach is capable of resolving all types of superimposed waveforms. Methods that combine the peel-off and modeling techniques have been developed in order to take advantage of each technique while curbing their undesirable properties. Loudon et al [1992], have implemented such techniques. Fully automated systems have not been developed. Most of these EMG decomposition techniques are based on a single channel. Multi-channel EMG recordings increase the probability of motor unit identification during strong muscle contraction [Fang 1999].

5.6 Existing EMG Decomposition Tools

There are number of techniques available for EMG decomposition. Recently, Kevin McGill [McGill 2005] has developed a freely-available, open source graphical EMG decomposition tool ('EMGLAB' developed in Matlab) and is working to implement EMG standards so that EMG data from multiple sources is readily available to all interested. This tool is primarily targeted towards single-channel EMG recording. LeFever and De Luca [LeFever and De Luca 1982] developed a multichannel decomposition (precision decomposition) technique based on template matching and firing time statistics. Stashuk and others [Stashuk 2001b] have developed an EMG signal decomposition system called DQEMG (decomposition-based quantitative EMG). DQEMG estimates MU firing rate pattern statistics, clustering based on MUP shape and MU firing pattern characteristics,

certainty-based supervised MUP classification, and temporal relationships between firing patterns of pairs of motor units. This system does not resolve superimposed spikes and, thus, is not suitable for detailed firing time series. Loudon et al. [Loudon et al 1992] used knowledge-based signal processing techniques for the decomposition of EMG signals. Their system automatically decomposes EMG signals recorded at force levels up to 20% MVC. Non-overlapping MUAPs are classified using a statistical pattern recognition method. Superimposed MUAPs are decomposed using both procedural and knowledge-based methods. Hamid Nawab et al. [Nawab et al 2007] developed a knowledge-based approach to implement decomposition. Their knowledge-based system's accuracy ranges between 90 and 95 %. Gut and Moschytz [2000] developed a communication signal-based interpretation of the EMG signal. They analyzed the communication between neurons and muscles. Hassoun et al [1994] developed a system for EMG signal decomposition called NNERVE (neural network extraction of repetitive vectors for electromyography) capable of decomposing. Zennaro et al [2003] developed a multi-channel tool to decompose multichannel long-term intramuscular EMG signals. Classification is based on template matching using wavelet coefficients. It should be noted however that despite the advances in EMG decomposition tools, none is perfect. Depending on goals, complete decomposition requires hours of manual editing. The results from decomposition are sometimes cross-checked by an experienced individual for any inconsistencies. A recent tool combines components from previous decomposition procedures in an expert systems approach using fuzzy logic [Erim and Winsean 2008]. This system attempts to replicate the thought process of an accomplished EMG decomposer. This approach is intended to reduce time that is spent on manual editing.

Chapter 6

Methods & Procedures

Participation in the *motor unit discharge rate* study involved a single session for control subjects and three study sessions performed over a 6-month time period (baseline, 3 months and 6 months) for ALS patients. In this thesis, we are only analyzing the baseline patient and control subject data. Data from the remaining two patient sessions are available for future work. Testing took take place in the Spaulding Motion Analysis Laboratory. The study was performed as described below.

6.1 Subject Recruitment

This study was approved by the Institutional Review Boards at Spaulding Rehabilitation Hospital and Worcester Polytechnic Institute. Each subject provided his/her written informed consent and was remunerated for taking part in the study. Eight control subjects, 56.6 $\pm$ 7.7 years of age (mean $\pm$ SD) were enrolled in the study. Each control subject was examined by a practicing physiatrist for exclusion criteria including neuromuscular disorders and the use of medications that could affect muscle activity. All eight control subjects were accepted into the study. Six subjects 54.7 $\pm$ 12.7 years of age (mean $\pm$ SD) with ALS were also recruited in the study. Individuals with ALS were recruited among patients routinely examined at the EMG clinic, Massachusetts General Hospital. Suitabil-

ity for inclusion of ALS patients in this study was determined based on the fact that they met clinical and electro-diagnostic criteria for definite ALS. All ALS patients were cognitively intact, medically stable and capable of communicating their informed consent. Each subject was considered capable of performing sustained isometric FDI muscle contractions of at least 30 seconds, had at least grade 3/5 strength in the FDI muscle, and were able and willing to participate in the study's baseline data collection, as well as three and six-month follow up data collection sessions lasting three hours each. Four of the ALS patients had dominant LMN dysfunction and two had dominant UMN dysfunction. Subjects in the study were recruited regardless of gender or ethnicity.

6.2 Instrumentation

A nerve conduction device, $TECA^{TM} SynergyN2$, was used to perform nerve conduction studies, see Figure 6.1. To monitor index finger abduction force we used a "constraining" device as shown in panel A of Figure 6.2. The device was adjustable and accommodated different hand sizes. Two force transducers (10 lbf and 25 lbf Interface - Miniature Beam Load Cell) were used to measure abduction and flexion forces of the index finger. The acquisition system was set up with two seventeen inch screens. The first screen was utilized by the researcher conducting the data collection to inspect the quality of the EMG data and force trajectories. The second screen showed subjects the abduction force trajectory to be followed during testing along with their achieved abduction and flexion forces. Subjects were instructed to minimize

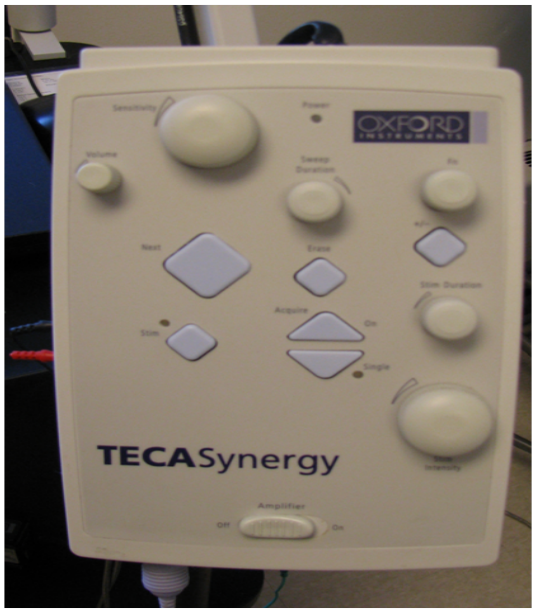

Figure 6.1: Nerve conduction device used in our study

forces in the flexion-extension orientation. A set of speakers was used in real-time to additionally assess the quality of the recordings based on the sound generated from the input EMG signals. High pitch sounds were considered as associated with high quality EMG data since the EMG decomposition is typically more reliable when motor unit action potential (MUAP) waveforms show sharp edges.

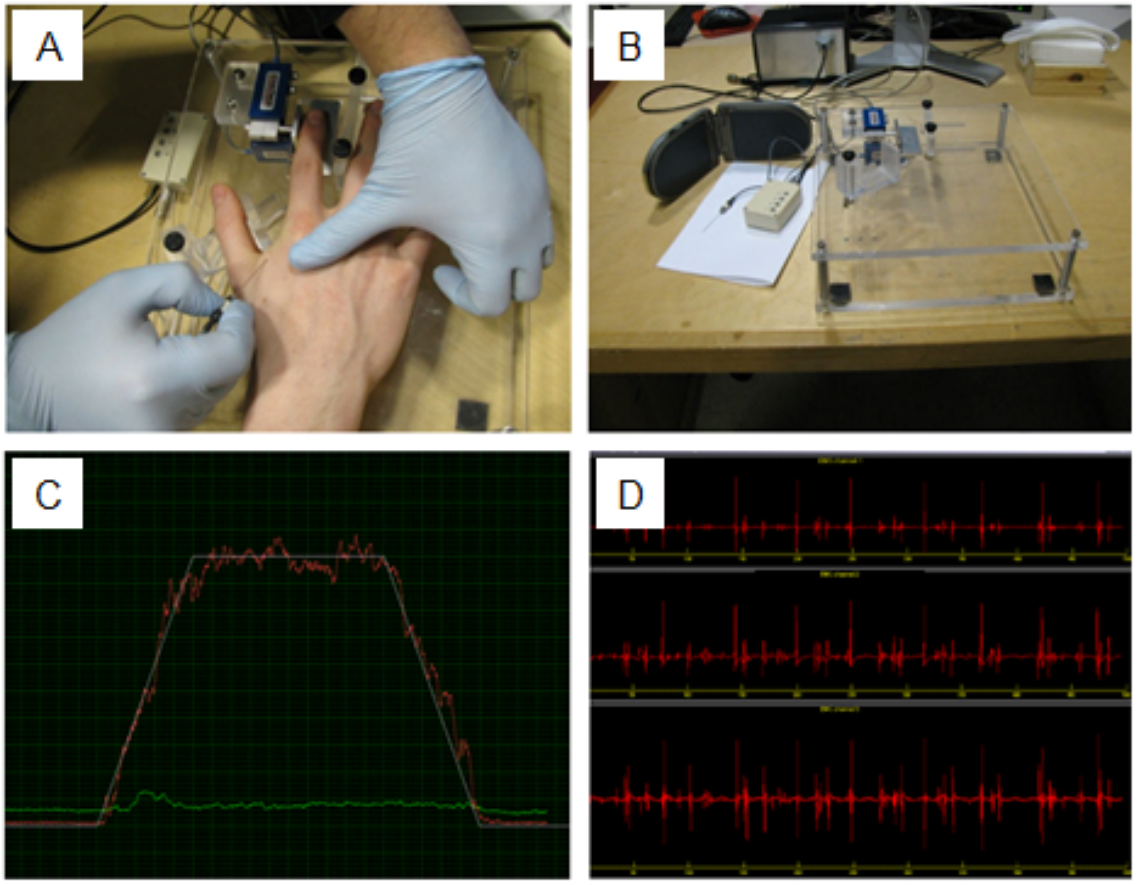

Figure 6.2: Motor unit data collection. A) Needle insertion. B) Hand constraint and measurement equipment used in data collection. C) Force trajectory to be followed. D) EMG signal in real-time

A 25-gauge stainless steel quadrifilar needle electrode was used to record electromyographic (EMG) signals. The quadrifilar needle electrode was composed of four electrodes made of platinum wires with diameter of 50μm. The wires were fed through the cannula of the needle and reached a side port where the electrodes were arranged in a 2x2 array with inter-electrode distance of 200μm (Figure 6.3). Four channels (differentially amplified) of EMG data were recorded.

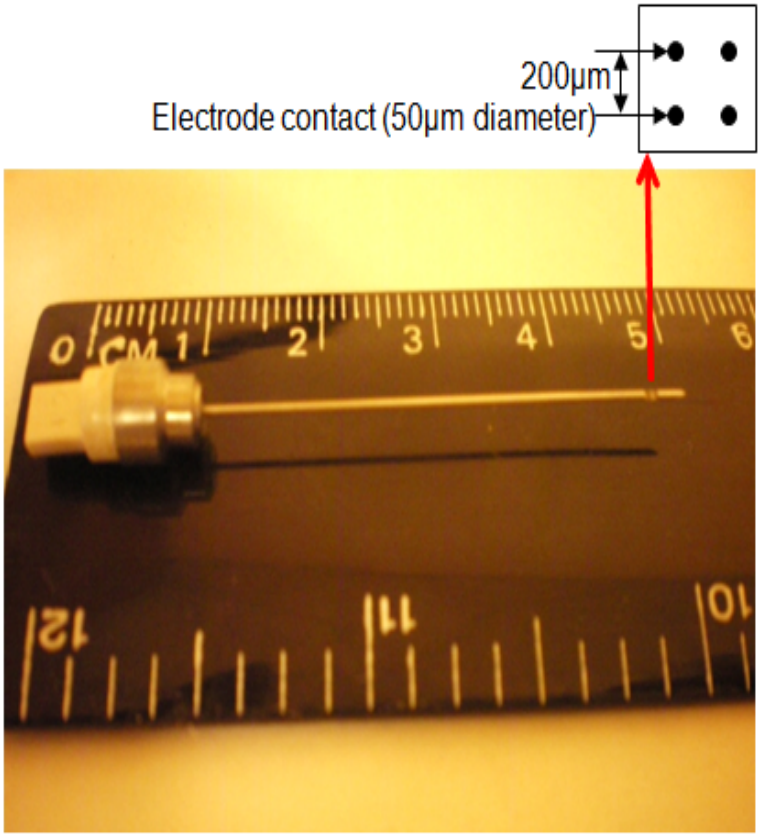

Figure 6.3: Quadrifilar needle electrode used in data collection

During the analog phase of data collection, data were high pass filtered at 300 Hz (single pole RC filter), amplified by a magnitude of 500, and low pass filtered at 10kHz (4-pole butterworth filter). Data were sampled at 25 kHz using a 16-bit acquisition card (NI6035E). During muscle contraction, waveforms are recorded from active muscle fibers within the detection volume of the quadrifilar needle electrode. MUAPs related to different motor units typically exhibit different shapes and amplitude values, due to the orientation of each recording area relative to the propagation of the electric field associated with the presence of depolarized zones travelling along the muscle fibers. All amplification and filter hardware, and the display software portion of the overall data acquisition system were designed and developed by our research team as detailed in Appendix A.

6.3 Experimental Protocol

Figure 6.4 shows an outline of the manner in which the study proceeded. All study procedures were approved by the local ethical committee. After consenting, the following functional assessment tests were administered for ALS patients:

- *The Revised ALS Functional Rating scale*, a standard clinical assessment tool based on interviewing and clinically observing patients.
- *Muscle stretch reflex assessment*, a standard clinical exam where the biceps, triceps, brachioradialis, knee and ankle reflexes were elicited using standard physical exam techniques and graded as 0 to 4+
- *The modified Ashworth scale*, a standard clinical assessment tool for assessing spasticity, was used to assess elbow flexor spasticity.

The following tests were performed in both ALS patients and control subjects:

- The compound muscle action potential (CMAP) amplitude, a standard clinical nerve conduction study technique was performed on the ulna motor nerve from the first dorsal interosseous (FDI) muscle.
- The FDI maximum muscle force was measured by instructing subjects to position their dominant hand in the ”constraining” device (panel B of Figure 6.2) designed to facilitate the isolation of force output generated by the FDI muscle during abduction. Subjects were asked to perform three maximum contractions (rapidly producing the maximum force of which they were capable of producing) lasting a period of three to five seconds each. Subjects were verbally encouraged to contract their FDI muscle to its maximum.

Subjects performed a practice index finger abduction while tracing a trapezoidal force template. Then a Velcro strap was wrapped around the forearm, near the elbow. Also,

an electrode with a conducting gel surface was placed on the arm just above the elbow as a reference. Once the strap was secured and the reference electrode attached, a quadrifilar needle electrode was then inserted into the FDI muscle (approximately 0.25-0.5 cm deep). Subjects were instructed to contract the FDI muscles at about 10% of MVC. The needle electrode was then positioned in a manner so as to obtain EMG signals that were assessed (via visual and auditory inspection) to be suitable for the analysis of motor unit firing rate characteristics. Based on our experience, we considered the uniqueness of the MUAP waveforms associated with each motor unit and the consistency of the MUAP shapes over time to predict the number of motor units whose firing rate characteristics could be derived. Data were then gathered during isometric contractions of 20% MVC and 50% MVC while subjects followed a trapezoidal template displayed on the computer screen. The template included an initial rest period (5.5s for 20% MVC and 6s for 50% MVC) when the FDI muscle was silent, an interval during which the level of contraction progressively increased to the desired force output (slope of 10% MVC/s), a period of constant-force contraction (plateau), and an interval during which the level of contraction was progressively decreased (slope of 10% MVC/s). The plateau of the trapezoidal trajectory lasted for 15 s for the 20% MVC tests and 8 s for the 50% MVC tests. Subjects rested for at least one minute after each contraction. Two contractions were performed at each force level (20% MVC and at 50% MVC). The needle was repositioned twice and two such recordings were performed from each additional site within the FDI muscles.

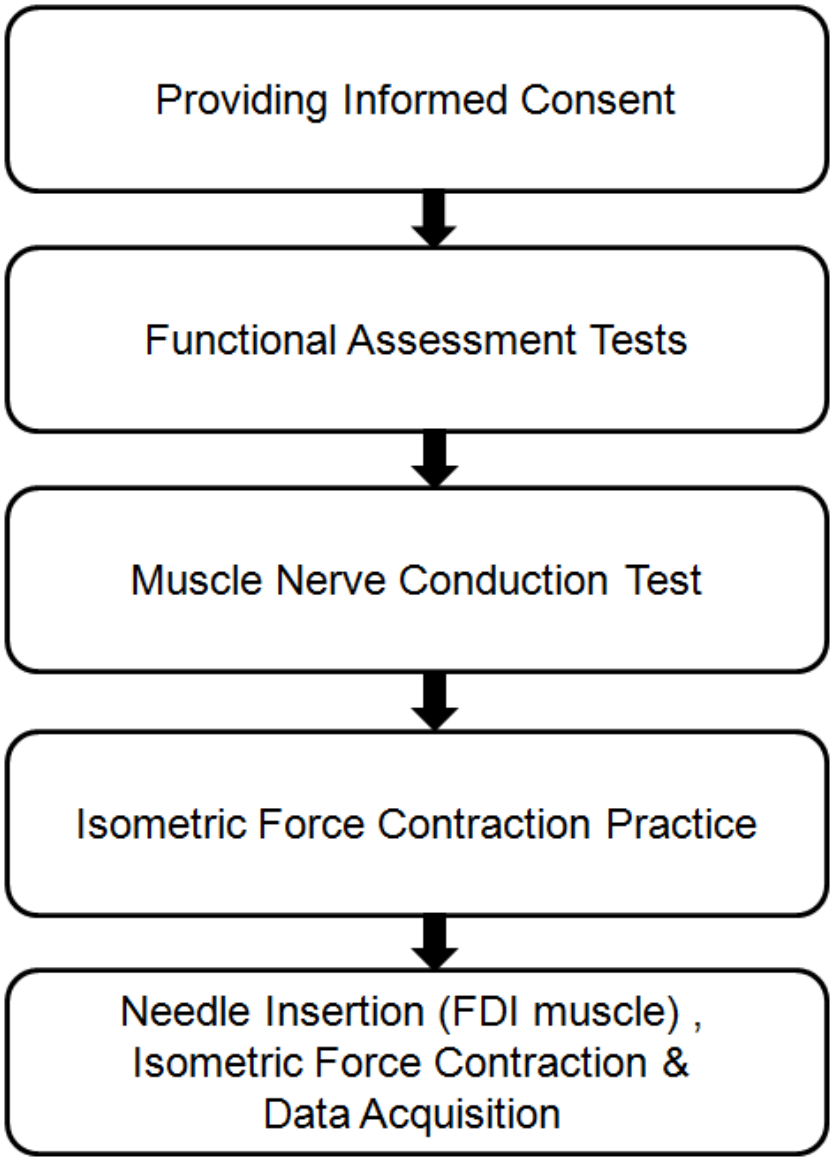

Figure 6.4: Outline of the the study procedure

6.4 Data Analysis

6.4.1 Decomposition

We analyzed the EMG signals basing on a procedure known as EMG decomposition. Motor unit decomposition is a method designed to identify the occurrence of MUAP waveforms related to the activity of a given set of motor units. Classically, decomposition is divided into four stages, namely: (1) pre-processing, (2) detection, (3) classification and (4) superposition resolution. A detailed description of decomposition was given in chapter 5. We utilized a graphical software tool (EMGLAB) developed by McGill et al [McGill 2005]. For the decomposition process, the EMG signals were high pass filtered at 1 kHz using a first order Butterworth filter. An automated decomposition algorithm [Florestal et al 2007] incorporated within EMGLAB was then utilized. After this process, visual editing of the results of the automated analysis was performed to assure reliability of the results. Exhaustive decomposition was performed on motor units that presented large magnitude (relative to background activity). Motor units were identified primarily based on shapes of MUAP waveforms. It is important to note that MUAP waveforms belonging to a particular motor unit undergo slow changes over time as shown in Figure 6.6. Slow changes in MUAP waveforms were accounted for by an adaptive template. There were cases when even the updated template could not match waveforms belonging to the same motor unit (increased EMG decomposition complexity). This was likely because MUAP waveforms from of two or more motor units fired simultaneously, creating complex waveforms (constructive superpositions) or even worse, showing no activity because waveforms may have cancelled each other out (destructive superpositions). In such situations, data were analyzed using an algorithm designed to automatically resolve superpositions [McGill 2002]. Cases of superpositions that were not resolved by the automated algorithm were resolved manually. In general, the analysis of the EMG data was more challenging in recordings from patients because MUAP waveforms in patients were

typically more complex than in healthy control subjects. In addition, changes over time in MUAP waveform shape in recordings from patients were more dramatic than in recordings from control subjects. Figure 6.5 shows examples of MUAP waveforms recorded from a control subject and a patient with ALS. The complexity of the polyphasic waveform recorded from the patient compared to the relatively simple waveform recorded from the control subject is apparent. The complexity of the MUAP waveform made the patient data difficult to decompose because the shape of the waveform changed over time rather fast. Due to this fact, we combined the use of automated decomposition software with manual editing tools [McGill 2005].

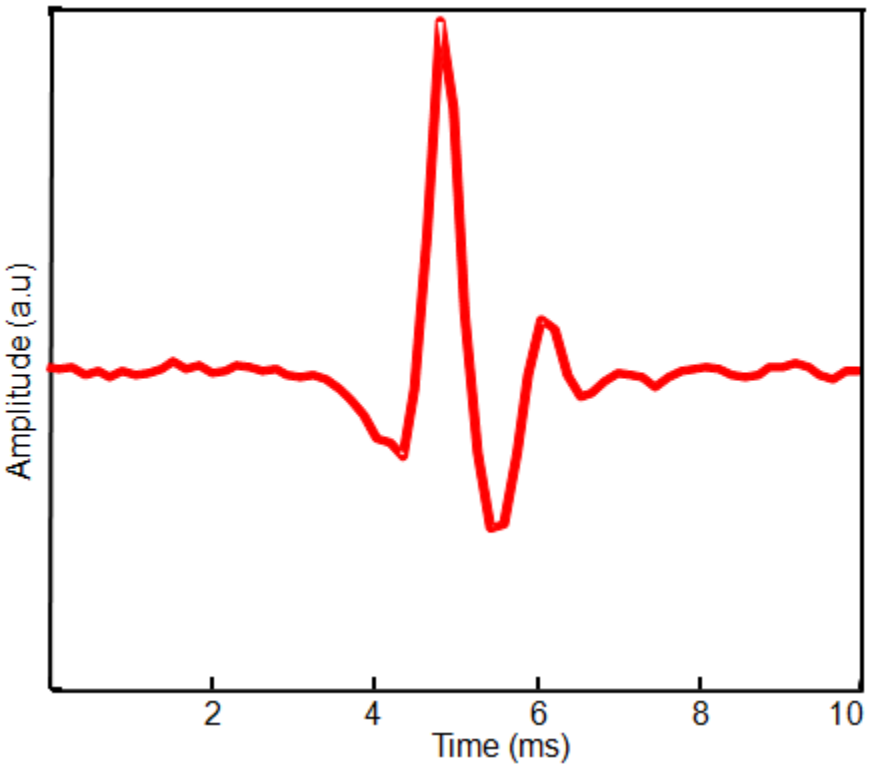

(a) Non ploy phasic action potential

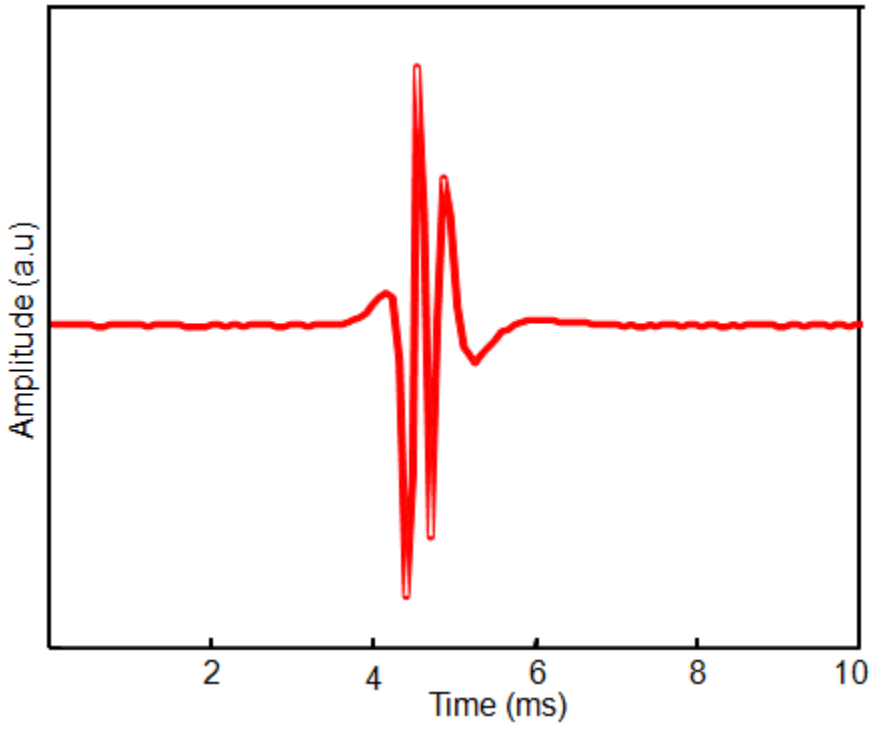

(b) Polyphasic action potential

Figure 6.5: Action potential in (a) was recorded from a control subject whereas action potential in (b) was recorded from an ALS patient.

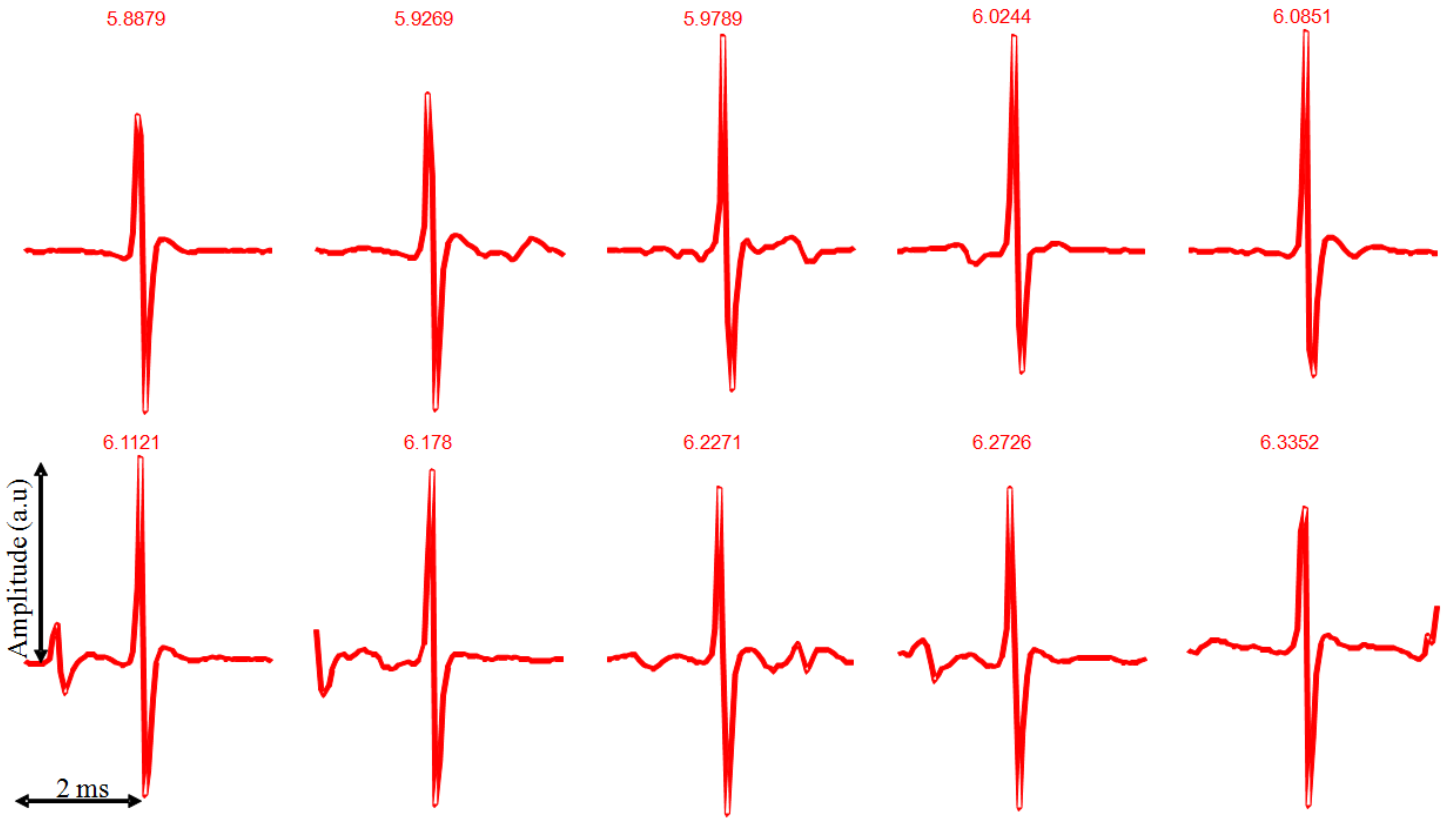

Figure 6.6: A group of MUAPs (MUAPT) classified as the same motor unit based on shape. Peak times (seconds) of each firing is also shown above each MUAP.

6.4.2 Motor Unit Firing Rate Time Series

We extracted several features from the motor unit firing activity that resulted from the decomposition process. Figure 6.7 shows firing activity of a motor unit during a 20% MVC contraction following a trapezoidal trajectory recorded over a period of twenty seconds. This activity, even along the interval where the force was stabilized, did not occur at even intervals.

To obtain the instantaneous firing rate times series (full details are given subsequently), we computed the forward differences of the firing times and then we inverted these differences to produce a rate. We visually identified a continuous portion (plateau segment) of force that was stable. Using MAtlab's built in functions, a re - weighted (bisquare weighting function) least squares fit was then performed to the instantaneous firing rate within the plateau segment. All points that fell outside of the 99% confidence interval bounds of the regression line were considered outliers and were eliminated. Then, interpolation was performed to obtain motor unit firing rates that were sampled periodically [Knight and Kamen 2006]. In particular, the firing rate data were resampled at 100 samples per second, using piecewise cubic Hermite interpolation (has no overshoots and less oscillation if the data are not smooth) algorithms provided by Matlab technical computing software.

Derivation of Firing Rate Time Series

Given a finite set of M motor unit firing times in ascending order, $ft(n)$, 1 $\leq$ n $\leq$ M, we determined the instantaneous firing rates, fr(n), as the inverse of the forward differences:

$$fr(n) = \frac{1}{ft(n+1) - ft(n)}, 1 \leq n \leq M-1 \tag{6.1a}$$

The times corresponding to the firing rates defined in 6.1a, above, were defined as

follows:

$$ft_r(n) = \frac{ft(n+1) + ft(n)}{2} \tag{6.1b}$$

Note that each of these times is the mid-point between the two associated firing times. Then, using the firing rate values (fr) and their corresponding firing rate times (ft_r), we performed the piecewise cubic Hermite interpolation. All subsequent analysis utilized this periodically sampled firing rate, which was determined over the stable force portion of the force trajectory plateau.

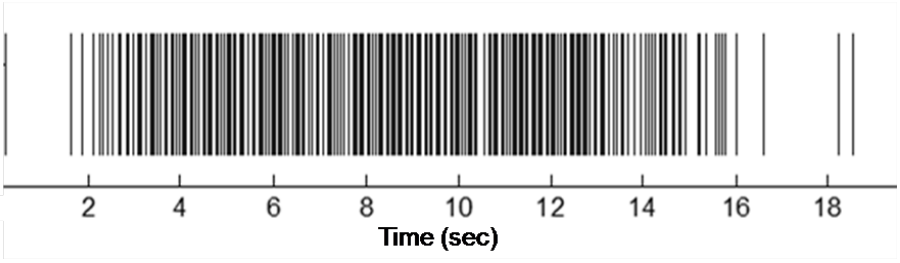

Figure 6.7: Each of the bars indicate firing instance (seconds) of the given motor unit during muscle contraction.

Plateau Segment

As shown in Figure 6.8, a continuous portion of force trajectory that was stable was determined for each trial. The interval was determined manually because some patients could not maintain a steady contraction along the plateau of the trapezoidal trajectory due to weakness as a result of disease.

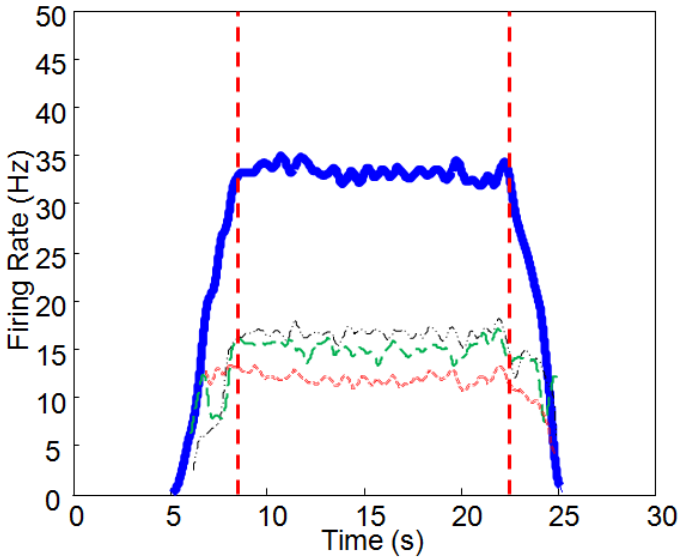

Figure 6.8: Vertical bar plots indicate bound portion of motor unit firing rate time series which was used to characterize motor units recorded during the given muscle contraction. The thick trajectory is the force contracted by the subject and the thin trajectory represents the firing rate of the motor units that were recorded and decomposed.

Motor Unit Firing Rate Time Series Trends and Initial Firing Rates

To characterize motor unit firing rate time series, several parameters were defined. Motor unit firing rate time series trends were defined as the slopes of lines that were fit to the motor unit firing rate time series in the time range over the portion of motor unit firing rate time series that corresponded to the region of force trajectory that was stable (Plateau Segment). In some patients it was observed that firing rate time series decreased quite dramatically as shown in Figure 7.1(a). In order to compare firing rates, we looked at the

initial firing rate. The initial firing rate was defined as the initial point of the regression line fit to motor unit firing rate time series in the region where force is stabilized using a least squares fit. The initial firing rate was used to characterize the firing rate of the time series.

Variability

In order to determine the variability of a time series, we fit a least squares error criterion to the motor unit firing rate time series that corresponded to the region of force (plateau segment) first. Following this, we removed the mean, by subtracting the regression line, from the original data. The sample standard deviation of these residuals was our measure of variability.

Mean Motor Unit Firing Rate

Mean motor unit firing rates were defined as the average of motor unit firing time series that corresponded to the region where the force was stable.

Doublets

Motor units fire at close intervals. In situations where similar shaped motor unit action potential waveforms (i.e., classified as from the same MU) that discharged at an interval of less than 20ms were classified as doublets [Christie and Kamen 2006].

Onion Skin

Onion skin is the relationship between motor units whereby earlier recruited motor units achieve higher firing rates than subsequent motor units and the de-recruited process is the inverse of the recruitment process (”first in last out”) as shown in Figure 6.9 [Erim et al 1999]. In order to quantify ”onion skin” phenomenon, first we pooled motor units observed from a particular subject at 20% MVC and separately at 50% MVC. Then

we fit regression lines to mean values against the recruitment threshold. A negative slope of the regression line indicated that onion skin phenomenon was not violated whereas a positive slope indicated violation of the onion skin phenomenon. The recruitment threshold was defined as the average force in a window of 7.5 ms beginning at the time of the first firing of the motor unit [Erim et al 1999].

Statistical Tests

Differences in motor unit firing rate time series behavior of ALS patients compared to control subjects were assessed using t-$tests$ (not assuming unequal variances as is the case in student's t-$test$).

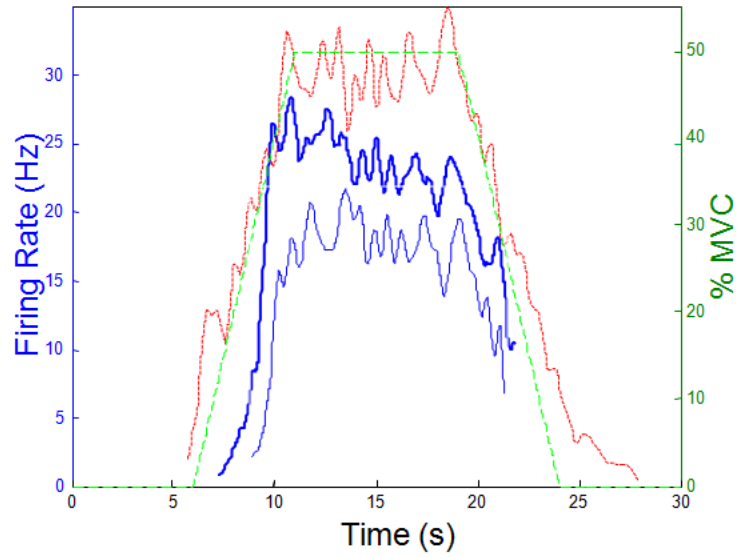

(a) Obeys ”Onion skin” phenomenon

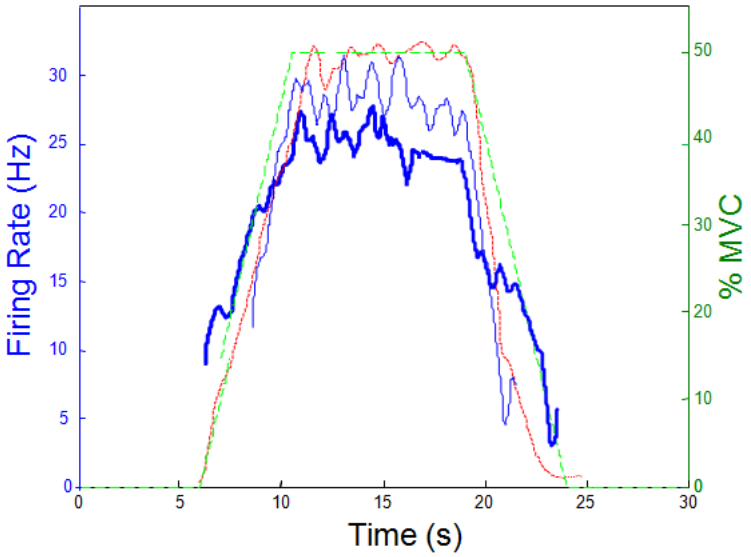

(b) Violates ”‘Onion skin”’ phenomenon

Figure 6.9: Two plots of motor unit firing rate time series plotted against the force trajectory during EMG recording. The thick and thin solid trajectories represent the motor unit firing rate time series. Long dashed trajectory represents the trapezoidal force template that the subject traced during the isometric force contraction. The short dashed trajectory represents the actual force generated by the subject during the contraction of the muscle. The two motor units shown in (a) conform to the onion skin phenomenon whereas those shown in (b) violate onion skin.

Chapter 7

Results

Data from a total of 82 fully decomposed motor unit firings were analyzed at contractions of 20% (13 from controls and 23 from ALS patients) and 50% (13 from controls and 33 from ALS patients) MVC. Data from 4 control subjects was analyzed. Motor unit firing rate time series analyzed corresponded to the stable region of the force trajectory. At 20% MVC the duration of the plateau was 15 s and 8 s for 50%MVC. On average, CMAP (Compound Muscle Amplitude Potential) for controls was 10.8 mV and the MVC was 23.4 N. Throughout this text, significance levels of $P < 0.05$ were used for all statistical comparisons.

Tables 7.1 and 7.2 show summary of tests that were administered before recording of EMG data. Tables 7.3 and 7.4 show results that were based on observations made from motor unit firing rate time series. The information provided in these tables is re-enforced by the figures that follow the tables.

Hypothesis 1: ALS patients with dominant lower motor neuron dysfunction will have increased MUDR

As shown in Figure 7.2, initial motor unit firing rate time series recorded from dominant LMN dysfunction ALS patients fired at a higher rate when compared to those of control subjects. In order to assess whether the difference in initial motor unit firing rate time series was significant, we performed a t-$test$ as described in section 6.4. At the 20%

MVC contraction, we failed to reject ($P > 0.05$) the hypothesis that motor unit firing rates of recordings from dominant LMN ALS patients were equal to motor unit firing rates of recordings from control subjects. The initial firing rates were not statistically significant. However on performing the same test at 50% MVC we rejected ($P < 0.05$) the hypothesis that motor unit firing rates of recordings from dominant LMN ALS patients were equal motor unit firing rates of recordings from control subjects. The difference was statistically significant.

Hypothesis 2: ALS patients with dominant upper motor neuron dysfunction decreased MUDR

In contrast to motor unit firing rates in dominant LMN ALS patients, we observed low firing rates in motor units recorded from dominant UMN dysfunction ALS patients when compared to control subjects. The t-$test$ found these results to be statistically significant ($P < 0.05$).

Variability

Hypothesis 3: ALS patients with dominant lower motor neuron dysfunction will have increased variability in motor unit firing rates compared to control subjects

Increased variability was observed in motor unit recordings from ALS patients with dominant LMN dysfunction rates compared to control subjects, see Figure 7.4. We found the difference to be statistically significant at both the 20% and 50% MVC ($P < 0.05$).

Hypothesis 4: ALS patients with dominant upper motor neuron dysfunction will have decreased variability We observed a decrease in variability of the motor unit firing rate time series in patients with dominant LMN dysfunction compared to both control subjects and patients with dominant UMN dysfunction. The differences were significant ($P < 0.05$) at 20% and 50% MVC.

$Subject$	$Diagnosis$	$Gender$	Age	$CMAP(mV)$	$MVC(N)$	$ALS-FRS$	$Ashworth$
A	ALS (LMN)	M	49	5.0	5.0	41	0
B	ALS (LMN)	F	59	9.2	14.2	41	0
C	ALS (LMN)	F	71	7.9	5.4	40	0
D	ALS (LMN)	F	44	10.2	16.4	44	0
E	ALS (UMN)	M	39	3.0	3.4	26	1
F	ALS (UMN)	F	66	10.8	9.3	24	1

Table 7.1: Summary of patient functional data recorded from ALS prior to recording of motor units.

$Subject$	$Diagnosis$	$Gender$	Age	$CMAP(mV)$	$MVC(N)$
A	Healthy	F	49	14.6	22.5
B	Healthy	M	54	9.8	16.0
C	Healthy	F	51	6.3	24.2
D	Healthy	M	60	6.3	15.4
E	Healthy	M	50	12.1	34.4
F	Healthy	M	65	16.2	20.3
G	Healthy	M	71	9.2	21.0
H	Healthy	M	68	12.2	28.2

Table 7.2: Summary of control subject functional data that was recorded prior to recording of motor units.

Slopes

Fast decrease in motor unit firing rates was observed in some ALS patients. The difference in slopes between predominant UMN ALS patients and control subjects was not statistically significant at both 20% and 50% MVCs however, the difference between predominant LMN ALS patients and control subjects was statistically significant at both 20% and 50% MVCs.

	$Substitution$	$\%Onion\ skin\ obey$	$Initial\ Firirng\ Rate\ (Hz)$	$SD\ (Hz)$
		$20\%\ MVC$		
Controls	none	75	16.22	2.06
LMN	none	75	18.87	4.73
UMN	none	100	9.22	1.68
		$50\%\ MVC$		
Controls	none	25	19.79	1.66
LMN	none	50	23.34	4.81
UMN	3	50	12.83	2.26

Table 7.3: Various characteristics we observed in motor unit firing rate time series (4 controls and 5 patients at 20% MVC; 4 controls and 6 patients at 50% MVC).

	$Standard\ Deviation\ (Hz)$	$SDvar(Hz)$	$Slope(Hz/s)$	$SD_{slope}\ (Hz/s)$	$n\ of\ MUs$
			$20\%\ MVC$		
Controls	1.90	0.54	-0.10	0.10	13
LMN	3.38	1.2	-0.24	0.29	12
UMN	0.99	0.17	-0.02	0.09	11
			$50\%\ MVC$		
Controls	3.00	0.71	-0.18	0.16	13
LMN	4.07	1.56	-0.39	0.26	25
UMN	1.70	0.52	-0.09	0.26	8

Table 7.4: Variability and slopes of motor unit firing rate time series.

t-tests

MU Parameter	Null Hypothesis	20% MVC		50% MVC	
		$\mathbf{H_o}$	$\mathbf{P-Value}$	$\mathbf{H_o}$	$\mathbf{P-Value}$
Firing Rates	ALS(LMN) = Controls	Acepted	9.4×10^{-2}	Accepted	2.2×10^{-2}
Firing Rates	ALS(UMN) = Controls	Rejected	2.8×10^{-9}	Rejected	8.0×10^{-6}
Variance	ALS(LMN) = Controls	Rejected	8.4×10^{-4}	Rejected	7.0×10^{-3}
Variance	ALS(UMN) = Controls	Rejected	2.3×10^{-5}	Rejected	5.2×10^{-6}
Slopes	ALS(LMN) = Controls	Rejected	1.1×10^{-2}	Rejected	4.6×10^{-3}
Slopes	ALS(UMN) = Controls	Acepted	2.1×10^{-1}	Accepted	6.4×10^{-1}

Table 7.5: T-test results of several motor unit firing rate parameters.

Fasciculations

During quiet intervals when subjects were resting, we noticed occasional muscle activity on the display screen as well as heard a crisp high frequency sound through the set of speakers. These were likely due to the occurrence of fasciculations. This activity was noted only in dominant LMN ALS patients.

Doublets

Occasionally some firings of the same motor unit occured within 20ms of each other (doublets). In the predominant LMN pathology, 29 doublets were observed. This was much higher compared to five for UMN and six for control subjects.

Polyphasic MUAPs

We identified differences in MUAP waveforms recorded from ALS patients. It was apparent that MUAP waveforms recorded from patients were generally more complex than MUAP waveforms recorded from control subjects, see Figure 6.5.

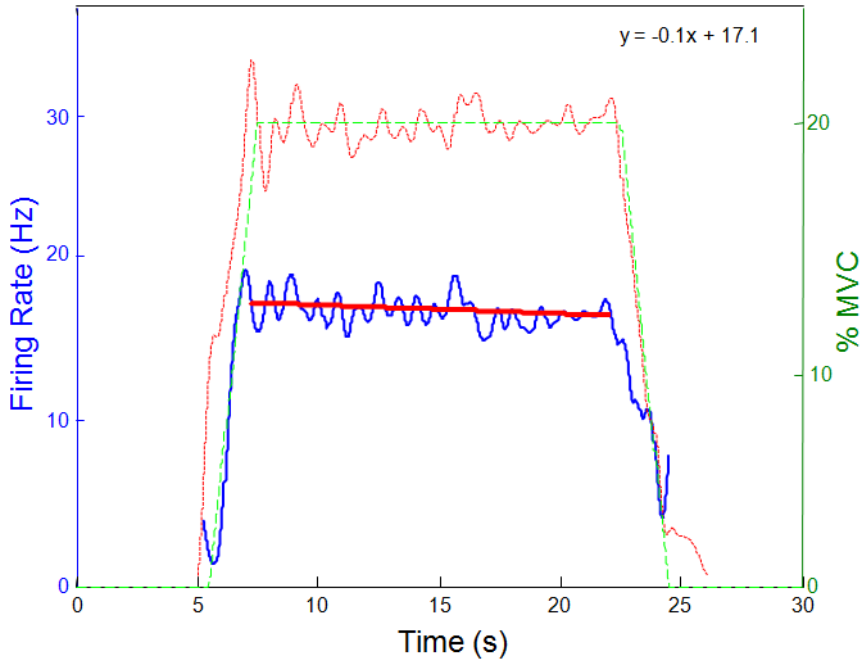

(a) Trend for control subject

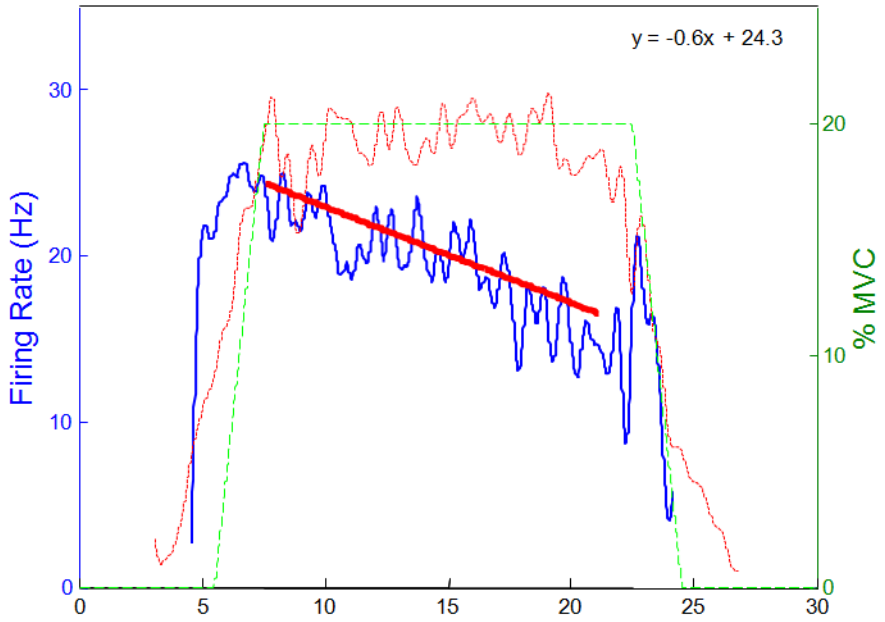

(b) Trend for ALS patient

Figure 7.1: Plots of motor unit firing rate time series recorded at 20% MVC. A trend line is drawn through a segment of the motor unit firing rate time series that corresponds to the stable region of the force trajectory. The thick and thin solid trajectories represent the motor unit firing rate time series. Long dashed trajectory represents the trapezoidal template that the subject traced during the isometric force contraction. The short dashed trajectory represents the actual force generated by the subjectject during the contraction of the muscle. Figure 7.1(a) shows two motor units that conform to the onion skin phenomenon whereas Figure 7.1(b) shows an example of onion skin violation.

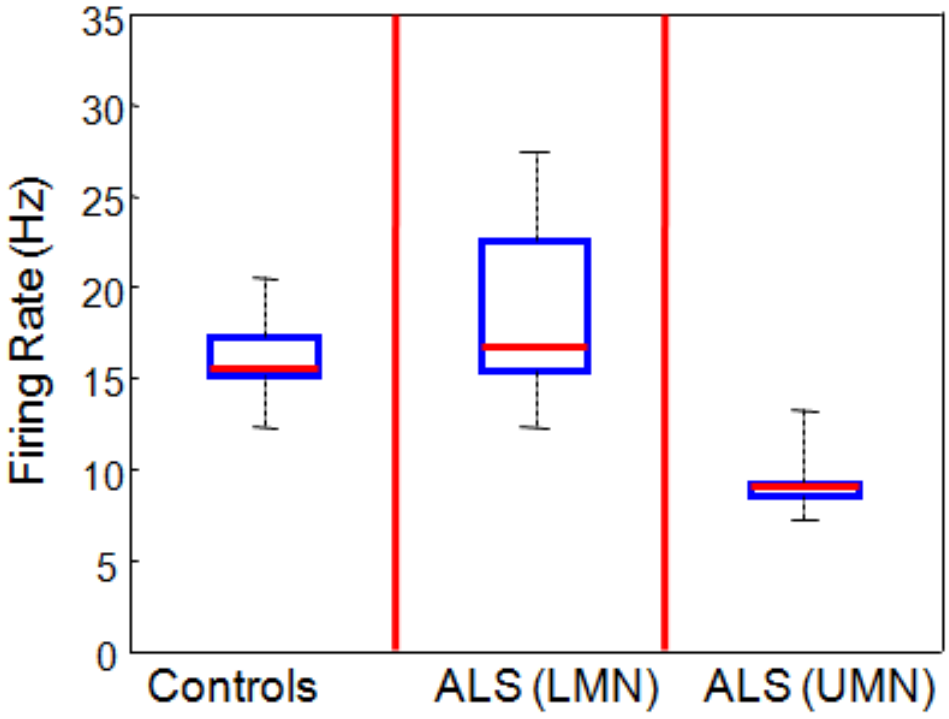

(a) 20% MVC

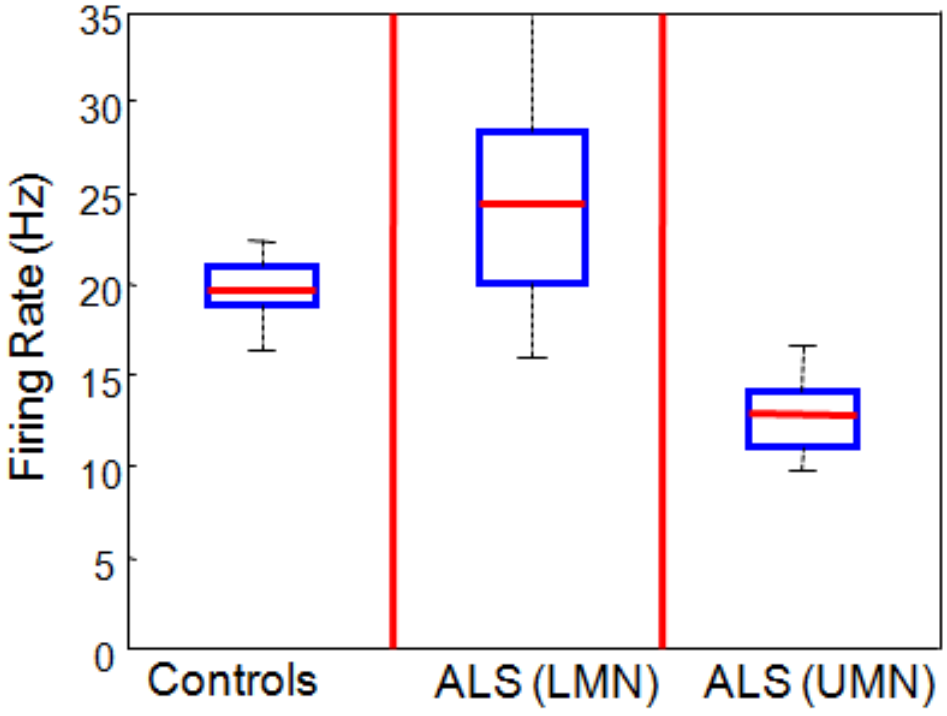

(b) 50 % MVC

Figure 7.2: Box plots showing motor unit firing rates between control subjects and ALS patients. Dominant LMN dysfunction patients have high firing rate.

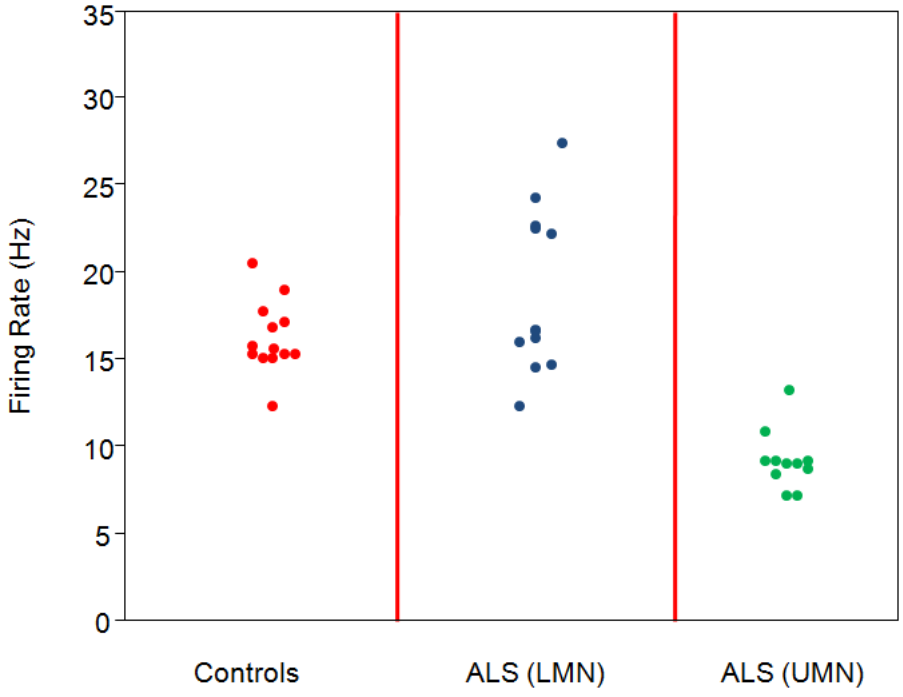

(a) 20% MVC

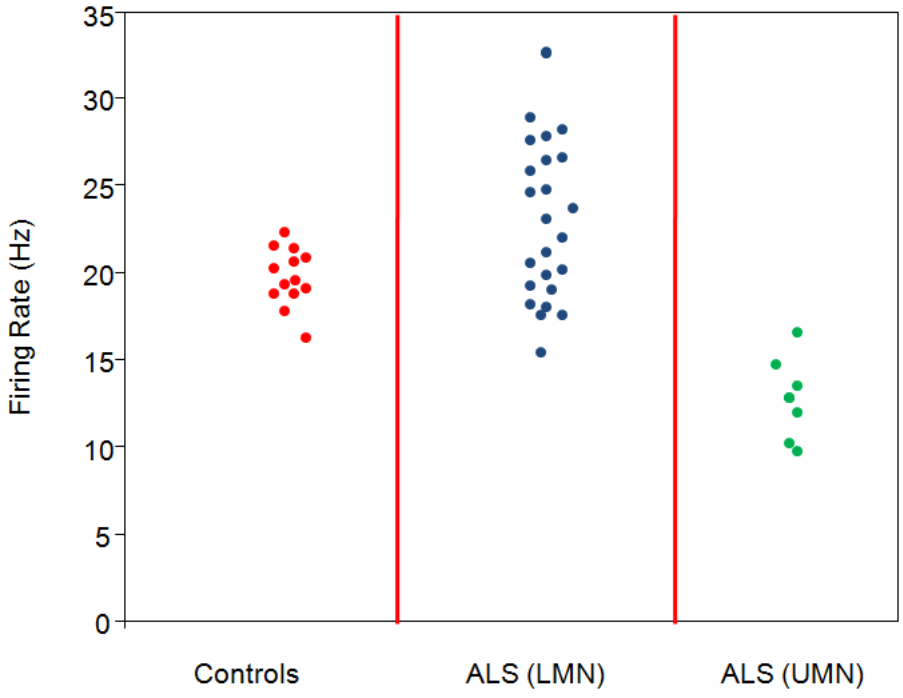

(b) 50 % MVC

Figure 7.3: Dot plots showing motor unit firing rates between control subjects and ALS patients.

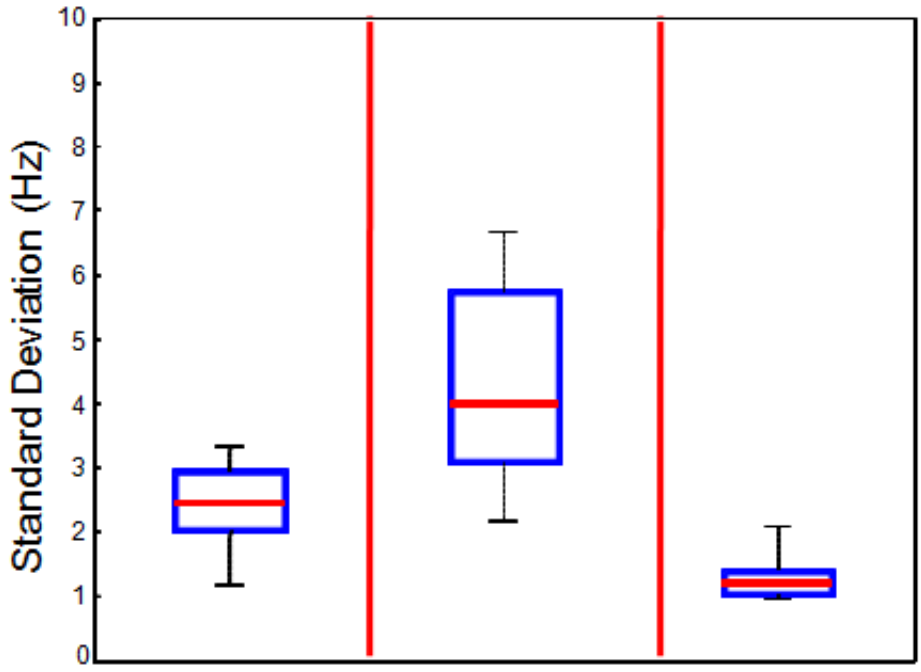

(a) 20% MVC

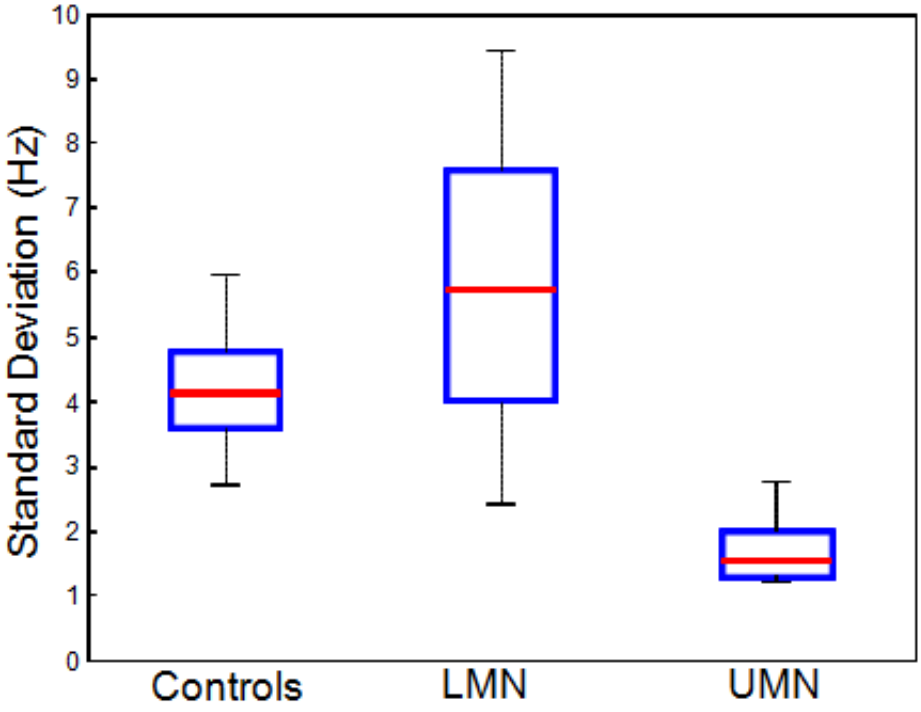

(b) 50 % MVC

Figure 7.4: Box plots showing variability of motor unit firing rate time series.

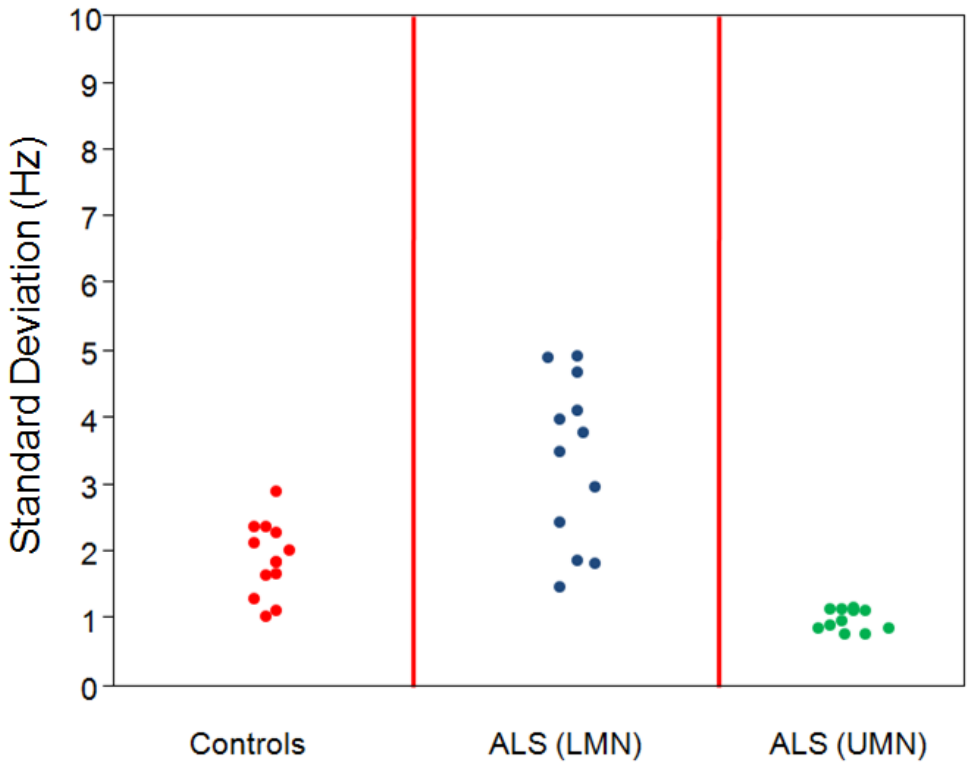

(a) 20% MVC

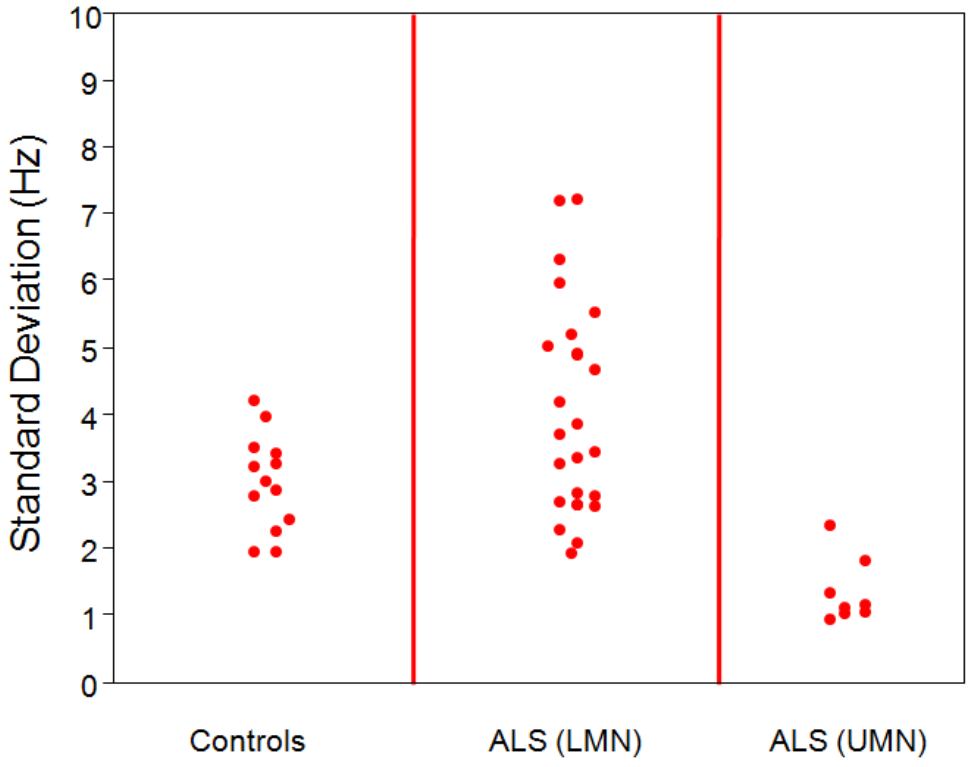

(b) 50 % MVC

Figure 7.5: Dot plots showing a comparison of variability in individual motor unit firing rate time series.

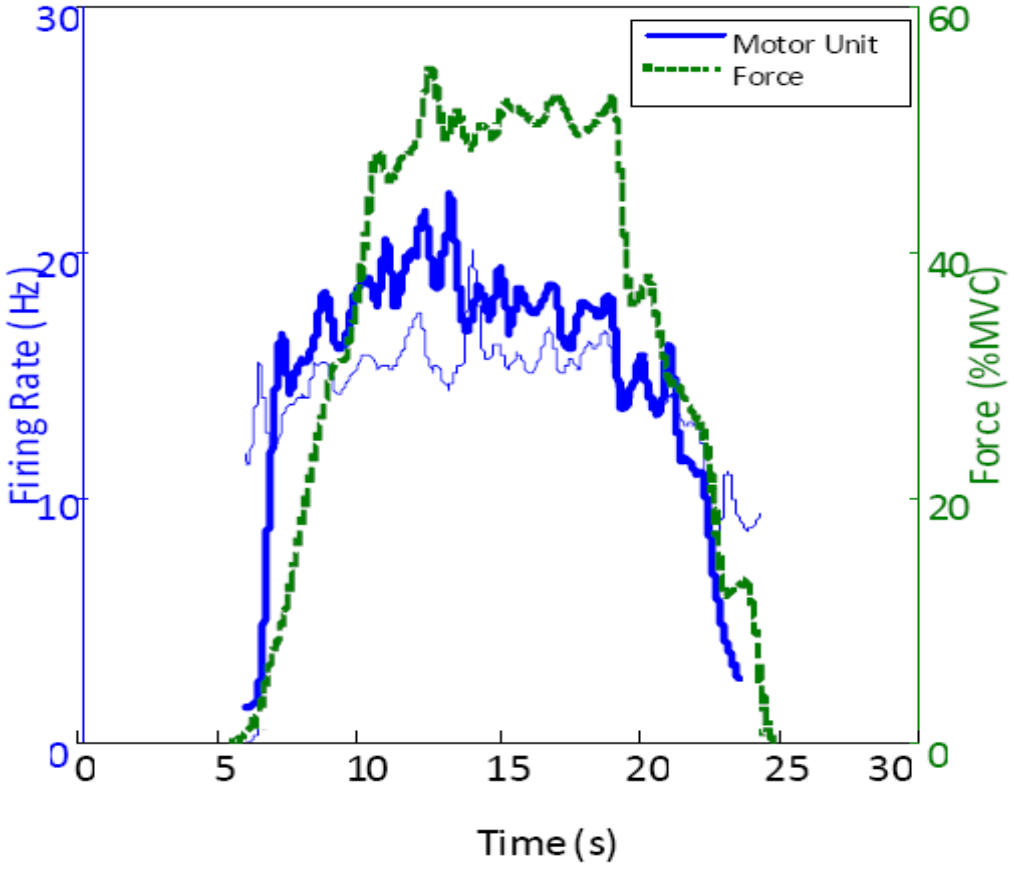

Figure 7.6: Firing rate time series from a 50% MVC contraction (control subject). The green trajectory is the index abduction force measured by a force transducer, and the blue trajectories are the motor unit firing rate time series of two of the detected motor units.

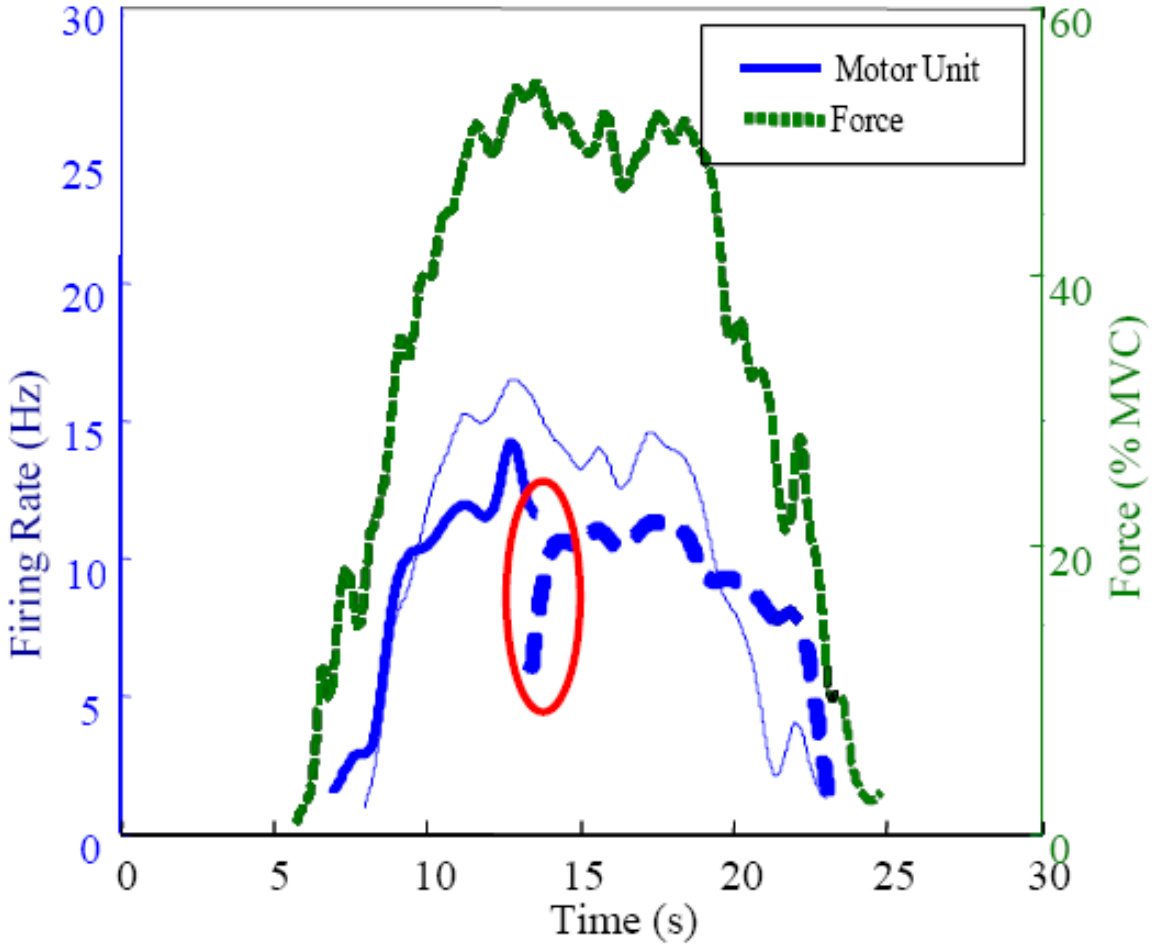

Figure 7.7: Firing rate time series from a 50% MVC contraction (patient with ALS). The green trajectory is the index abduction force measured by a force transducer, and the blue trajectories are the motor unit firing rate time series of two of the detected motor units. This figure shows a motor unit substitution. Thin dashed line is force trajectory and the others represent motor units.

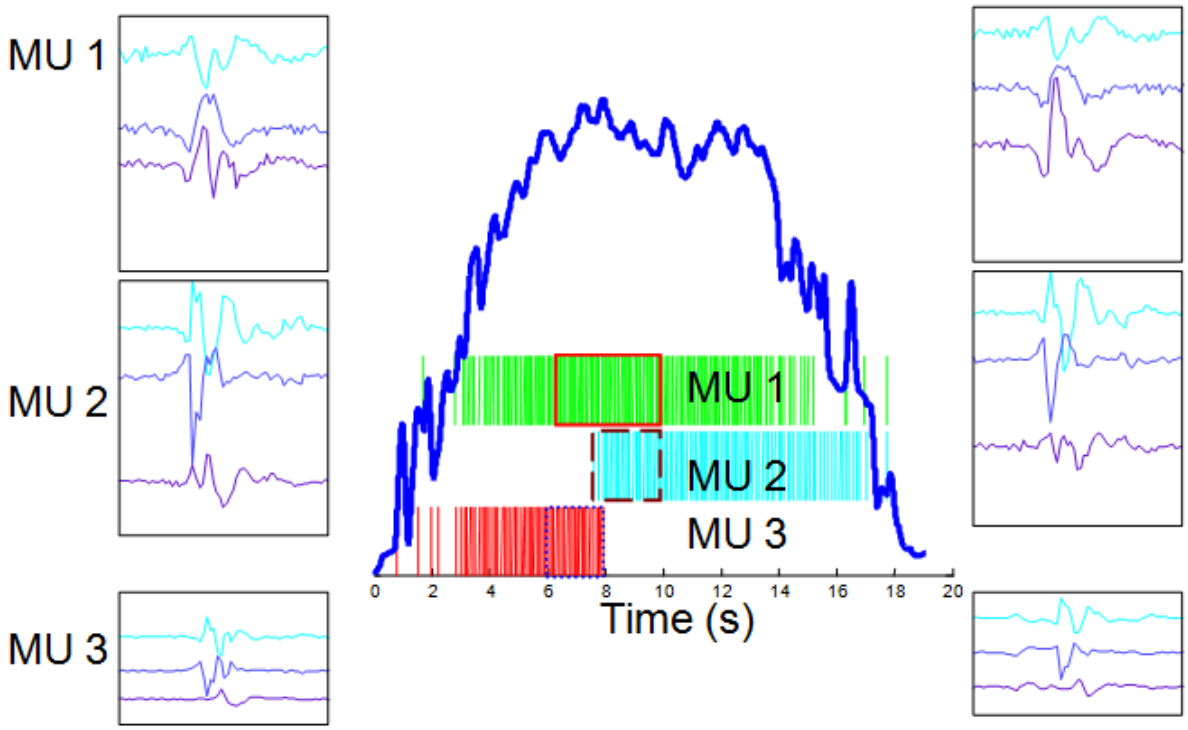

Figure 7.8: Bar plot corresponding to same data as shown in Figure 7.7 showing substitution. MUAP waveforms of the different motor units are included to show that indeed substitution occurred as opposed to needle movement that would inevitably alter waveform shapes representing a given motor unit. Each of the three channel MUAPs on the left represent their respective motor units at the start of the window drawn across the bars and on the right hand side they represent their respective motor units observed at the end of the window. MU 1 overlaps the other two motor units indicating that there was needle movement and during that same period MU3 stops firing and MU2 starts firing.

Chapter 8

Discussion

This study, to our understanding, is the first regarding the characterization of motor unit behavior in patients with ALS. We observed several interesting features in motor unit firing rate time series recorded from ALS patients. As this was the first study in ALS patients, we also recorded motor unit firing rate time series from individuals with no known form of neuromuscular disorders (controls). Results from the control group exhibited characteristics similar to those observed by others in healthy populations of similar age. For example, firing rates were comparable to those reported by Erim [Erim et al 1999]. We compared results observed in control subjects to those observed in ALS patients and saw differences. Furthermore, there were differences in motor unit firing rate characteristics between dominant LMN and dominant UMN ALS dysfunction.

Initial Motor Unit Firing Rate

In some patients, there was a fast decline in motor unit firing rates. As a result, instead of comparing firing rates based on average values, we used the initial firing rate. Firing rates observed from control subjects were similar to those obtained by others [Erim et al 1999] in elderly populations. Increased motor unit inital firing rate was observed in predominant LMN patients when compared to control subjects. Motor units inflence muscle force generation. Since, due to ALS disease, motor units are lost, the increase in firing rates

was likely a compensatory mechanism, to account for lost motor units, that would enable the patient reach a target force. Predominant UMN ALS patients had decreased firing rates. Predominant UMN ALS patients also lose motor units and one would anticipate an increase in firing rates. However, due to lack of ”central drive”, a motor unit firing rate decrease was observed.

Variability

Variability in predominant LMN patients, compared to control subjects, increased. This was likley because of increased motor unit firing rates. In predomonant UMN ALS patients, we observed decreased variability in motor unit firing rate time series when compared to control subjects. This was likely due to reduced upper motor neuron involvment.

Motor Unit Firing Rate Slopes

During sustained muscle contraction, in the region where the force was stable, motor unit firing rates gradually decreased with time. This is in agreement with motor unit studies done by others [Erim et al 1999]. In some patients, however, we observed dramatic changes in motor unit firing rates as shown in Figure 7.1(b). Fast decline in motor unit firing rates were observed mostly in dominant LMN ALS patients. This was likley due to fatigue as motor units fired at increased rates. Slopes in motor unit recordings from dominant UMN ALS patients were similar to those of control subjects. It could be that fatigue in predominant UMN ALS patients is revealed through other mechanisms such as motor unit substitution which was observed in this group at the 50% MVC.

Onion Skin

At 20% MVC, 75% (3 of 4) of control subjects obeyed onion skin, 75% of predominant LMN ALS patients obeyed onion skin and all ALS patients with predominant UMN pathology obeyed onion skin. Violations of onion skin were observed in subjects at the 50%

MVC. In studies done on the FDI muscle, it has been reported [Erim et al 1999] that in young adults, motor unit firing rate time series obeyed onion skin, where as in elderly subjects onion skin was violated. The mean age of control subjects in our study is less than that of the elderly population in Erim's [1999] study however, it is larger than that of the young population. We would expect to have similar results to the elderly population as observed in other studies [Erim et al 1999]. Our results did not identify any differentiating trend in onion skin phenomenon between control subjects and ALS patients. Hence disobeying onion skin may not indicate whether pathology exists or not.

Polyphasic Potentials

We identified differences in MUAP waveforms recorded from ALS patients. Some MUAP waveforms recorded from patients were generally more complex than MUAP waveforms recorded from control subjects. ALS causes motorneuron loss. Thereafter, surviving axons branch off and reinnervate the orphaned muscle fibers by collateral sprouting. Polyphasic potentials are likely due to reinnervation and denervation of a group of orphaned fibers [Erim et al 1999].

Doublets

Doublets were observed more frequently in the predominant LMN ALS pathology; 29 doublets compared to five for UMN and six for control subjects. This result is in agreement with studies done on doublets by others [Rowiñska et al 1999] where it was found that doublets occurred most in lower motor neuron lesions. Piotrkiewicz et al [2008] observed that the incidence of MUs capable of firing double discharges was significantly higher in ALS patients (28.8%) than in controls (3.9%). However, they did not specify whether the observation was more prevalent in dominant LMN ALS patients. We have found that the incidence of doublets in dominant UMN ALS patients is comparable to that of control subjects.

Substitution

An interesting observation of motor unit firing rate time series was made as shown in Figures 7.6 and 7.7. It was observed that motor unit substitution occurred in individuals with ALS despite the short duration of the contractions performed in the study. Three observations of motor unit substitution were made in the dominant UMN dysfunction ALS patients. Motor unit substitution has been observed before in healthy subjects, but only when contractions of long duration (i.e. minutes) were performed [Westgaard and de Luca 1999]. The observation of motor unit substitution during contractions of short duration suggests an early onset of fatigue in individuals with ALS with dominant UMN dysfunction. Substitution was observed only at 50% MVC. Some investigators have observed that substitution often occurs as a consequence of a decrease followed by an increase in the excitation to the motorneuron pool [Westgaard and de Luca 1999].

Limitations

It was difficult to recruit patients with ALS. One of the reasons is that ALS a debilitating disease that progresses very fast. We were interested in recruiting patients with substansive symptoms so that we could monitor them for a period of six moths. This further put limitations on the recruitment process.

In addition to recruitment, the process was further complicated by the technique we use to obatin precise neuronal information. The process of decomposition from which we can obtain neuronal information is a time consuming process. It is time consuming because most decomposition algorithms are not fully automated. Visual editing by an EMG decomposer takes a long time. The technique can provide precise information however it is not ready for clinical applications yet. Finally in computing statistical tests, we did not adjust for multiple comparisons.

Chapter 9

Conclusion and Future Work

9.0.3 Conlusion

In this study, we characterized motor unit behavior of recordings performed in dominant LMN ALS patients, dominant UMN ALS patients, and control subjects. This objective was achieved by employing a custom built data acquisition system and freely available EMG decomposition software. One of the limitations we had were: (1) small number of subjects and (2) the decomposition process takes several hours to complete. Despite the small number of patients, we observed that there were differences in motor unit firing rate and variability between ALS patient groups and controls subjects. The main observation we made was increased firing rates and increased variability of motor units in dominant LMN dysfunction ALS patients when compared to control subjects; and decreased firing rates and decreased variability of motor units in dominant UMN dysfunction ALS patients when compared to control subjects.

These findings may be useful in early diagnosis of neuromuscular disorders. In addition, these parameters may be utilized in the future to study the rate of disease progression. In addition, features extracted from firing rate time series could be useful as outcome measures in clinical trials. The main advantage of assessing motor unit firing rate is that the disease might be quantified more accurately compared to CMAP and MUNE

meausures that have limited disease (motor neuron) quantification. There are limitations in achieving the result however. EMG signal decomposition for example, due to its complexity, requires a significant amount of time in order to achieve satisfactory results. As a result, it is not practical for clinical purposes at this time. Currently, MUAP parameters are used in the diagnosis of neuromuscular disorders. It is probable that motor unit firing rate time series may provide additional useful information not yet used for clinical diagnosis, mainly because of the difficulty in identifying activities of a given motor unit. Improved techniques in analyzing the data are needed in order to realize the benefits of examining motor unit discharge rates, because even motor unit recordings over a short period of time, about 5 seconds, can reveal relevant neuronal information. For example, variability from a fully analyzed motor unit may be an indicator of pathology and the rate of its progression. It will be useful to develop fast and robust EMG decomposition algorithms that can be applied in clinical settings since the results of decomposition are likely to provide useful information.

9.0.4 Future Work

Our immediate next step is to investigate the in-phase common fluctuations (cross correlation) of concurrent motor unit firing rate time series and to look into nonlinear parameters such as sample entropy. We intend to do a comparison between control subjects and ALS patients. We have performed motor unit recordings in six ALS patients at three and six months after the initial recordings. In the future, we plan on analyzing these data sets (longitudinally assess motor unit firing rate time series). We hope that we will be able to track slow changes in motor unit behavior as the disease progresses. We hope that insight into how ALS disease progresses will be gained.

Appendix A

Development of Data Acquisition System

A.0.5 Hardware Development

We designed and built all hardware components used in the acquisition of the electromyographic (EMG) data. We developed a four-channel EMG amplification unit for recording EMG signals. The amplification unit consisted of four buffers (one for each channel) and differential amplifiers with a gain of 10 in the first stage. The second stage of the amplification unit consisted of a single pole RC high pass filter with a cut-off frequency of 300 Hz, a four pole butterworth low pass filter with a cut-off frequency of 10 kHz and an amplifier with a gain of 50.

A personal computer workstation equipped with an A/D board (16 channel National Instruments 6035E) and LabView software was used to record and display data in real time. A less advanced version of the setup was assembled prior to initiating the study, but modifications turned out to be necessary as summarized below. A significant amount of work was devoted to refining the design and implementation of the pre-amplification unit. Three versions of the preamplifier were built and tested before satisfactory results were achieved. We compared one AC-coupled and two DC-coupled pre-amplifiers. With the first DC-coupled pre-amplifier, we often observed saturation of the input stage. The bias current of the instrumentation amplifiers utilized to build the pre-amplification unit were

excessive given the very small diameter (50μm) of the electrodes utilized. We then built an AC-coupled version of the pre-amplification unit. This version allowed us to overcome the problems we experienced with saturation of the input stage, but turned out to be too noisy. A third version of the pre-amplification unit was therefore designed and implemented by our team with instrumentation amplifiers with extremely low bias current. Polarization of the electrodes was still observed, but below 10% of the input range; therefore with no significant impact on the input range and no negative effect on the quality of the recordings resulted.

Initially we intended to record EMG signals using fine wire electrodes. However the quality of recordings was not satisfactory. This was another problem that we had to resolve; the need for improving the quality of the recordings performed using fine wire electrodes. Although utilized to perform motor unit recordings from other muscles, the fine wire technique led to relatively poor results in our recordings of motor unit activity from the First Dorsal Interosseus (FDI) muscle. We hypothesized that problems were originated by the fact that when using fine wire electrodes, it is difficult to optimally position the electrodes. The relative position of the electrodes and active muscle fibers is in fact difficult to control, i.e. it is a function of the specific area where the electrodes end up after inserting the cannula containing the bundle of fine wires and then removing the cannula to leave the electrodes in place. We also hypothesized that refinement of the position of the electrodes are possible by utilizing a needle with four 50 μm electrodes positioned 200 μm apart from each other and located on one side of the cannula. Figure 2 shows a schematic representation of the needle electrode that we currently use. We worked closely with Viasys (a manufacturer of equipment for neurophysiological recordings) to obtain electrodes of the type described above and that were compatible with the pre-amplification unit we originally designed for fine wire electrodes. This type of electrode is referred to as quadrifilar and allows one to obtain recordings that are superior in quality to those achieved using a fine wire technique.

A.0.6 Software Development

The data acquisition software was developed using LabView. We developed with three software components: (1) the graphical interface for the researchers, which was designed to allow investigators to monitor the quality of the recordings during data collection; (2) the patient user interface, which was designed to provide feedback during the index finger abduction task performed by healthy control subjects and patients with ALS during the experimental sessions; and (3) the ”engine” underlying the graphical user interfaces that allowed continuous data collection and real-time display of the recordings. Figure A.1 shows the graphical user interfaces for the researchers (left panel) and the subjects (right panel). The graphical user interface was modified as we made progress with the data collection and gained practical experience. For instance, we found that researchers were overwhelmed by the amount of information we provided by our first design of the user interface. We simplified the data display by using a raster scan method, i.e. we had the data ”scrolling through” the screen as if we were using an oscilloscope in raster mode. Also, we provided some control of display features to researchers so that they could set how fast data scrolled through the screen.

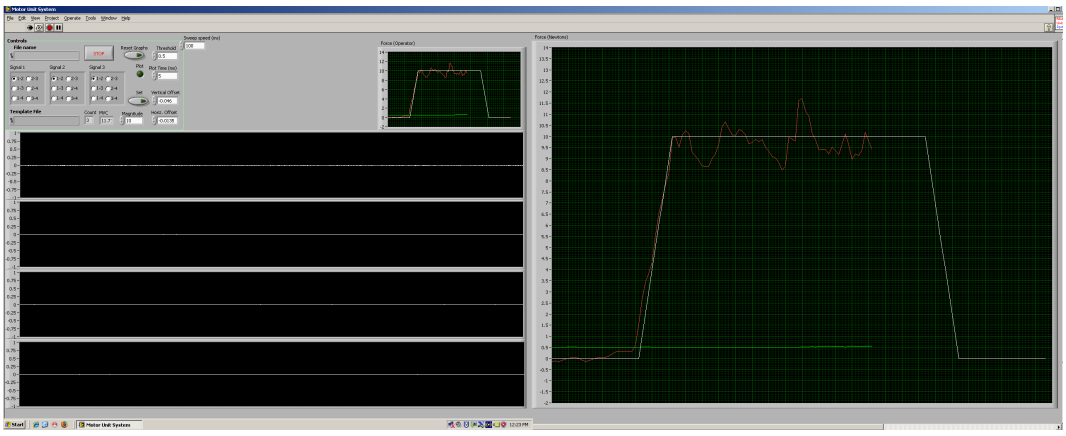

Figure A.1: Data acquisition display interface which we designed using LabView software

Appendix B

Interactive Multi-Channel EMG Decomposition Tool

B.1 Introduction

Most researchers that work with EMG signals record single channel EMG. As a result, most existing EMG decomposition algorithms address single channel EMG. For our purposes, to ensure high quality EMG data, we record multichannel EMG. Below is a description of an interactive, multichannel EMG decomposition tool that was initially developed for this project. Note that this tool was not used in the analysis of the data. Rather, it was replaced by the open access EMGLAB tollbox. It is described herein for completeness.

B.2 Multichannel EMG Decomposition Tool Box

In the following, all of the elements constituting the MatLab software (MU Decomposition toolbox) for multi-channel motor unit (MU) decomposition are described at length. Motor unit decomposition is a process whereby an EMG signal is processed in order to identify motor unit action potentials (MUAPs) and to group them into classes that pertain to a particular MU. The software is composed of a graphical user interface (GUI) that will

appear by entering the command $main\_MU$ at the command prompt. The GUI is composed of three main panels on which MUAPs along different channels are plotted. The left hand side of the GUI contains pushbuttons and list-boxes. This set of pushbuttons and list-boxes provides a means by which a user can interact with the GUI. Also, on the left hand side of the GUI is an information box. It displays relevant guidelines on how to proceed with the decomposition process. Upon starting the GUI, only the START button, located at the bottom left hand corner of the GUI, is active. Pressing this button sets the global variables that will be called at different stages of the decomposition process, and initializes workspace and objects (pushbuttons). The global variables that are set at this level include: the window length of the MUAPs (default setting is 8 ms), which can be altered by the user, and the sampling frequency (set at 25,000 Hz). All the functions that are called by interacting with the different objects in the GUI are designed in such a manner that MatLab workspaces are saved on the hard disk at the end of each decomposition phase. Subsequent sessions of the software use the saved information. This choice has been preferred to the classical operation of passing variables between functions, following a twofold objective: firstly to minimize the amount of memory and processing time dedicated to the software, so that the computation is manageable and secondly to make it possible to repeat a procedure by choosing different parameters if needed, without having to re-start the whole decomposition procedure.

Figure B.1: Flow diagram of $MU\_extractor$, Each function is briefly described through the light blue rounded squares, whereas the data structures are shown in yellow, and the events triggering the functions are represented in black.

All of the temporary workspaces are named $tmp\_MU\_\#\#\#$.mat where $\#\#\#$ is substituted with the name of the function (relating to decomposition stage) that creates them. A flow diagram of the different MatLab functions contained in the MU Decomposition Tool Box is shown in Figure B.1, together with the definition of the input and output variables, and the MatLab workspaces necessary to perform the operations. A screen capture of the MU Decomposition Tool Box, as it appears during the execution of the detection stage, is presented in Figure B.2.

Figure B.2: The MU Extractor GUI as it appears during the execution of one of the procedures.

B.3 Loading Data

The whole procedure starts by clicking Load EMG data, which invokes the function MU_open. This function loads the EMG files, which were saved under LabView with a 123 extension. Loading LabView data files directly eliminates the need of converting LabView data into a MatLab workspace format. At present, this function assumes the presence of multiple segments, where each segment represents a thirty-second recording (trial) of EMG data. If the experimental protocol for trial duration or channel order were to be changed, both the LabVIEW virtual instrument for data acquisition, and the parameters for loading data, would need to be changed accordingly. At the end of the procedure, the entire trial will be shown in the three panels. The top panel shows a plot of force data, whereas the lower two panels show plots of motor unit activity of the four EMG channels recorded, two per panel. An overall trial of eight repetitions corresponds to more than 250 M bytes and as a result the software will be slow. It is bearable since this operation is done only once. This function saves the overall trial in the workspace $tmp\_MU\_open.mat$

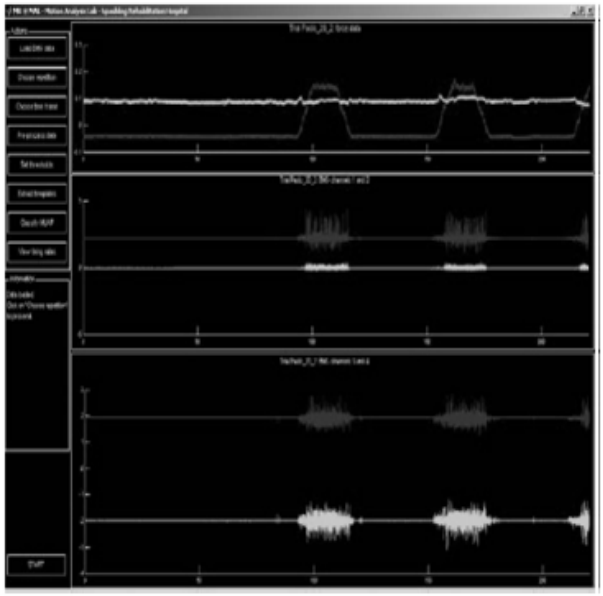

Figure B.3: Showing one whole session containing different repetitions of the task.

B.4 Choosing the repetition

A repetition (part of a trial) here refers to a thirty-second recording of motor units when the subject produces a force. This part of the software is executed by clicking on Choose repetition pushbutton, which invokes the function $MU\_segment$. In this part the user has the option of choosing a trial that represents one of the different repetitions of the

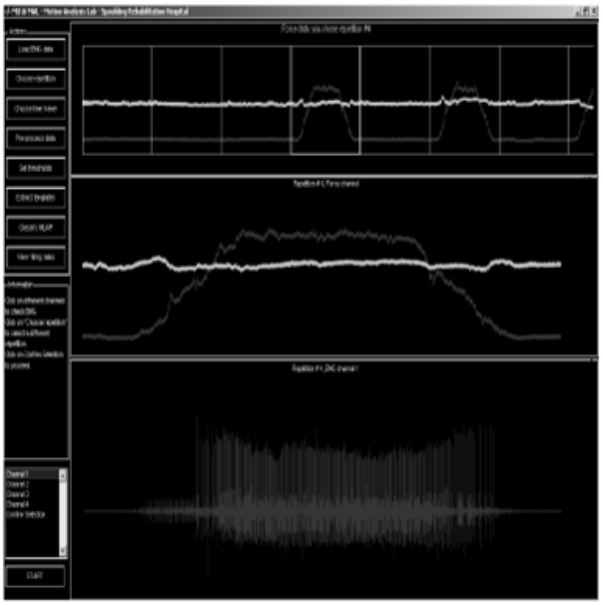

Figure B.4: showing chosen repetition enclosed in Yellow Square.

entire session recording, by directly clicking on that particular repetition. In this case, the trial enclosed in the yellow square is the chosen trial. The middle panel of the GUI shows two plots of the forces generated by the subject. The blue plot shows vertical force that will show negligible values due to shaking. The other force data are plotted in red and relates to MU activity. The bottom panel of the GUI shows motor unit activity on one of the channels. It clearly indicates that motor unit activity increases with increasing force. The user can scroll among the different channels by using the list box on the left bottom side. When the selection of a chosen repetition is confirmed, the software saves the selected repetition in the MatLab workspace $tmp\_MU\_segment.mat$.

B.5 Choosing the time frame

The current design of the GUI invites the user to choose a time frame once the repetition has been chosen. The selection of this time frame is based on the graphical display and the selected portion of the EMG signal is where the initial templates are generated from. The $select\_time\_frame$ feature is invoked by clicking on Choose time frame. The

purpose of this section of the decomposition process is to select a time from which the initial templates will be generated. Our approach is to select roughly a 500 ms window along the plateau of the force data plot. To perform this operation, the user can choose the window by clicking on two different time locations in the upper panel. We anticipate that most MUs will appear during this time since this period corresponds to the time of maximum force generation. This half-second of data is saved and will later be plotted so that the threshold for detecting spikes can be set across all the channels. At the end of the procedure, the functions will store in memory the frame range to be used to set the thresholds and extract the templates.

Figure B.5: Shows chosen frame (yellow bars). A plot of motor units between the two bars appears in the lower panels of the GUI

B.6 Preprocessing data

This part of the software is one of the four core stages in EMG decomposition. It is invoked by clicking on Preprocess data, and is performed by the function $MU\_preprocess$. It performs three operations: *First*, it computes two additional software-derived channels. Since the four channels are taken as a differential voltage between the successive sensors (i.e. *s1=potential1 - potential2*, *s2=potential2 - potential3*, *s3= potential3 - potential4*, *s4=potential4 - potential1*), the software digitally extracts the remaining two combinations (*s5=potential1 - potential3* and *s6= potential2 - potential4*). These software derived channels may not be as accurate as hardware derived channels and hold redundant information.

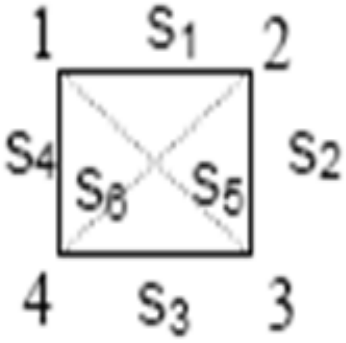

Figure B.6: Schematic of reconstructed signals from 4 different voltages acquired.

However they may provide useful information that could be missing on the hardware channels. *Second*, the EMG data are band pass filtered. The user can choose the cut-off frequencies for the band pass filter. The filter itself is FIR with an order of 200. The default values of the filter frequencies are set at 1000 Hz and 8000 Hz, for the high pass, and low pass cut-off frequencies, respectively. The filtering is done by forward filtering and then reverse filtering, which ensures zero phase distortion. It has been found that both IIR and FIR implementations might introduce ringing, so in some cases it has been found necessary to bypass the filtering. Inserting the value 0 for the corner frequencies bypasses filtering. And *Third*, sub sample and low pass filter force data. Also in this case, the function lets the user choose the corner frequency of the low pass filter, and the selected new sampling rate for the force channel. The default values have been set at 100 Hz, and 500 samples per second. At the end of the procedure, the function will store the whole preprocessed repetition, and the corresponding time frame for setting the thresholds, in $tmp\_MU\_preprocess.mat$ and $tmp\_MU\_preprocess\_frame.mat$, respectively.

B.7 Setting the thresholds (Detection)

The algorithm for MU decomposition has been developed in a parallel fashion with no hierarchy among channels either in the detection phase or in the classification phase. It is therefore critical, as a way of ensuring a more robust approach, to set the thresholds for each of the six channels independently, so that the probability to detect MU waveforms with different signal to noise ratios among channels is maximized. It has been agreed

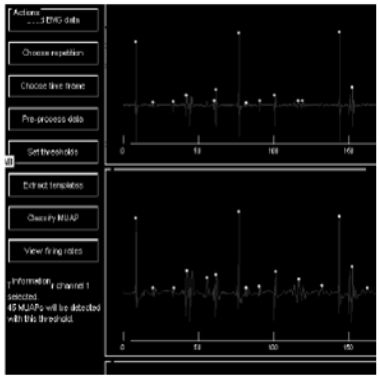

Figure B.7: Waveforms with a dot at their peak amplitude indicate that their peak amplitudes are above the set threshold for detection.

upon to manually (via visual inspection) set the threshold, instead of selecting it automatically based on statistical features of the signals under consideration. One of the reasons the threshold is selected manually is due to the intrinsic nature of the experimental protocol. It consists of 5 seconds of rest, 20 seconds of contraction, and 5 seconds of rest. This makes it more difficult to identify the threshold based on a statistical approach; plus, the manual procedure is not very time consuming, as compared to the automatic selection, and is more reliable. This procedure is accomplished by the MU_detect and MU_update_triple functions, which are invoked by clicking on Set thresholds. The GUI has a zoom in feature that permits a user to clearly see which MUAPs are above noise and given this visual feedback a reasonable threshold is set. The GUI also shows the number of MUAPs that would be detected within the time frame chosen during the Choosing the time frame phase, should one proceed with this particular threshold. Peaks of each detected MUAP waveform are also shown on the panel, to help the user understand if there are MUAP waveforms missing. Figure B.7 shows a detailed picture of the GUI as it appears in this phase. If the threshold is negative, because the user would like to consider the negative peaks, the procedure will work by detecting values below that threshold. After all the thresholds have been set for all the channels, the function saves the detected MUAP waveforms and the thresholds in the workspace $tmp\_MU\_detection.mat$. The detection of the MUAP waveforms is performed according to the following:

1. All spikes above a set threshold (on a channel by channel basis) are detected. This ensures that we will classify MUAPs that are above the noise level.

2. Looking at all spikes that appear above the set threshold and are at least 50% of

the MUAP window apart identifies distinct MUAPs. Based on the default value of the window size of 8 ms, if a spike occurs 4 ms or greater away from the previous spike that is above noise then it is considered a new MUAP. This rule also means that if the time interval between two spikes of an 8 ms window is less than 4 ms on the same channel, the spikes in question are considered constituents of one MUAP. With reference to Figure B.8, some of the different possibilities are shown: the first MUAP (AA) is detected over all three channels, with negligible temporal offset between them, the second MUAP (BB) is not detected by any of the channels, since it appears at less than 4 ms from the first detection. The third MUAP (CC) is detected by two of the three channels, still with negligible temporal offset across channels. The fourth MUAP (DD) is not detected, for the same reason explained for BB. The same issue applies to MUAPs EE and FF. GG is detected only in the third channel, whereas HH is detected on the other two channels. At the end of the detection phase, thus, 11 MUAP waveforms are detected.

B.8 Extracting Templates

The overall procedure has been designed in such a way that a number of templates are available before the beginning of classification. Templates are manually extracted from the 500 ms frame that was selected as described in subsection B.5. The assumption made here is that most MUs of interest will be active during the plateau of the force

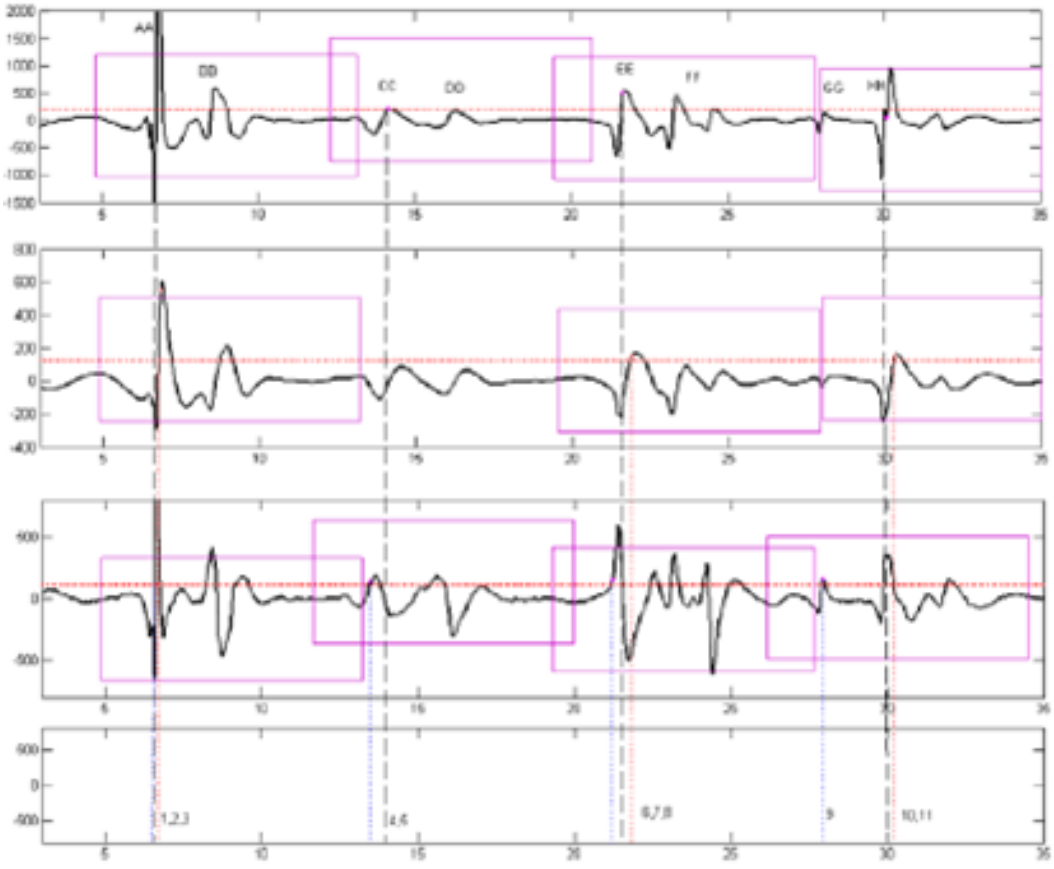

Figure B.8: A sample showing EMG data on three different channels, the time occurrences of the detected MUAPS along and across the channels are also represented in the bottom panel.

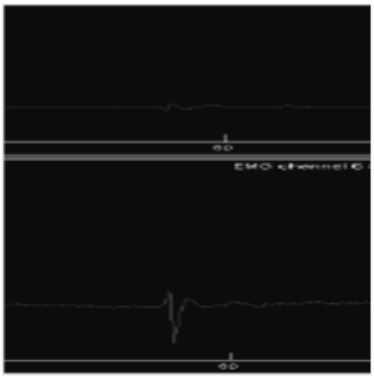

Figure B.9: showing an almost non existent MUAP on the top channel and clearly defined MUAP on .

generated. So by selecting a window of approximately 500 ms, see Figure B.5, the algorithm is able to extract templates that pertain to most MUs that are recruited. Waveforms corresponding to these templates are expected to appear throughout the entire recording of EMG data. To accomplish this objective, the Extract templates push button invokes the function $MU\_extract\_templates$. This function only operates on the frame range selected in the extract frame phase. The $MU\_extract\_templates$ function's inputs are the information pertaining to MUAPs that have been detected during the detection phase. This information includes the time at which a detected MUAP occurs (start time of the detected MUAP), and the channel in which it has been detected. The following two parameters can be chosen by the user before the procedure begins: Inter channel delays (temporal off-set of the occurrence of MUAPs across channels that pertain to the same MU), and the weighted vector cross-correlation threshold.

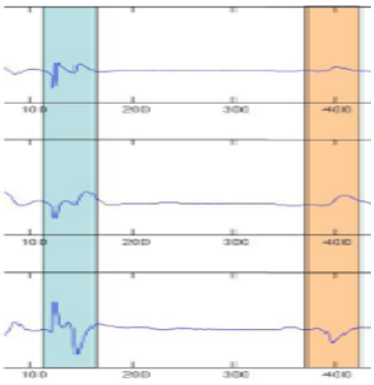

Figure B.10: A sample of a MUAP wave form across 3 different channels: for each of the three channels, a normalized cross correlation will be computed.

Weighted vector cross-correlation is preferred because we are matching multi-channel waveforms (MUAPs that display across channels but are considered one MU because they occur at almost the same time). The reason it is preferred is because it is possible to have a MUAP on one channel, with a high signal to noise ratio and that same MUAP on another channel with a low signal to noise ratio as shown in Figure B.9. From Figure B.9, it is clear that the MUAP on the upper channel is noisy and we will be correlating noise instead. To overcome this problem, the power (weighted) of each MUAP of a multi-channel template is computed. In order to see whether a selected multi-channel wave form cor-

responds to a given template, cross correlation values of corresponding channels are computed, multiplied by their corresponding weights and then summed and normalized by the sum of weights.

A detailed description of how the algorithm handles the extraction of templates follows below

1. First and foremost, temporal information across channels is merged. The algorithm compares occurrence times across channels. Temporal offsets that are within half the window size are considered to represent the same MU across channels. Temporal information of the MUAP with the highest power is registered.

2. Then, to identify unique wave forms (templates) that will represent the different MUs, a classification is performed. Wave forms (pertaining to the same MU across all channels, i.e. occurring at almost the same time) that correlate well with at least three other waveforms (note that a wave form here refers to a set of waveforms that have similar temporal information across channels) are considered templates. The classification is based on average weighted vector cross-correlation.

3. Now, if the weighted cross-correlation value is over the threshold chosen by the user, the two MUAP waveforms will be considered as candidates for corresponding to the same class.

4. It might happen that a MUAP waveform is a candidate for more than one class: in this case, it will be considered as belonging to the class for which the highest value of the weighted vector cross correlation is present

5. If occurrences of the same class appear at less than 10 ms intervals, one of them (the one with the lowest weighted vector cross correlation value) is retained.

6. Templates are checked against each other to ensure that all templates are unique. Those templates that are similar are, at this stage, merged.

B.9 Classification

Each template extracted during the 'Extract Template' phase represents a distinct motor unit (MU). The extracted templates and the pre-processed data set serve as the inputs to the classification algorithm once the Classify MUAP push button is pressed. This button calls the $MU\_detect\_classify\_frames$ function. Four parameters can be selected at this stage: the jitter, weighted vector cross-correlation threshold for classification, buffer size (number of averaged MUAPs to update templates), and weighted vector cross-correlation threshold for new template creation.

1. The classification starts at the beginning of the chosen repetition (a motor unit recording) by taking a one second window of the pre-processed data. Within this one-second window, the algorithm first detects spikes above channel thresholds (determined during the 'setting the thresholds' phase) as explained in the detection procedure under the 'setting threshold' stage. The predetermined templates (each being a vector of waveforms across channels) are then slid along the data. The technique employed performs parallel-normalized cross correlation (weighted vector cross-correlation) across all channels at a given time instant. From a set of cross correlations across all the channels, a weighted vector cross-correlation is determined and if it is above a set threshold, the MUAP in question is classified as possibly belonging to the same class as the template. Again, if this waveform has been classified (i.e, is above threshold) with more than one MUAP template, it will be classified with the MUAP template with the highest weighted vector cross-correlation value. Once it has been classified, only the occurrence time in the channel whose corresponding MUAP template has the highest variance is retained.

2. Next, the algorithm aligns every classified spike with its corresponding template and then takes the average as a way of keeping the template updated and this keeps track of gradual changes in spike shapes due to the non-stationary nature of the

MUAPs. The number of averaged spikes is limited to ten spikes that are closest in time by default, and can be changed by the user. This means that once the buffer reaches a count of ten classified MUAPs, any newly classified MUAP will be added to the buffer and the first MUAP will be dropped before the template is updated. It follows a FIFO (first in first out) approach.

3. An attempt to identify new templates during the classification process is made. The algorithm searches through the set of unclassified MUAPs. If it finds a MUAP that has at least five closely related spikes (i.e. with values of the weighted vector cross correlation higher than the threshold) in this particular window, a new template and therefore class is generated. The newly generated template is compared to all existing templates to ensure that it is indeed a unique template with respect to the already existing templates. In case this newly generated template matches any of the existing templates, it is merged with that particular template.

4. At this point, those MUAPs that are still unclassified are manually checked. This is achieved by visually sliding templates along the detected spikes and if there is a match, a MUAP is added to a class to which the given template pertains.

B.10 Super position Resolution

Currently the classification algorithm attempts to classify most MUs automatically. However, since the algorithm is not perfect, it is common to have MUAPs that cannot be classified automatically by the classification algorithm. MUAPs that are not classified are represented as 'x's in the lower panel of the GUI whereas circles represent MUAPs that have been classified. Three of the probable reasons as to why some MUAPs cannot be classified are described below;

Figure B.11: A motor unit that has been classified manually (colored). The template which matches the motor unit shown in white. This template is composed of six waveforms from across all channels.

1. A particular MUAP that has been detected may actually belong to a particular MU but it may not be assigned to that class simply because its cross-correlation is slightly below the set threshold due to the presence of noise.

2. A detected MUAP in question may be a superimposition (sum) of two or more waveforms pertaining to different motor units that might have fired at roughly the same time. This summation distorts the waveform and therefore it cannot be classified.

3. Some unclassified MUAPs will belong to a class of a MU that was not detected because it does not appear at least five times in a period of a second and therefore was disregarded as a class (MU).

To work with this part of the software, an interactive way of classifying the remaining MUAPs has been developed. By clicking on the Manual classify push button that appears on the bottom left, the user will be able to interact with the lower panel, by clicking and picking each of the unclassified MUAPs. This portion of the software is called $tmp\_MU\_manual\_classify$. When an unclassified MUAP is picked, the upper panel will show the template across all channels, superimposed with the first template, aligned to maximize the cross-correlation coefficient. If the user is happy with the matching, he/she can click on classify: in this case, the instances of that template will be updated with the new classified one, and the unclassified group will be updated as well. The push button, next, will let the user scroll through the different templates, to check for the best matching template. If the detected MUAP waveform appears as a superimposition of the different detected MUAPS, the user is left to choose between two different ways, as proposed by McGill [McGill 2002]. First is the known identities case, in which case the templates involved in a superimposition are known a priori. In this case the user can pick the templates that appear as the most likely constituents of the superimposition. The software then resolves the superposition by finding the minimum RMS error between the combination of different superposition between templates, and the current detected MUAPs. In

this case, the best matching superposition is shown, and the GUI lets the user choose if this superposition resolution fits. The second way to resolve superposition is to let the software decide which is the best combination between the different templates. In this case, the software makes an exhaustive search among all the possible templates and superpositions, and for each combination of templates, extracts the superposition with minimum RMS error. The user can also manually select possible combinations among different templates, and identify those that fit best. Since the procedure performs an exhaustive search among all the possible combinations between extracted templates and corresponding delays, the procedure is slightly slow (i.e. around 25-30 s per template combination), so that, if the number of templates is higher than five, this part is practically very slow and should not be performed. In both cases (i.e. known identities, and unknown identities), if there's no good fit, the user can disregard the superposition. If the result of the superimposition has been accepted, the time occurrences of the classes compounding the superposition are updated. In any case, the manually classified waveforms will not be used to update the templates, since their weighted vector normalized cross correlation value is below the threshold, and they might introduce noise or artifact coming from other MUAPs in the case of superpositions.

B.11 View Firing Rates

Once the EMG data have been wholly analyzed (the analysis of an entire recording might last 60-90 minutes), the user has an option of clicking on the View firing rates push button, to see the mean firing rate of each motor unit and the motor unit firing rate time series. In the upper and middle panels of the GUI, the mean firing rate of each motor unit will be presented, with color codes corresponding to their respective templates in the lower panel. The lower panel displays the motor unit firing rate time series as a classic bar plot, which shows the location of each of the MUAPs of individual motor units, via single lines

in correspondence to MUAP time occurrences, superimposed on the time series of the force exerted by the muscle. This plot is generally used to show the motor unit recruitment behavior as a function of force generated by the muscle as shown in Figure B.12. The mean firing rate time series is arrived at by taking the inverse of forward differences between the spikes. A moving average filter is used to smooth the resulting firing rate information. In order to to be able to utilize classical data analysis techniques such as the Fourier transform, the time series of the firing rates is then periodically resampled using cubic Lagrange interpolation.

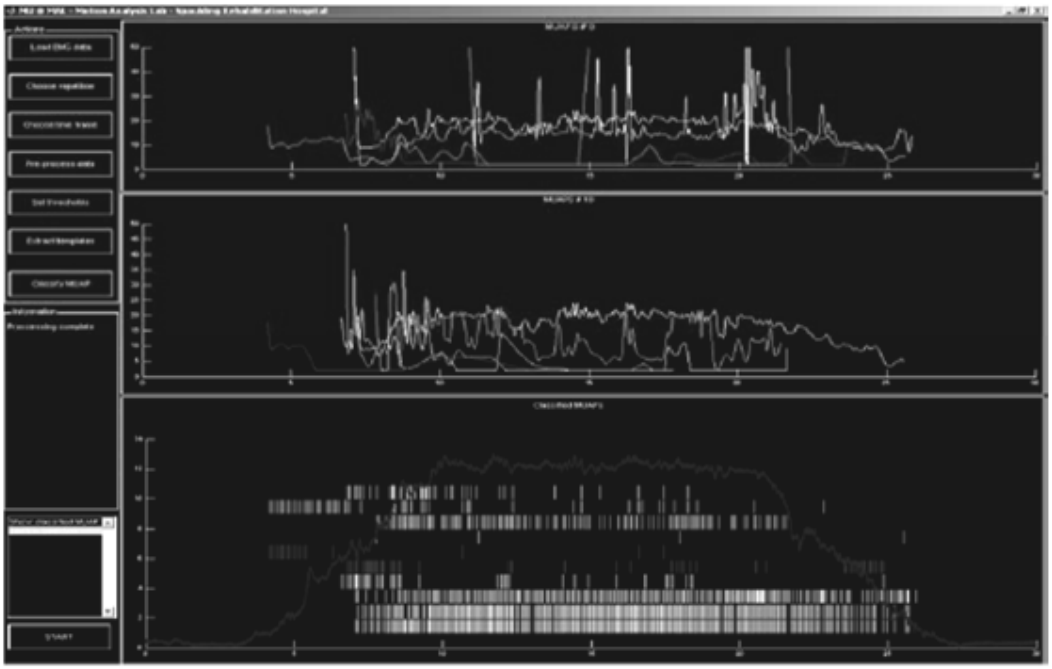

Figure B.12: Motor unit time series. Each bar plot in the bottom panel shows the interfering interval of a distinct motor unit. The top panels show firing rate of an individual motor unit.

B.12 Conclusion

The goal of the EMG decomposition system is to reliably break down complex EMG signals into its constituents. The decomposition system consists of four main stages. The first stage pre-processes the four channel recorded EMG data. The second stage

performs detection. The third stage classifies the detected MUAPs into groups pertaining to different motor units. The fourth stage resolves superimpositions that cannot be clearly classified. Classification is implemented by template matching based on cross-correlation. The resolution of superimposed MUAPs is based on the 'Optimal Resolution of Superimposed Action Potentials' algorithm developed by McGill [McGill 2002]. An 'EMG viewer', developed by Clancy, is be used to manually resolve superposition that cannot be resolved by the 'Optimal Resolution of Superimposed Action Potentials' developed by McGill.

Appendix C

Stochastic Processes

C.1 Stationary Stochastic Processes

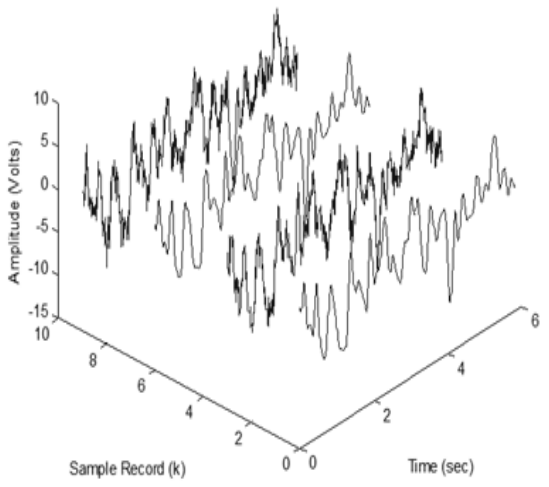

Figure C.1: Showing sample functions of a random process.

Figure C.1 shows a group (ensemble) of functions which can be either real or complex valued functions. This ensemble of functions is denoted by $\{\ x_k\ (t)\ \}$, where k and t are variables representing sample function and time, respectively, and can be defined through their probability distributions. Collectively, they are known as a stochastic process (also known as a random process or time series). A sample function by itself is defined as $x_k(t)$, where t is varying and k is fixed. It can be perceived as the outcome of a single experiment. Therefore all possible experiments represent a sample space of index k. Stochastic processes are classified as either stationary or non-stationary. Any observation that is considered to be a stochastic processes can have its properties defined at any given time instance. It is possible, for example, to estimate its first moment at

a given time t. This is achieved by taking the instantaneous value of each sample function at a given time t and finding the mean of those values together (ensemble average across k) as given in equation C.1a. Similarly, the autocorrelation function can be estimated by taking the ensemble average of the product of instantaneous values at two different instances, t and $t+\tau$. The assumption made here is that each sample function is equally likely. In this document we limit ourselves to stochastic processes that are stationary and ergodic (stationary stochastic processes are classified as either ergodic or non ergodic).

$$\mu_x = \lim_{N\to\infty} \frac{1}{N} \sum_{k=1}^{N} x_k(t) \tag{C.1a}$$

$$R_{xx}(t, t+\tau) = \lim_{N\to\infty} \frac{1}{N} \sum_{k=1}^{N} x_k(t) x_k(t+\tau) \tag{C.1b}$$

When the the $\mu_x(t)$ and $R_{xx}(t, t+\tau)$ values of a stochastic process do not vary as t changes, this particular stochastic process is said to be stationary in the wide sense (*weakly stationary*). In other words, for a stochastic process that is stationary in the wide sense, its mean is a constant and its autocorrelation is only dependent on the time displacement τ. In a situation where an infinite set of higher-order moments of a stochastic process can be realized in order to have all underlying probability distribution functions that describe the process and given that the moments do not vary with time, then this process is said to be stationary in the strict sense (*strongly stationary*). For practical purposes however we would only verify wide sense stationarity.

C.1.1 Ergodic Stochastic Processes

There are cases when it is not possible or convenient to observe more than a single time history of a stochastic process. For any given sample function $x_k(t)$, one cannot generally conclude that it is a suitable representation of the entire stochastic process to which it belongs. However, for a stationary stochastic process, it is possible to compute moments for individual sample functions. The k^{th} sample function mean value $u_x(k)$,

autocorrelation and auto covariance functions computed by time average are defined in the equations below:

$$\mu_x(k) = \lim_{T\to\infty} \int_0^T x_k(t)dt \tag{C.2a}$$

$$R_{xx}(\tau, k) = \lim_{T\to\infty} \int_0^T x_k(t)x_k(t+\tau)dt \tag{C.2b}$$

$$\begin{aligned} C_{xx}(\tau, k) &= \lim_{T\to\infty} \int_0^T [x_k(t) - \mu_x(k)][x_k(t+\tau) - \mu_x(k)]dt \\ &= R_{xx}(\tau, k) - \mu_x^2(k) \end{aligned} \tag{C.2c}$$

For a stationary stochastic process, if $\mu_x(k)$ and $R_{xx}(\tau, k)$ are the same for any sample function, then the stochastic process is said to be ergodic. Therefore, for a stochastic process to be ergodic, first it has to meet stationarity criteria. Ergodicity also means that the time averaged mean value, autocorrelation and auto covariance functions (as well as other time averaged values) are equal to their corresponding ensemble average, autocorrelation auto and covariance functions $\mu_x(k) = \mu_x$, $R_{xx}(\tau, k) = R_{xx}(\tau)$ and $C_{xx}(\tau, k) = C_{xx}(\tau)$ respectively. In summary, an ergodic stochastic process is a sub set of a stationary stochastic process. Any given sample function of an ergodic stochastic process is a true representative of all other sample functions.

C.2 Analytic methods

C.2.1 Digital Filtering

Filtering of time or space series in order to manipulate frequency or wave numbers of signals is essential and is increasingly done digitally. Digital filters utilize a processor to manipulate (typically multiplications and additions) sampled signals. If desired, the output of digital signal processors (sampled values of the filtered signal) can be transformed

back into analog form. A class of linear time invariant (LTI) systems that are characterized by linear difference equations with constant coefficients is the most important to the application of digital signal processing [Proakis and Manolakis]. Even though it is also possible to construct nonlinear filters, in this document we focus on filters which are linear and time invariant. The general equation characterizing LTI constant coefficient systems is given by

$$y(n) = \sum_{m=0}^{M-1} b_m x(n-m) - \sum_{l=1}^{L-1} a_l y(n-l) \tag{C.3}$$

where x is the input sequence, y is the output sequence and n is the discrete time index.

Linear time invariant systems are subdivided into two systems (filters):

- finite impulse response (FIR)
- infinite impulse response (IIR)

In implementing filters, it is essential to have minimal phase distortion while achieving the desired frequency response of time series. We will concentrate our analysis on filters which are themselves linear time invariant systems. This will enable us to apply all of the techniques that we have previously developed for LTI systems to analyze the performance of the filter. However, it is also possible to construct more complicated nonlinear filters which are not LTI systems.

Finite Impulse Response Filtering

Finite impulse response (FIR) filters are systems which have finite duration impulse responses. They are easy to implement (convolve time series with the impulse response of filter). One advantage that FIR filters have is that they are inherently stable since they do not have feedback (recursive components). In addition, FIR filters introduce very minimal distortion of the signal because of they can have a linear phase response characteristic.

If the a_l coefficients in equation C.3 are equal to zero for all l, then the difference equation characterizes an FIR filter and it is given by

$$y(n) = \sum_{m=0}^{M-1} b_m x(n-m) \tag{C.4}$$

Infinite Impulse Response Filtering

Unlike FIR filters, IIR (recursive) filters are not inherently stable due to feedback and further, do not have a linear phase response characteristic. First of all designing IIR filter is cumbersome since one has to ensure that they are stable and because they can exhibit significant phase distortion.

C.2.2 Autocorrelation Function Estimation

Autocorrelations can be estimated in two different ways. The first method is through computing an average of products among sampled values. The second method is through the estimation of the auto-spectral density using Fast Fourier Transforms (FFT), and then taking the inverse Fourier transform. The first method (averaging of products) is relatively simple but expensive in terms of its computation where as the FFT approach is efficient and more practical and is described below.

Autocorrelation via FFT

Let $x(n)$ be a signal, with N samples that are equally spaced, that is stationary and has zero mean. Based on the Wiener - Khinchine relations, its autocorrelation can be defined as,

$$R_{xx}(\tau) = \frac{\sum_{k=0}^{N-1} S_{xx} e^{j2\pi k \frac{n}{N}}}{N} \tag{C.5}$$

where S_{xx} is the auto spectral density function of $x(n)$. In other words the autocorrelation function is determined by taking the inverse Fourier transform of the auto spectral den-

sity function. Due to underlying periodic assumptions of the discrete Fourier transform, this procedure is 'circular in character [Bendat and Piersol]. The resulting autocorrelation function will therefore appear as though it were computed from a periodic function. This problem is overcome by adding N zeros to the original signal. Once the data are appropriately zero padded, we can obtain the autocorrelation by taking the inverse Fourier transform of the product of the Fourier transform of $x(n)$ and the complex conjugate of Fourier transform of $x(n)$.

C.2.3 Spectral Density Functions

The power spectral density defines how the variance (power) of a signal is spread with frequency. Estimates of functions of auto power spectral densities can be achieved in two ways;

- Classical (non-parametric) Methods
- Model based (parametric) techniques which are usually employed in situations where it is only possible to acquire short data records and none of the other techniques give satisfactory results.

A long time ago, the power spectral density of a signal used to be computed by taking the discrete Fourier transform of the autocorrelation estimate of the signal. A more common approach, recently, is formed by taking the squared modulus of the fast Fourier transform (FFT) of the signal, scaled by the length of the FFT. In this section, a description of the discrete Fourier transform (DFT) and power spectral density estimation based on the direct DFT of a signal will be given.

The Discrete Fourier Transform

Let x(nT) be a sampled causal sequence, where T is a sampling interval. The Fourier transform of x(nT) is given by

$$X(f) = \sum_{n=-\infty}^{\infty} x(nT)e^{-j2\pi fn} \tag{C.6}$$

For a finite sequence of length N,

$$X(f) = \sum_{n=0}^{N-1} x(nT)e^{-j2\pi fn} \tag{C.7}$$

The inverse Fourier transform is given by

$$x(nT)(\tau) = \frac{\sum_{k=0}^{N-1} X_k e^{j2\pi k\frac{n}{N}}}{N} \tag{C.8}$$

The drawback with the above representation of Fourier transforms, for digital applications, is the frequency variable is not discrete. In order to define a discrete Fourier transform, a sampled version of the frequency waveform is desired. If we assume that $X(\omega)$, where $\omega = 2\pi fn$, is periodic with period 2π, only samples in the fundamental frequency are necessary. Taking N equidistant samples in the interval $0 \leq \omega \leq 2\pi$ with a spacing of $f_\omega = \frac{2\pi}{N}$ we can evaluate ω by

$$\omega = \frac{2\pi k}{N} \tag{C.9}$$

$$X(\frac{2\pi k}{N}) = \sum_{-\infty}^{\infty} x(n)e^{-j2\pi kn/N} \tag{C.10}$$

Since the above summation above can be subdivided into an infinite number of summations, we can take a single summation using the same number of samples in one period of the repeating frequency domain waveform as is in one period of the time domain. The DFT pair obtained is a good approximation to the continuous variable Fourier transform

pair. Then the discrete Fourier transform is given by

$$X(k) = \sum_{n=0}^{N-1} x(n) e^{-j2\pi kn/N} \tag{C.11}$$

and the inverse discrete Fourier transform is given by

$$x(n) = \frac{1}{N} \sum_{n=0}^{N-1} X(k) e^{-j2\pi kn/N} \tag{C.12}$$

Auto Spectral Density

The most common method of estimating the power spectrum of a signal is the direct FFT approach. It is efficient and easy to implement however several techniques are performed as a way of improving the estimates. Given a set of data $x(n)$ of length M and that this data set is stationary with zero mean, first we segment it into n continuous segments of equal length N. The power spectrum estimate of each segment is estimated and then averaged as given by

$$\hat{S}_{xx} = \frac{1}{nN} \sum_{i=1}^{n} |X_i(f_k)|^2 \tag{C.13a}$$

for two sided spectrum and

$$\hat{T}_{xx} = \frac{2}{nN} \sum_{i=1}^{n} |X_i(f_k)|^2 \tag{C.13b}$$

for a one sided spectrum where

$$X_i(f_k) = \sum_{n=0}^{N-1} x(n) e^{-j2\pi kn/N}$$

Note that equation C.11 generates values at discrete frequencies of $f_k = \frac{k}{T} = \frac{k}{N\Delta t}$. But if we normalize Δt to 1, then $f_k = \frac{k}{T} = \frac{k}{N}$

Zeropadding

Zero padding of the data sequence does not add new information but rather interpolates the spectrum. Figures C.2 and C.3 show power spectral densities of a non-zero and a zero padded version of the data respectively.

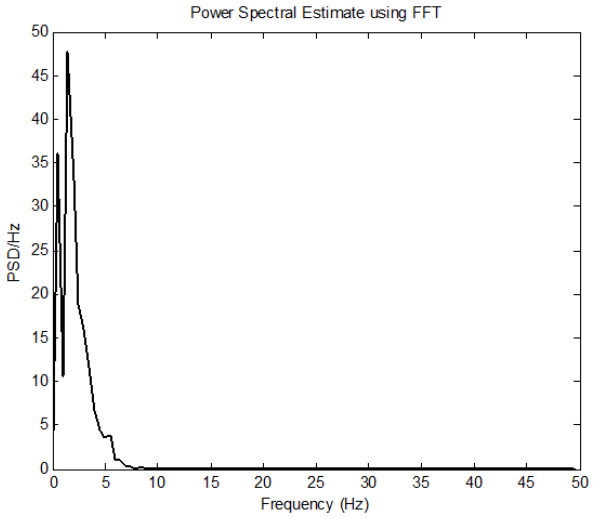

Figure C.2: Power spectral density of non-zero padded time series data

It is important to note that zero padding does not improve frequency resolution which is solely determined by the length of data segment under inspection.

Windowing

Using the DFT to estimate the power spectral density poses some challenges. In deriving the DFT of a single record, an assumption that the data sequence is a single period from a periodic sequence was made. Due to discontinuities at the boundaries of pseudo periods, very high frequency components will be introduced in the data sequence. To mitigate this problem, a technique called *windowing* is employed. Discontinuities at the edges of each period of the data sequence are reduced. In other words, the windowing method reduces the sequence amplitudes at the boundaries in a gradual manner, significantly reducing the aliased frequency components. One of the trade offs with windowing, since data are

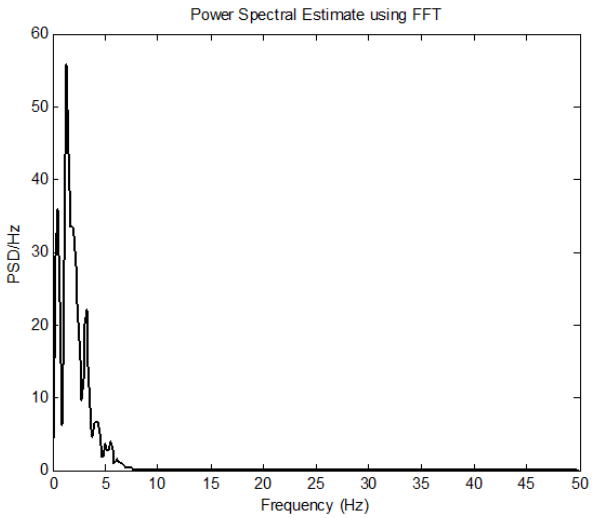

Figure C.3: Power spectral density of zero padded version of data whose power spectral density is shown in Figure C.2, plotted against the force trajectory during isometric muscle contraction

modified before the DFT is computed, the frequency estimate will be biased. Further more, the main lobe increases in width, a phenomenon known as leakage of power. It is desirable to use a window that does not compromise the quality of the power spectrum. One of the most commonly used window is the Hanning given by

$$w(n) = \begin{cases} \frac{1}{2}(1 - cos(\frac{2\pi n}{N-1})), & 0 \leq n \leq N-1 \\ 0, & otherwise \end{cases} \tag{C.14}$$

Where N is the number of samples.

Averaged periodogram

The periodogram PSD estimation for a sequence x(n) of length N is defined by equation C.13 above. In the practical world, signals are associated with noise (or the signal is stochastic itself), and therefore the DFT of a single sequence from a continuous time frequency does not give satisfactory results. To evaluate how good the estimate is, confidence intervals are defined as described in [Bendat and Piersol]. A method to improve

the spectral estimates is by taking multiple sequences from the same signal, assuming that they are identically distributed (IID) random variables, and ensemble average their power spectrum. An issue that arises when taking segments of data from the main sequence is that of spectral resolution, or the minimal separation distance between two adjacent spectral peaks in which the peaks can still be distinguished. The variance exhibited by periodogram-based spectral estimates may be reduced by a factor of approximately 1/K by simply averaging the periodograms from K different realizations of a stationary random signal. As the theory dictates, the variance of the spectral estimates is reduced by employing periodogram averaging. Since only a finite length data segment is typically available for analysis, there is an inherent trade off using periodogram averaging between the number of segments to average and length of the data segments used to compute the periodogram estimates. The periodogram approach, introduced by Bartlett was further modified by Welch. The modifications include

- overlapping
- windowing data before computing periodogram

Due to windowing, variability increases in the resulting spectral estimates [Bendat and Piersol]. This is so because data at the beginning and at the end is essentially discarded. For example, the normalized random error is, $\epsilon = 1/\sqrt{(n)}$ for non windowed data where as if windowed with a Hanning window it becomes $\epsilon = \sqrt{(2/n)}$. This has increased the variance by two. Overlapped techniques can be employed, generating more windows as a way of decreasing variability. A 50% overlap is commonly used and it recovers about 90% of stability lost [Bendat and Piersol]. The one sided Power spectral density of a modified periodogram is given by

$$\hat{P}_{xx}(f) = \frac{2}{NL}|\sum_{n=0}^{N-1} x(n)w(n)e^{-j2\pi fn}|^2 \tag{C.15}$$

L is the normalization factor of the window $w(n)$ used and is defined by

$$L = \frac{1}{N}\sum_{n=0}^{N-1} w^2(n) \tag{C.16}$$

C.2.4 Coherence

Coherence between two stationary zero mean random processes $x(t)$ and $y(t)$, at a given frequency f, is given by

$$\lambda_{xy}(f) = \frac{S_{xy}}{[S_{xx}S_{xy}]^{1/2}} \tag{C.17}$$

where $S_{xy}(f)$ is the cross spectral density and $S_{xx}(f)$ and $Syy(f)$ are the auto spectral density functions. The squared magnitude of coherence provides a bounded measure of linear association between two time series [Myers et al 2004]. For a perfect linear relationship, coherence is 1 and 0 for uncorrelated signals. Since in practice we are normally limited to single realization of a given stochastic process, it becomes necessary to segment the time series into multiple windows. Then the estimate of the magnitude coherence squared is given by

$$\hat{C}_{xy}(f) = \frac{|\sum_{n=0}^{N-1} X_n(f)Y_n^*(f)|^2}{\sum_{n=0}^{N-1}|X_n(f)|^2 \sum_{n=0}^{N-1}|Y_n(f)|^2} \tag{C.18}$$

where $*$ denotes complex conjugation, N is the number of data segments employed and $X_n(f)$ and $Y_n(f)$ are the discrete Fourier transforms of the nth data segments of $x(n)$ and $y(n)$. The confidence with which the magnitude coherence squared, $\hat{C}_{xy}$, is estimated for a given probability α given by [Myers et al 2004]

$$E_\alpha = 1 - (1-\alpha)^{1/(N-1)} \tag{C.19}$$

where N is the number of windows.

C.3 Entropy

C.3.1 Introduction

There are slow changes that take place in the behavior of physiological phenomena especially in patients that have progressive diseases. One of the goals of this study is the ability to track slow changes that take place in firing rate time series in patients that have motor neuron diseases. Techniques capable of quantifying such small differences in time series data are very important. Typically, quantification of biological time series is based on measures such as the mean, variability and frequency content. These measures may not provide insight into persistence of certain biological patterns. Efforts to quantify regularity have been centered around various entropy techniques [Chen et al 2005]. Entropy is a measure of randomness and predictability of a stochastic process. It generally increases with greater randomness.

C.3.2 Sample Entropy

Sample entropy (SampEn) is a variant of approximate entropy (ApEn) developed by Lake [Lake et al 2002] . ApEn was developed by Pincus and a detailed description is given [Pincus]. Just like ApEn, SampEn is a statistical index that quantifies the regularity of a signal. SampEn is becoming more widely used because, unlike ApEn which is inherently biased because self matches are counted to avoid the occurance of the natural logarithm of zero [Chen et al 2005] , it yields more consistent results. As described in the algorithm below, SampEn measures the logarithmic likelihood that runs of patterns are similar for a number of observations m remain similar for $m+1$. SampEn is a non-negative value. Low SampEn values indicate regularity while large values indicate a higher degree of irregularity. SampEn is described below.

Given a time series x(n) of length N

1. Generate m-vectors, X_1 to X_{N-m+1}

$$X_i = [x_i, x_{i+1}, ..., x_{i+m-1}] \tag{C.20}$$

$i = 1, 2, .., N - m + 1$

2. Then compute the distance, between vectors X_i and X_j as the maximum absolute difference:

$$D_m[X_i, X_j] = max([x_i, x_{i+1}, ..., x_{i+m-1}]) \quad i = 1, 2, .., N - m + 1 \tag{C.21}$$

3. For each i define, $i = 1, 2, .., N - m + 1$

$$B_i^m(r) = \frac{1}{N - m - 1} \times (no.of d_m[X(i), X(j)] \leq r) \quad i \neq j \tag{C.22}$$

4. Similarly define

$$A_i^m(r) = \frac{1}{N - m - 1} \times (no.of d_{m+1}[X(i), X(j)] \leq r) \quad i \neq j \tag{C.23}$$

5. Now define

$$B^m(r) = \frac{1}{N - m} \sum_{i=1}^{N-m} B_i^m(r) \tag{C.24}$$

and

$$A^m(r) = \frac{1}{N - m} \sum_{i=1}^{N-m} A_i^m(r) \tag{C.25}$$

6. Finally the SampEn value is defined as

$$SampEn(m, r, N) = -\ln(A^m(r)/B^m(r)) \tag{C.26}$$

Specification of parameters m and r is crucial to the computation of the SampEn value.

In developing ApEn, which is some what similar to SampEn, Pincus has suggest that r be set between 0.1 and 0.25 of the standard deviation of the data and that m be set to 1 or 2 [Pincus]. The developers of SampEn [Lake et al 2002] suggest using an autoregressive model to determine m. However it is questionable whether this selection still is appropriate for high sampling rates and the use of false nearest neighbors (FNN) to determine m is suggested [Chen et al 2005]. An optimal threshold value r is determined by minimizing a relative error as given below [Lake et al 2002]

$$max(\frac{\sigma_{CP}}{CP}, \frac{\sigma_{CP}}{-log(CP)CP}) \tag{C.27}$$

where CP is a conditional probability and is defined as

$$CP = \frac{A^m(r)}{B^m(r)} \tag{C.28}$$

σ_{CP} is the variance of CP.

C.4 Synchrony

C.4.1 Phase Synchrony Based on The Hilbert Transform

Phase synchrony is defined as the appearance of a certain relationship between phases of interacting systems while amplitudes remain uncorrelated [Bhattacharya 2001]. The measure of phase synchrony therefore assesses the degree of synchrony and when applied to physiological signals, may be useful in diagnosing diseases. Traditionally, the analysis of functional coupling of neuronal assemblies has been done through the magnitude squared coherence (MSC). However, it is not able to provide information regarding the feedback that exists between systems under investigation [Sakkalis et al]. In order to determine the phase lock value PLV of two given continuous time series $x(t)$ and $y(t)$,

first we define the analytic signals as follows:

$$Z_x(t) = x(t) + \jmath\tilde{x}(t) = B_x^H(t)e^{\jmath\phi_x^H(t)} \tag{C.29a}$$

$$Z_y(t) = y(t) + \jmath\tilde{y}(t) = B_y^H(t)e^{\jmath\phi_y^H(t)} \tag{C.29b}$$

where $\tilde{x}(t)$ and $\tilde{y}(t)$ are the Hilbert transforms of $x(t)$ and $y(t)$, respectively as described in subsection C.4.2. Next, we define the phase difference of the analytic signals;

$$\phi_{xy}^H(t) = m\phi_x^H(t) - n\phi_y^H(t) \tag{C.30}$$

where m and n are positive integers, and ϕ_x^H and ϕ_y^H are the locking phases of time series $x(t)$ and $y(t)$ respectively. Finally, the phase synchronization index is defined as

$$\gamma H \equiv sqrt(\langle cos\phi_{xy}^H(t)\rangle^2 + \langle sin\phi_{xy}^H(t)\rangle^2) \tag{C.31}$$

where $\langle . \rangle$ denotes the time average. From equation C.31, the phase lock value γH will be one if the phase difference is a constant as this will be indicative of perfect synchronization and zero if they is no synchronization whatsoever.

C.4.2 Hilbert Transform

A Hilbert transform is essentially a digital filter that has, approximately, unity gain and a 90 degree phase shift at all frequencies. One of its uses is to generate an analytic signal from a real-valued time domain signal $x(t)$. The analytic signal is defined as

$$z(t) = x(t) + \jmath\tilde{x}(t) \tag{C.32}$$

A magnitude function $A(t)$ can be defined from $z(t)$ and a phase function $\theta(t)$, where $A(t)$ describes the envelope of the original signal $x(t)$ and $\theta(t)$ describes the instantaneous

phase versus time.

Computation of Hilbert Transform

$\tilde{x}(t)$ is the convolution integral of $x(t)$ and $(1/\pi t)$

$$\tilde{x}(t) = x(t) * (\frac{1}{\pi t}) \tag{C.33}$$

Note that if we let $\tilde{X}(f)$ be the Fourier transform of $\tilde{x}(t)$, then $\tilde{X}(f)$ is defined by the product of the Fourier transforms of $x(t)$ and $\frac{1}{\pi t}$ since the Fourier transform of $\frac{1}{\pi t}$ is given by

$$F[\frac{1}{\pi t}] = -\jmath sgnf = \begin{cases} -\jmath, & forf > 0 \\ \jmath, & forf < 0 \end{cases} \tag{C.34}$$

Letting the Fourier transform of $z(t)$ be $Z(f)$,

$$Z(f) = X(f) + \jmath\tilde{X}(f) \tag{C.35}$$

A simpler method is to obtain $Z(f)$ from $X(f)$. Setting $Z(0) = X(0)$ and

$$Z(f) = \begin{cases} 2X(f) & forf > 0 \\ 0, & forf < 0 \end{cases} \tag{C.36}$$

we can obtain $z(t)$ by taking the inverse Fourier transform of $Z(f)$. $\tilde{x}(t)$ is then defined as the imaginary part of analytic signal $z(t)$.

Bibliography

[Adam and DeLuca 1999] Alexander Adam and Carlo J. De Luca, *Decomposition and Analysis of Intramuscular*, Chapter 27 In: Windhorst U and Johannson H (Eds.), Modern Techniques in Neuroscience Research, Springer, Heidelberg, 1999.

[Bendat and Piersol] Julius .S. Bendat, Allan G. Piersol, *Random Data: Analysis and Measuremneet Procedures*, Second Edition.

[Bhattacharya 2001] Joydeep Bhattacharya *Reduced Degree of Long-Range Phase Synchrony in Pathological Human Brain*, Acta Neurobiol. Exp. 2001, 61:309-318.

[Chen et al 2005] Xinnian Chen, Irene C. Solomon and Ki H. Chon, *Comparison of the Use of Approximate Entropy and Sample Entropy: Applications to Neural Respiratory Signal*,Proceedings of IEEE Engineering in Medicine and Biology 27th Annual Conference Shangai, China, Sept 1-4, 2005.

[Christie and Kamen 2006] Anita Christie and Gary Kamen *Doublet Discharges in Motorneurons of Young and Older Adukts* J. Neurophysiol 95: 2787-2795, 2006.

[DeCarvalho et al 2005] deCarvalho, M., J. Costa, and M. Swash, *Clinical trials in ALS: A review of the role of clinical and neurophysiological measurements*. ALS and Other Motor Neuron Disorders, 2005. 6: p. 202-212.

[DeOliveira 2005] Adriano de Oliveira Andrade, *Decomposition of Electromyographic Signals*, PhD Thesis.

[Erim et al 1999] Zynep Erim et al, *Effects of Aging on Motor-Unit Control Properties*, The Journal of Neurophysiology Vol. 82 No. 5 November 1999, pp. 2081-2091, 1999.

[Erim and Winsean 2008] Zynep Erim et al, *Decomposition of Intramuscular EMG Signals Using a Heuristic Fuzzy Expert System*, IEEE Transactions on Biomedical Engineering, 55(9):2180-2189, 2008.

[Fang 1999] Jianjun Fang, *Decomposition of Multiunit Electromyographic Signals*, IEEE Transactions on Biomedical Engineering, Vol. 46, No. 6, June 1999.

[Florestal et al 2007] J F. Florestal, P A. Mathieu and K C. McGill, *Automatic Decomposition of Multichannel Intramuscular EMG Signals*, Journal of Electromyography and Kinesiology 2007.

[Gut and Moschytz 2000] R. Gut and G. S. Moschytz, *High-precision EMG signal decomposition using com-munication techniques.* IEEE Transactions on Signal Processing, 48(9):2487 2494, 2000.

[Guyton] Guyton & Hall, *Textbook of Medical Physiology.* p.68,p82-84.

[Hammarberg 1994] Björn Hammarberg, *A SIGNAL PROCESSING APPROACH TO PRACTICAL NEUROPHYSIOLOGY, A Search for Improved Methods in Clinical Routine and Research.* Conference of the IEEE Volume , Issue , 3-6 Nov 1994 Page(s):347 - 348 vol.1.

[Hassoun 1994] M. H. Hassoun, C. Wang, and R. Spitzer, *Nnerve: Neural network extraction of repetitive vectors for electromyography* - part I: algorithm. IEEE Transactions on Biomedical Engineering, 41(11):1039 1052, 1994.

[Hoeven] Hoeven, Johannes Harmen van der, *Conduction velocity in human muscle : an EMG study in fatigue and neuromuscular disorders* Dissertation, 1995.

[Hudson] Hudson, *Amyotrophic Lateral Sclerosis, Concepts in Pathogenesis and Etiology.* p.144.

[Johnson et al 1973] M. A. Johnson, J. Polgar, D. Weightman and D. Appleton *Data on the Distribution of Fibre Types in Thirt-six Human Muscles: An Autopsy Study* Journal of neurrological Sciences, 18 (1973) 111-129.

[Kamen et al 1995] Kamen, G., Sison, S. V., Du, C.C.D., and Patten, *C. Motor unit discharge behavior in older adults during maximal effort contractions.* J. Appl. Physiol. 79: 19081913, 1995.

[Kantz and Schreiber 1995] H. Kantz and T. Schreiber, *Nonlinear Time Series Analysis*, Cambridge University Press (1997).

[Knight and Kamen 2006] Christopher Knight, Gary Kamen, *Motor Unit Firing Rates During a Complex Sinosoidal Force Task in Young and Older Adults* ,J Appl. Physiol. 2006.

[Koch et al 2006] Volker M. Koch, Kevin C. McGill, and Hans-Andrea Loeliger, *Resolution of Superpositions in EMG Signals using Belief Propagation: Results for the Known Constituent Problem*, EMBC 2006.

[Konrad 2005] Peter Konrad, *The ABC of EMG, A Practical Introduction to Kinesiological Electromyography*.

[Krivickas 2008] Lisa S. Krivickas, MD, *Anatomy and Physiology of the Motor Unit*, Lecture notes 2008.

[Lake et al 2002] Douglas E. Lake, Joushua Richman, M. Pamela Griffen, and J. Randall Moorman, *Sample Entropy Analysis of Neonatal Heart Rate Variability*, Am J Physiol Regul Integr Comp Physiol 283: R789-R797, 2002.

[LeFever and De Luca 1982] Ronald S. LeFever, Carlo J De Luca, *A Procedure for Decomposing the Myoelectric Signal Into Its Contituents Action Potentials Part I: Technique, Theory, and Implementation*, IEEE Transactions on Biomedical Engineering, Vol. BME-29, No. 3, March 1982.

[Leigh and Swash 1995] P.N Leigh and M. Swash, *Motor Neuron Disease.*Biology and Management p.11, p.4, p.53, p93 p139.

[Loudon et al 1992] G. H. Loudon, N. B. Jones, and A. S. Sehmi, *New signal processing techniques for the decompositon of emg signals.* Medical & Biological Engineering & Computing, 30(11):591599, 1992.

[Malmivuo] Jaakko Malmivuo, *Bioelectromagnetism.*

[McGill 2002] Kevin McGill, *Optimal Resolution of Superimposed Action Potentials*, IEEE Transactions On Biomedical Engineering, Vol. 49, No. 7, July 2002.

[McGill 2005] Kevin C. McGill et al, *EMGLAB: An interative EMG decomposition program*, Journal of Neuroscience Methods, 2005

[Merletti et al 1992] Merletti, R., Lo Conte, L. R., Actis, M. V., and Cisari, C. *Age related changes in surface myoelectric signals.* Scand. J. Rehab. Med. 24: 2536,1992.

[Myers et al 2004] Lance J. Myers, Zeynep Erim and Madaleine Lowery, *Time and Frequency Domain Methods for Quantifying Common Modulation of Motor Unit Firing Patterns*, Journal of NeuroEngineering and Rehabilitation, 2004, 1:2 doi:10.1186/1743-0003-1-2.

[Nawab et al 2007] S. Hamid Nawab, Robert Wotiz, and Carlo J. De Luca, *Improved Resolution of Pulse Superpositions in a Knowledge-Based System for EMG Decomposition*, Proceedings of the 26th Annual International Conference of the IEEE EMBS.

[Papoulis and Pillai] Athanasios Papoulis, S. Unikrishna Pillai, *Probability Random Variables and Stochastic Processes* , Fourth Edition.

[Piccolino 1997] Piccolino M, *Luigi Galvani and animal electricity: two centuries after the foundation of electrophysiology.* Trends in Neuroscience 20: 443-448. doi:10.1016/S0166-2236(97)01101-6 (1997).

[Pincus] Steven M. Pincus, *Irregularity and Asynchrony in Biologic Network Signals*,methods in enzymology, vol331.

[Piotrkiewicz et al 2008] Piotrkiewicz M, Kudina L, Mierzejewska J, Hausmanowa-Petrusewicz I, *Analysis of double discharges in amyotrophic lateral sclerosis.* Muscle Nerve. 2008 Jul;38(1):845-54.

[Preston 2004] David C. Preston, Barbara E. Shapiro; *Electromygraphy and Neuromuscular Disorders* 2004.

[Proakis and Manolakis] John G. Proakis, Dimitrid G. Manolakis *Digital Signal Processing*, Principles, Algorithms & Applications Third Edition, Pearson Education.

[Purves et al] Purves et al. *Neuroscience* p. 48-49.

[Raez et al. 2006] M. B. I. Reaz, M. S. Hussain1 and F. Mohd-Yasin, *Techniques of EMG signal analysis: detection, processing, classification and applications*, Biol. Proced. Online 2006; 8(1): 11-35 March 23, 2006.

[Rasheed et al 2006] Sarbast Rasheed, *Adaptive fuzzy k-NN classifier for EMG signal decomposition*, Medical Engineering & Physics 28 694-709 2006.

[Rasheed 2006] Sarbast Rasheed, *A Multiclassifer Approach to Motor Unit Potential Classification for EMG Signal Decomposition*, PhD thesis.

[Rowiñska et al 1999] Rowiñska-Marciñska K, Zalewska E, Hausmanowa-Petrusewicz I, *Double discharges of motor units in neuromuscular disorders.* J Physiol Paris. 1999 Jan-Apr;93(1-2):175-82.

[Sakkalis et al] Vangelis Sakkalis, Ciprian Doru Giurcneanu, Petros Xanthopoulos, Michalis Zervakis, Vassilis Tsiaras, Yinghua Yang, and Sifis Micheloyannis, *Assessment of linear and non-linear EEG synchronization measures for evaluating mild epileptic signal patterns.*

[Shefner et al 2004] Shefner, J., et al., *The use of statistical MUNE in a multicenter clinical trial*. Muscle and Nerve, 2004. 30: p.463-469.

[Stashuk 2001a] Dan Stashuk, *EMG signal decomposition*, Journal of Electromyography and Kinesiology, 11 (2001) 151-173.

[Stashuk 2001b] Dan Stashuk, *EMG signal decomposition: how can it be accomplished and used?*, Journal of Electromyography and Kinesiology 11 (2001) 151-173.

[Ushiba et al 2003] Yamada R, Ushiba J, Tomita Y, Masakado Y, *Decomposition of Electromyographic Signal by Principal Component Analysis of Wavelet Coefficient*, IEEE EMBS Asian-Pacific Conference on Biomedical Engineering 2003; Keihanna, Japan. pp. 118-119.

[Westgaard and de Luca 1999] R.H. Westgaard and C.J. de Luca *Motor Unit Substitution in Long-Duration Contractions of the Human Trapezius Muscle*, J. Neurophysiol 82:501-5-4, 1999.

[Yamamoto and Takano 1994] Yamamoto, T.; Takano, H , *Application of muscle sound to assess muscle tonus of the electrically stimulated muscle for FES.* Engineering in Medicine and Biology Society, 1994. Engineering Advances: New Opportunities for Biomedical Engineers. Proceedings of the 16th Annual International.

[Young] Ronald E. Young, *Muscle Physiology Lecture Muscle Site.* Website, 2002. `http://www.mona.uwi.edu/fpas/courses/physiology/muscles/MotorUnits.jpg`

[Zennaro et al 2003] Daniel Zennaro, Peter Wellig, Volker M. Koch, George S. Moschytz, and Thomas Läubli, *A Software Package for the Decomposition of Long-Term Multichannel EMG Signals Using Wavelet Coefficients*, IEEE Transactions on Biomedical Engineering, Vol. 50, No. 1, January 2003.